DEVELOPMENT OF A SOIL BIN TEST FACILITY FOR SOIL DYNAMICS STUDIES

by

MUHAMMAD RAZIF MAHADI

A thesis submitted to the Faculty of Graduate Studies of the University of Manitoba in partial fulfillment of the requirements for the Degree

of

Master of Science

Department of Biosystems Engineering
University of Manitoba
Winnipeg, Manitoba, CANADA

Development of a Soil Bin Test Facility for Soil Dynamics Studies

BY

Muhammad Razif Mahadi

A Thesis/Practicum submitted to the Faculty of Graduate Studies of The University of Manitoba in partial fulfillment of the requirement of the degree

Of

Master of Science

ABSTRACT

A soil bin test facility was developed at the University of Manitoba for indoor soil dynamics studies, specifically on soil-machine interaction research in agriculture. The soil bin permitted soil-machine interaction research being studied continuously without weather interruption and allowed researchers to control soil conditions. The soil bin featured fixed soil containers and a moving carriage. The soil containers were designed to enable quick soil preparation and testing different soil types in one test run. An 11.19 kW electric motor was fixed to a position at one end of the soil bin. The moving carriage was towed by the electric motor via a chain and sprocket system and traveled at a design maximum speed of 2.78 m/s. Conceptual designs of a 3-directional dynamometer for measuring soil-tool interaction forces and a single wheel tester for measuring breaking torque of soil-wheel interaction were also studied and presented.

ACKNOWLEDGEMENTS

First, I would like to thank to my program advisor, Dr. Ying Chen, for her advice, guidance, and support throughout the entire program. I would also like to thank to Dr. Nariman Sepehri and Mr. Don Petkau for serving as examining committee members and providing invaluable guidance on my thesis work. I would like to acknowledge the Department of Civil Service of the Government of Malaysia and my employer, the Universiti Putra Malaysia, for providing financial support and the opportunity to study in a wonderful university and gaining valuable experience for my future professional development.

I would also like to thank to Dale Bourns, Gerry Woods, and Matt McDonald for their endless comments, suggestion, and assistance in fabricating and assembling the soil bin test facility. I extend my gratitude to Associate Dean Rudolf Shilling and Dr. Qiang Zhang for their assistance in coordinating the placement of the assembled parts. I also appreciate Derek Inglis, Baraket Assefa, Samuel Ima, and Manickavasagan Annamalai for their assistance in this project.

Invaluable gratitude goes to my wife, Wan Nur Fariza Wan Abu Bakar, for her support and encouragement that has been the driving force for me to excel in my studies and career.

TABLE OF CONTENTS

LIST OF FIGURES

LIST OF TABLES

CHAPTER 1

INTRODUCTION

1.1 Introduction

Soil bin is a generic term for a test facility for studying soil dynamics, specifically on soil-machine interaction research in agriculture. The application of soil bin for soil-machine interaction research was initially established by several research institutes, such as the National Tillage and Machinery Laboratory (NTML) in the United States, the U.S. Army Tank Automotive Center Land-Locomotive, the Vicksberg Waterways Experimental Station, and Caterpillar Tractor Co. (Clark and Liljedahl 1968). Soil bins can be used for indoor and outdoor testing. But, many soil bins are intended for indoor testing. There are two broad divisions of soil-machine interaction studies. The first is on the applications of tools related to soil engaging and materials incorporation operations. The second is on the applications related to tractive devices, such as wheels and tracks. Soil bins were used more often in the first division than in the second.

Ideally, soil-machine interaction tests are conducted in fields for development of a prototype machine or evaluations of an existing machine, so that the tests could emulate the actual farm situation. Several problems often limit field-testing. The problems come from two sources, the weather condition and the soil condition. Testing can only be conducted when the weather is suitable for farming operations. But weather condition and changes in climate affect farming operations (Hammer et al. 2000). Manitoba has a variable weather condition (MMSW 2002), which permits farming operations during the

growing season only. So, the weather condition limits the time period for conducting a field test in Manitoba.

Soil condition consists of soil types, soil moisture content, and roughness of soil surface. Soil types may vary greatly within one field (Clark and Liljedahl 1968) and also from one field to another. Therefore, replicating the same soil condition is a challenge in field-testing. Moisture content, which influences the mechanical and dynamical properties of the soil, varies within one field. Natural field condition is bumpy that might affect the machine traveling speed and the working depth of a test-tool. But, controlling these parameters is essential for valid comparisons of measurements of tools or traction devices. (Gill and Berg 1968). These infield conditions parameters are beyond the control of researchers in field conditions.

Soil bins provide several benefits to soil-machine interaction studies. If located indoor, tests can be conducted all year round without weather interruption. Soil bins also allow researchers to control soil type and soil moisture content (Stafford 1979). In addition, researchers can replicate the same soil condition in a soil bin easily for every test. Monitoring and controlling of travel speed and working depth of the test tools can also be done easily in a soil bin. Experiments using soil bins can also reduce experimental errors due to the precise control on the tool working depth and travel speed (Chen 2002).

Soil bins provide tremendous benefits to researchers. But there are several limitations in soil bin testing. Firstly, soil bins are built under dimensional constraints. For instance, the design dimensions of most soil bins may be chosen to accommodate only three test-tools for testing in one pass (Liu et al. 2002). Therefore, most soil bin testing is limited to a small number of test-tools. Secondly, soil bins have a limit in maximum loads. Chen et al. (2004) could not test both seed-opener and fertilizer-opener for testing in one pass in a soil bin because the total loads of those devices exceeded the allowable load capacity of the carriage. Thirdly, most indoor laboratories are closed confinement. Thus any high odor materials cannot be tested with indoor soil bins. Rahman et al. (2004) replaced hog manure with water or dyed liquid when they tested liquid manure injection tools in an indoor soil bin. Other limitations may include the existence of vegetation and crop residue that affect the actual performance cannot be replicated in a soil bin.

A soil bin is important for studying soil-machine interaction in the laboratory. Experiments with soil bins can overcome the limits imposed by time constraint to develop a new design prototype or to evaluate an existing design. But, one should realize that there are some limitations to soil bin testing. Thus, field-testing still plays a role in soil machine-interaction studies. Soil bin testing should be used to investigate the initial phenomena of soil-machine interaction. The results from a soil bin testing may be validated with field tests.

There is a need for a soil bin test facility to conduct soil-machine interaction studies at the Biosystems Engineering Department, University of Manitoba. The soil bin should

be able to meet the demand for testing and developing prototype tools, comparing the performance of existing tools, and studying the phenomena of soil and machine interaction.

1.2 Objectives

The prime objective of this study was to design and develop a new indoor soil bin at the Department of Biosystems Engineering, University of Manitoba. The specific objectives were to develop the design concepts, analyze the design, fabricate, and assemble the soil bin. In addition, the conceptual design of a 3-directional dynamometer and a single wheel tester that were needed for soil-machine interaction studies was also expounded.

CHAPTER 2

LITERATURE REVIEW

2.1 Basic components

In general, a soil bin consists of five basic components. The first component is a soil container to contain soil. The second component is a carriage or a device to mount test-tools. The third component is the drive system to move the carriage. The fourth component is a soil-processing device to prepare the soil condition for a desired test. The fifth component is instrumentation for data collections. Other components may be added as necessary. An example of an additional component is a camera for capturing the image of soil movement while a tool cuts through the soil (Jayasuria and Salokhe 2003).

2.2 Design layout

Basically, a soil bin layout describes the physical appearance of a soil bin and its design configuration. There are two general types of design layouts, and both of them are related to the design of the soil container. The layouts can be classified upon the shape of the soil container (circular or straight) or based on the moving component (soil container or test-tool).

Every design layout has its advantages and disadvantages as describes by Siemens and Waber (1964). For instance, a circular soil container is good for continuous testing,

such as testing the weariness of a high-speed tillage tool. However, one must consider that the difference in traveling speed between the outer edge and the inner edge of the tool must be included in the analysis. Otherwise, the data is meaningless. This fact increases the complexity of the analysis. Meanwhile, a straight soil bin reduces the complexity of the soil bin design and permits easier data analysis. A straight soil bin can better represent the condition of a tool moving in linear motion in a field operation.

The design of a moving soil container reduces the complexity of the design for carriage, as the test tool can be mounted to a stationary frame. A stationary frame can also be equipped with more instrumentation than a moving one (moving carriage). But, the soil in a moving container can be exposed to vibration from the motion of the container, which reduces the rigidity of the soil in that container. Furthermore, the amount of power required is directly proportional to the load. Thus, moving a soil container requires tremendous amount of power to accelerate the heavy soil to an intended speed. But, relatively smaller amount of power is required to move a carriage. Moving soil container design also requires more space than moving carriage. Therefore, the design with moving carriage and stationary soil container design is the better option.

2.3 Soil bin classification

Soil bins can be classified into large-scale soil bins and small-scale soil bins. The size of the soil bin influences the type of testing, the amount of data collected, and the number of test tools per test run. The significant difference between a large-scale and a small-scale soil bin is the overall length of the soil bin. The overall length of the soil bin

consists of the working length and the effective length of the soil bin. The overall length directly refers to the length measured from one end to another of the entire soil bin structure. The working length refers to the total traveling distance of test tool. The effective length is the distance over which a test tool is moving in a constant speed. It is important to note that the effective length for measurements is important. According to Gill and Berg (1968), tool draft varied with the tool traveling distance. Hence, draft and other data should be taken at the constant tool traveling speed. Usually the longer the soil bins, the more data points can be collected in one pass.

A soil bin at the National Soil Dynamics Laboratory (NSDL), in the United States is a good example of a large-scale soil bin. The length of the soil bin is 75 m long, 6 m wide, and 0.6 to 1.5 m deep. Another large-scale soil bin is located at the Obihiro University of Agricultural and Veterinary Medicine, Japan (Taniguchi et al. 1999). The soil bin is 100 m long, 4.3 m wide, and 1.0 m deep.

The soil bin designed by Siemens and Weber (1964), Stafford (1979), Durant et al. (1980), Godwin et al. (1980), and Onwualu and Watts (1989) are some examples of small-scale soil bins. The length of those soil bins ranges from 5 to 13 m. Therefore, one can classify any soil bins longer than 20 m as large-scale bins and those shorter or equal to 20 m as small-scale soil bins.

It was reported that large-scale soil bins are able to test a test-tool at a test speed up to 4.8 m/s (Burt et al. 1980; Taniguchi et al. 1999). Most small scale soil bins have a

maximum test speed range of 1.0 to 3.0 m/s. In a rare occasion, Stafford (1979) designed a soil bin with a test speed of up to 5.5 m/s for a total working length of 10 m.

Soil bin length directly affects the capability of collecting a sufficient amount of data and achieving a high test speed. The capability to reach a high test speed is also influenced by the size of the motor that drives the carriage. A closer observation reveals that the motion profile of a test-tool consists of three sections: the acceleration, constant speed (effective length), and the deceleration sections. Regardless of the motor capability, a motor requires some distance for acceleration to achieve the desired constant speed. The higher the target test speed, the longer the distance needed to accelerate and decelerate under the same motor power. Furthermore, the higher the target test speed, the shorter the time it takes to travel over the working length. Thus, if the length of a soil bin is long enough, one should have an ample distance to be allocated for acceleration and deceleration sections, and a high test speed is feasible as well.

2.4 Soil bin components

2.4.1 Soil container

The primary function of a soil container is to contain soil. A soil container can also be used to provide support to the carriage rails (Godwin et al. 1980; Onwualu and Watts 1989). It has also been discussed that the design of a soil container is influenced by the need of having a moving container or stationary container.

The dimensions of a soil container are the major factors in a soil bin design, influence the overall dimensions of the soil bin. Basically, the dimension selection has two constraints. The first constraint is the space limitations. This factor determines the possible length of the soil bin and consequently affects the motion profile of the test tool. The second constraint is boundary effects on the test results. By definition, the boundary effect is interference from the sidewalls and the bottom floor of the soil container.

There are no specific theories for determining the dimensions of a soil container. Previous reports had made several assumptions to come up with a valid dimensional value. Sowers (1962) cited by Clark and Liljedahl (1968) stated that for testing a track type traction device, a length to width ratio of 5 or larger for the container could satisfy the testing without boundary effects. Harrison (1961) cited by Clark and Liljendahl (1961) suggested that a width to depth ratio of 3 to 1 was adequately enough to prevent boundary effects. Clark and Liljedahl (1961) improvised a method for traction device testing, based on the theory of shallow foundation of bearing capacity. This theory was normally used in civil engineering. Initially, it was assumed that a traction device had an infinitely long footing in longitudinal direction, so the problem could be reduced to a two-dimensional analysis for selecting the width and depth of the soil container. The width and depth of the soil container was determined based upon the width and weight of a test wheel or track. They were determined by calculating the failure zones produced by the soil-traction device interaction. A rule of thumb, suggested by Schafer (1988), cited by Onwualu and Watts (1989), focused on the width and depth selection for tool testing.

The method treated the value for minimum soil container width as a function of the working depth and width of the tool.

A soil container can be designed to be a big tank that covers the whole length of a soil bin (Onwualu and Watts 1989). It can also be designed to occupy only the constant speed section, which is more cost-effective. A soil container can be designed to be a combination of small sections for testing various soil types in one test run (Stafford 1979). It can also be designed to have an adjustable width and length to satisfy variety of test purpose (Godwin et al. 1980).

Some soil containers were designed with transparent sidewalls (Jayasuria and Salokhe 2003), so that the soil displacement within the soil container can be observed. An uncommon design was proposed by Liu et al. (2002), in which the soil container could be lifted at one end by a pair of hydraulic cylinders in order to simulate a slope surface condition for tillage erosion studies.

2.4.2 Carriage

The primary function of a carriage is to transport test tools. Other functions include transporting soil processing devices and housing instrumentation. Siemens and Waber (1964) suggested that a carriage should be rigid enough to subject the weight of test tools and the forces that are produced by the tools. Another important consideration in the design of a straight soil bin is to ensure that the carriage motion is maintained in a straight path. For this reason, Onwualu and Watts (1989) employed a set of four rigid

wheels, running along the rails on the vertical plane of the sidewalls. Stafford (1979) ran the carriage on an overhead rail. Godwin et al. (1980) used a steel angle as the guide rail, so that the rigid wheels rolled on the steel angle instead of on the flat surface of a rail. The tendency for carriage tilting should also be considered. Onwualu and Watts (1989) used another sets of rigid wheels running along the bottom surface of an I-beam rail to prevent the carriage from tilting.

2.4.3 Soil processing devices

Soil processing devices are used to prepare soils in the soil container for testing. The devices may consist of several components such as a rotary tiller, a leveler, and a compaction roller. The devices may be mounted on a specifically designed carriage for the soil processing devices (Durant et al. 1980), or shares a common carriage with the test tool (Onwualu and Watts 1989). When the carriage is shared, either a tool or a soil-processing device will be mounted to the carriage at one time.

2.4.4 Drive system

An electric motor is the common driving power source. Stafford (1979) used a DC electric motor (20 kW) to drive the carriage. The maximum test speed was up to 5.5 m/s. A distance of 3 m was designed for acceleration and deceleration sections and the effective length was 4 m. Onwualu and Watts (1989) employed a combination of an electric motor and a hydraulic motor and pump. Durant et al. (1980) used an electric

motor to drive a hydrostatic transmission system. Godwin et al. (1980) used a stationary tractor engine (internal combustion) to drive the carriage.

2.4.5 Instrumentation

The most common instrumentation is a force dynamometer that measures forces of the test-tools in horizontal, vertical, and lateral directions (Stafford 1979). There are many types of dynamometers that can be used for soil bin applications. Those dynamometers can be classified into frame types and linkage types (Kirisci et al. 1993). In a frame type dynamometer, force transducers are mounted into a frame that is to be installed between the tool to be tested and a soil bin carriage or a tractor drawbar. The dynamometer used on the previous soil bin in the Department of Biosystems Engineering is a frame type dynamometer. This dynamometer measured three orthogonal forces (horizontal or draft, vertical, and lateral) and had been used for many soil-tool interaction studies (Rahman and Chen 2001; Chen 2002). Like most frame type dynamometers, this dynamometer was large, which changed the position of the tool relative to the toolbar, which is not desired in drawbar force measurements. A linkage type dynamometer can overcome this drawback, as it is more compact in structure.

Linkage type dynamometers have been developed by many researches. Zoerb et al. (1983) and Kirisci et al. (1993) designed instrumented hitch pins to replace the usual implement hitch pin. The strain gauges installed in the pins generated force signals that were recorded as the drawbar force of an implement. Most pin type dynamometers are 1-D dynamometers that can measure drafts only. Vertical and lateral forces of a tool or an

implement are also important in many studies. Furthermore, pins cannot accommodate bending moments exerted on the drawbar by a tool or an implement.

Another linkage type dynamometer is ring dynamometers, such as extended octagonal ring (EOR) dynamometers (Siemens and Weber 1964; Hoag and Yoerger 1975; Godwin 1975; Gu et al. 1991). They were developed for accommodating large bending moments and measuring two or three forces. The latest development for EOR dynamometers includes large capacity double EOR dynamometers developed by Tessier et al. (1992), McLaughlin et al. (1998), and Chen et al. (2005) for measuring forces exerted by an implement on the tractor drawbar.

In any dynamometer design, the locations of transducers or strain gauges are critical. The optimal strain gauge locations are those where the measurement of one force is not affected by that of another force. In other words, the optimal locations should minimize or eliminate the crossing effects between the force measurements in three directions. One of the drawbacks of EOR dynamometers is the difficulty in selecting the strain gauge locations to minimize the crossing effects.

In summary, a compact dynamometer was needed to replace the previous frame type soil dynamometer used in the previous soil bin. The compact dynamometer should measure three orthogonal forces, minimize the crossing effects between three forces, and be able to accommodate large bending moments.

2.5 The role of soil bin in soil-machine interaction

Soil bins have been used to test soil engaging tools and materials incorporation tools. Soil engaging tools include tillage tools and seeding openers. Materials incorporation tools include manure injection tools and straw incorporation tools. Studies conducted on these tools included measurements of draft requirement and characteristics of soil disturbance caused by the tool (Rahman and Chen 2001), evaluations of existing tools (Chen and Ren 2002), and development of a prototype tool (Chen 2002). A soil bin was also utilized for evaluating straw and soil movement resulting from a tillage tool (Liu 2005) and the distribution pattern of liquid manure in soil following manure injection (Rahman et al. 2004). Chen et al. (2004) studied the performance of drill and crop as affected by various drill configurations in a soil bin.

2.6 The role of soil bins in soil-traction studies

Researchers have been using soil bins to investigate the phenomena of soil-traction and soil compaction. Raheman and Singh (2002) studied the effect of steering forces on a driven tractor wheel in a soil bin. Canillas and Salokhe (2002) developed a decision support system to predict soil compaction based on a soil bin research. Carmen (2002) evaluated the degree of compaction caused by a towed wheel in a soil bin. Others (Watyotha et al. 2001; Hendriadi and Salokhe 2002) utilized a soil bin to gain a better understanding in cage wheel design to improve the traction of the cage wheel.

Many soil-traction studies in a soil bin were conducted by utilizing a single wheel tester. The function of a single wheel tester is similar to that of a soil bin carriage. However, the single wheel tester is not necessarily movable like a carriage. It can be fixed stationary on a soil bin when testing.

2.6.1 A single wheel tester

A single wheel tester is a test jig. With this tester measurements are taken under different vertical loads. Those measurements include input torque, drawbar pull, input velocity, and output velocity. These data are collected by transducers and data acquisition systems. Later the data are used to calculate traction performance parameters. Single wheel testers can be designed in various scales to suit the test objectives. There were small-scales and large-scale single wheel testers. The large-scale testers are usually used for field-testing, while smaller-scale testers are used in the laboratories or operated on soil bins.

2.6.2 Large-scale single wheel testers

Burt et al. (1980) reported the development of a single wheel tester used by the National Tillage Machinery Laboratory (NTML) in the United States. The test tire was driven by a system that consisted of a radial piston hydraulic motor, a chain drive, a speed reducer, and a closed loop servo for angular velocity control. The angular velocity could be controlled at 0.3 and 4.2 rad/s. Maximum torque was 42 000 N-m and could be reached within 2.1 rad/s. A hydraulic cylinder and a closed loop control were used to

regulate the vertical load to the test tire. Maximum applied load was 71.2 kN, but because of the opposite reaction from the torque reaction force, the net dynamic load was 44.0 kN at the maximum torque value.

Upadhyaya et al. (1986) developed a unique, mobile single wheel tester. The machine was equipped with the necessary sensors to measure forward speed, wheel load, wheel angular speed, torque, and drawbar force. The machine could be operated either on a control draft option or a control slip option. The maximum tire size that could be mounted on the machine was 1 m in width and 2 m in diameter. The maximum wheel load that could be applied was 26.7 kN while the maximum torque was 230 N-m at a rotational speed of 2103 rpm.

Shmulevich et al. (1996) developed a large-scale single wheel tester for field-testing. The tester was mounted at the rear of a tractor and towed around a field. The tractor hydraulics was used to drive the test tire and also power other equipment. The machine could be equipped with a tire up to 2 m diameter. Vertical load could be applied up to 50 kN and the maximum torque was 31 kN. Alcock and Wittig (1992) also reported a similar device. While Shmulevich et al. (1996) used a single frame machine, Alcock and Wittig (1992) used a dual frame with an inner frame sliding within an outer frame.

2.6.3 Small-scale single wheel testers

Clark and Liljedahl (1969) designed a small-scale single wheel tester for testing the effect of single, dual, and tandem wheels. The tester was operated in a soil bin 6.7 m

long, 0.9 m wide, and 0.3 m depth. Ram and Pathak (1969) used a single wheel tester to investigate the tractive efficiency of soil. A pneumatic tire without lugs was used as the test tire. The tire size was 0.4 m in diameter and 0.1 m wide. The test tire was driven by a 0.4 kW 3-phase electric motor with a gearbox, a sprocket, and chains arrangement. The soil processing carriage was used as the horizontal wheel load. Two straight rails were installed side by side in order to permit the test device to move only in forward or reverse motion.

Wanjii et al. (1997) used a single wheel tester to study the distribution of normal and tangential soil stresses of a rigid wheel. The tester consisted of an outer frame and an inner frame. The inner frame could move freely in vertical direction within the outer frame. Normal and tangential dynamometers were installed to the rigid wheel to measure normal and tangential stresses acting on the wheel. The target vertical load and angular velocity of the wheel were 1.09 kN and 0.9 rad/s, respectively. But during the test, the angular velocity fluctuated between 0.55 to 0.92 rad/s. A hydraulic motor was used to drive the rigid wheel.

2.6.4 Design factors

A single wheel tester is designed based upon several factors. Two of the most important factors are the needs to drive the tire and to provide variable vertical loads to the test tire. In an active drive study, the test tire is required to have a direct drive to overcome the motion resistance. In this case, a motor is connected to the test tire to provide a driving torque. A hydraulic motor was used by Upadhyaya et al. (1986) and

Shmulevich et al. (1996) to provide torque. An electric motor was used by Ram and Pathak (1978). One must consider the fact that the speed of the motor must be reduced to a level which is acceptable to the test. Ram and Pathak (1978) used a chain and sprocket arrangement to reduce the speed of the motor.

Many traction tests study the effects of various vertical loads. A single wheel tester may be equipped with a hydraulic cylinder, installed vertically from the center of the wheel to vary the vertical load (Upadhyaya et al. 1986). Another method to vary the vertical load is by means of adding a weight block. In some cases, the vertical load may remain constant (Ram and Pathak 1978).

Frame configurations may be considered in the design of a single wheel tester. The function of the frame is to hold the related components and instrumentation. The frame should be design to reflect the required parameters. Zoz and Grisso (2003) described three configurations of a frame design. The simplest configuration is to have a frame with a single arm, where one end of the arm is connected to the test tire and the other end is connected to the main frame. A force transducer is connected between the end of the single arm and the main frame. The transducer in this case measures the drawbar pull produced by the tire-soil interaction. Although the design is simple, one has to consider the weight transfer effect for this configuration because the vertical load also influences the torque to the test tire. The second configuration eliminates weight transfers by utilizing two parallel arms. But, measuring the drawbar pull is difficult. The third configuration has two parallel arms with joints, so that the test wheel is free to move

along the vertical direction. This configuration is employed in many single wheel tester designs.

CHAPTER 3

DESIGN CONCEPTS AND CRITERIA

3.1 Constraints and limitations

Space availability to install the soil bin and the maximum testing speed desired were two vital factors in the soil bin design. It was decided to build an indoor and straight soil bin to accommodate those tests during the winter season and to better represent a typical field operation. The indoor space availability limited the overall length of the soil bin. The intention was to place the soil bin in the future Biomachinery Laboratory at the Engineering and Information Technology Complex, University of Manitoba. The longest measurement from wall to wall of the laboratory is 15 m. Therefore, the overall soil bin length should be lesser than 15 m. Thus, the soil bin would fall into the category of a small-scale soil bin.

Agricultural field machines (such as a tractor) are normally operated under a speed of 10 km/h. Therefore, the maximum speed of the soil bin was set as 10 km/h (2.78 m/s). As aforementioned, testing can be achieved by either moving soil container or moving tool carriage. For the limited space, moving tool carriage instead of soil container was the better choice. Thus, the available space could be used optimally for constructing the soil bin.

3.2 Components

3.2.1 Soil container, rail, and rail-support

The optimum shape for a soil container would be a rectangular box, where the carriage could be designed to move along the longitudinal direction of the soil container. The soil container could be sectional and filled with different soils. Thus, one test run could cover different soil types, which is effective for studies in comparisons of the effect of soil types. The soil container might not necessarily cover the whole length of the soil bin system; instead the soil container was chosen to only cover the constant speed section (effective length) of the soil bin. Thus, the amount of material required to make the box would be less and the amount of soil required would also be reduced. Furthermore, soil processing before a test would be completed quicker. Thus, the soil container having three sections (or three rectangular boxes) was considered for the soil bin. A rail should be assembled on top of each soil containers side walls to enable carriage motion. The soil container supported the rails at the center, while both ends of the rails were supported by rail supports.

3.2.2 Carriage

The carriage structure must be rigid to carry a test-tools and to overcome the draft of the test-tools. It is essential that the carriage moves in a straight path, so that the collected data points are consistent. Assembling a steel angle on top of the carriage rail and using groovy type rigid wheels for the carriage would ensure a straight path, as long as the groovy wheels roll on the steel angle. The carriage must have a toolbar or toolbar

plate to mount test-tools. The carriage must also have a capability to adjust the position of the test-tools in lateral and vertical directions.

3.3.3 Drive system

The drive system provides power to move the tool carriage. Power can be provided by a motor (electrical, hydraulic, or gasoline engine). Selection of motor type depends upon the convenience of operating the soil bin. Application of a Variable Speed Drive (VSD) control to regulate the motor speed was preferred instead of a traditional gear reducers unit, because a VSD allowed for simple drive system designed, easy operation, and easy to include variety of control instrumentation, such as limit sensors and brakes. Considering the power supply available at the intended soil bin location, an AC 3-phase electric motor with a VSD should be the optimal choice for the soil bin drive system.

3.3 Design sketch

A conceptual sketch was developed to show the major components of the soil bin and the way these components were connected (Fig. 3.1). The ends of the soil bin were labeled as motor end and tensioner end. An electric motor was located at the motor end to tow the carriage. A chain tensioner was located at the tensioner end to control the tension of the chain. A soil container was located at the center of the soil bin. A rigid rail was installed on top of the soil container. Both ends of the rail were supported by rail-supports.

The carriage moved on top of the rails. Two stages of chain and sprocket systems linked the carriage to the electric motor. The first stage had two sets of chain and sprocket system. Each set was assembled to one side of the soil bin in longitudinal direction. Specifically, the first stage of the chain and sprocket system consisted of the carriage, two roller chains A, four carriage sprockets, and a drive shaft at both ends. Chain A was connected to the carriage via chain connectors. The second stage of the system consisted of a roller-chain B, a drive sprocket (installed at the center of the drive shaft at the motor end in lateral direction), and a motor sprocket an electric motor. A test-tool was mounted on a dynamometer, while the dynamometer was mounted to the vertical adjustment frame of the carriage.

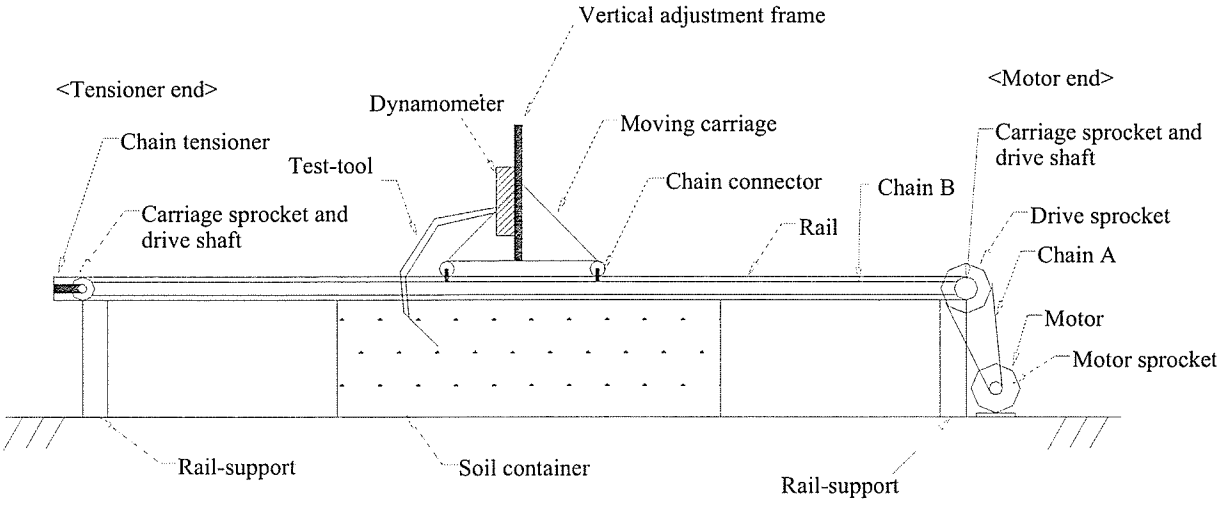

Fig. 3.1 Conceptual sketch the soil bin

CHAPTER 4

ANALYSIS OF COMPONENTS

4.1 Dimensions of the soil container

The design of a soil container must consider the dimensions for inner width and depth. The dimensions should be selected to satisfy testing without boundary effects from the container's sidewalls and bottom floor. The method suggested by Schafer (1988), cited by Onwualu and Watts (1989) for selecting the container dimensions for testing a tillage tool, was used as a guide to select the dimensions for the inner width and depth of this soil bin.

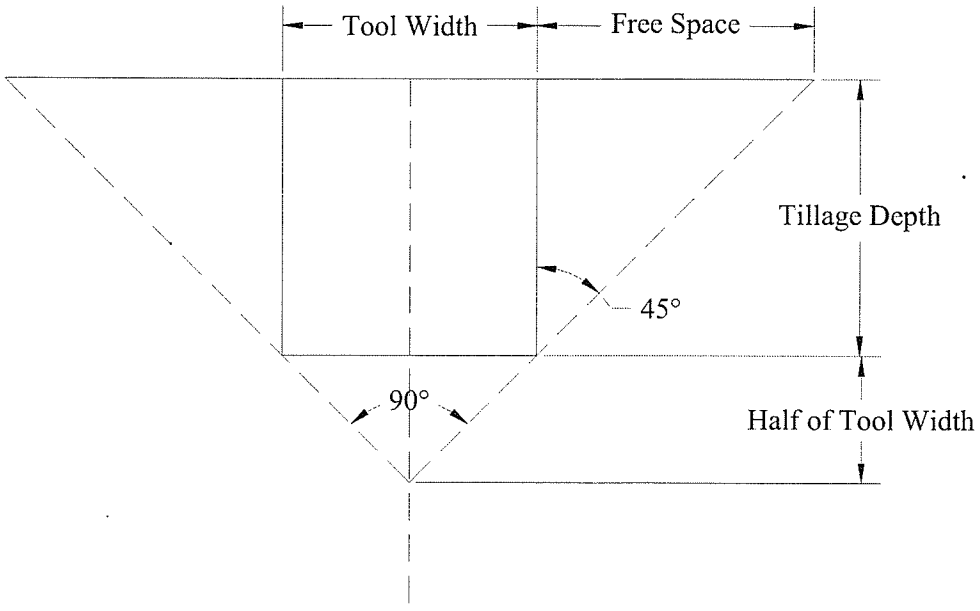

Fig. 4.1 Determination of inner width and depth based on Schafer (1988), cited by Onwualu and Watts (1989)

This method assumes that for any test-tool width, the amount of free space from the edge of the test-tool to one side of the container sidewall is equal to the tillage depth (tool

working depth) (Fig. 4.1). Then the minimum width is the sum of the free space on both sides and the tool width itself. The minimum depth is the sum of the tillage depth and half of the tool width.

In selecting the width and depth of the soil bin, the width of test-tool was based on the biggest sweep width possible. A sweep type tool of 0.57 m wide, working at a depth of 0.15 m, used by Rahman and Chen (2001), seemed to be the case representing the widest tool operated at the greatest depth. Using this example, the minimum inner width required for the soil container was 0.87 m and the minimum inner depth was 0.44 m. To allow for a greater flexibility of testing other tools, greater values were selected for the dimensions of the soil container. The final designed inner width and depth were 0.91 m and 0.61 m, respectively. These values for width and depth will also allow for testing multiple narrower tools in one test run and for testing tires for traction or soil compaction studies.

4.2 Rail length and testing time

From Chapter 3, the overall length of the soil bin was designed as 15 m. A length of 3 m was allocated for placing the drive system components and chain tensioners at the ends of the soil bin. The rail length was 12 m. A length of 2 m of the rail was allocated for the carriage. Thus the working length was 10 m, which included all the three sections of carriage (or tool) motions: length for acceleration, length for constant speed (effective length), and length for deceleration. Within the 10 m working length, a length of 2 m was allocated for both acceleration and deceleration sections. Thus, the effective length was 6

m, which was considered sufficient for the effective length for most tests. Assuming the tool moves in a uniform linear motion, the acceleration of the carriage was estimated with eq. (4.1).

$$a = \frac{V^2 - V_0^2}{2S} \tag{4.1}$$

Where,

a = acceleration (m/s^2)

S = distance travel (m)

V = final speed (m/s)

V_o = initial speed (m/s)

Based on eq. (4.1), to move a test-tool from zero speed to the maximum testing speed of 2.78 m/s within a distance of 2 m, the acceleration was 1.93 m/s^2. The time required for acceleration can be found by eq. (4.2):

$$t = \frac{V - V_0}{a} \tag{4.2}$$

Where,

t = traveling period (s)

Using eq. (4.2), one knows that the traveling period, t to accelerate the carriage from zero to a maximum constant speed of 2.78 m/s was 1.44 s. Similarly, the traveling period, t to

decelerate the carriage from maximum constant speed to zero was also 1.44 s. Based on the selected length for constant speed section (6 m), the time required to remain in constant speed was 2.16 s. Therefore, for a working length of 10 m at maximum test speed, a test run (tool motion from tensioner end to the motor end) should take approximately 5 s to complete.

4.3 Equivalent angular speed and acceleration

Based on Fig. 3.1, the power from the power supply is transmitted to the carriage by means of two stages of chain and sprocket system. To design the driving system, one should consider the equivalent angular motion parameters related to the linear motion parameters of the carriage. Linear speed and angular speed are related by eq. (4.3):

$$\omega = \frac{V}{R} \tag{4.3}$$

Where,

ω = angular speed (rad/s)

V = linear speed (m/s)

R = radius of the sprocket (m)

Considering a carriage sprocket radius of 0.05 m and a maximum linear speed of 2.78 m/s, the equivalent angular speed was 55.6 rad/s or 531 rpm. Therefore, with this carriage

sprocket, the drive shaft should be rotated to a maximum speed of 531 rpm within 1.44 s in order to achieve the maximum design linear test speed.

Linear acceleration and angular acceleration are related by eq. (4.4):

$$\alpha = \frac{a}{R} \tag{4.4}$$

Where,

α = angular acceleration (rad/s^2)

Considering the same radius for carriage sprocket (R = 0.05 m) and the linear acceleration of 1.93 m/s^2, the equivalent angular acceleration was 38.6 rad/s^2.

4.4 Power requirement

The requirement of motor power was determined based upon two factors: the mass moment of inertia of the carriage and the draft force produced by the test tool. Torque from each factor was estimated independently and added up to form the total torque requirement. The requirement for motor power was determined from the total torque. The drive system was considered as a constant load problem.

4.4.1 Estimation of draft force of test tool

There is no single value of draft force which can be used for the soil bin design, as draft force of a tool increases with the working depth and travel speed (McKyes 1985). Draft force also varies with the tool width, and the bigger the width, the higher the draft

force is. For example, disc type tools have lower draft forces than sweep type tools, as the latter tools are wider. Soil types used in the soil bin also affect the draft of test tool. In this study, the draft force for a large sweep, reported by Rahman and Chen (2001) was used as a reference for determining the power requirement of the motor. The sweep was fairly wide (0.573 m) and it produced a draft of 1700 N at the working depth of 0.15 m.

4.4.2 Mass moment of inertia

Carriage. Estimation of the mass moment of inertia of the carriage requires estimation of the mass of the carriage. The mass of the carriage included the mass of the carriage assembly, test tools, and roller chains A and B (Fig. 3.1). A dynamometer should also be included in the carriage assembly. A total mass of 250 kg was considered for these components. The mass moment of inertia of the carriage was estimated by eq. (4.5):

$$J = m R^2 \tag{4.5}$$

Where

J = mass moment of inertia (kg-m^2)

m = mass (kg)

The radius of carriage sprocket, R was 0.05 m. Thus, mass moment of inertia of the carriage was 0.625 kg-m^2.

Drive shaft. The mass moment of inertia of the drive shaft was estimated based upon a solid cylinder condition, eq. (4.6):

$$J = \frac{\pi}{2} l \rho (R^4) \tag{4.6}$$

Where,

ρ = material density (kg/m^3)

l = length of the cylinder (m)

Appendix C (section C.1) describes the calculation of the mass moment of inertia for two units of drive shafts, which was 1.82 x 10^{-2} kg-m^2.

Drive sprocket. The mass moment of inertia of the drive sprocket was estimated based upon a hollow cylinder configuration. The method is described in eq. (4.7).

$$J = \frac{\pi}{2} l \rho (R_o^4 - R_i^4) \tag{4.7}$$

Where,

R_o = outer radius (m)

R_i = inner radius (m)

Appendix B (section B.3) describes the dimensions and calculation of moment of inertia of the drive sprocket, which was 1.23×10^{-2} kg-m^2

Carriage sprockets. Equation (4.7) was also used to calculate the mass moment of inertia of the drive sprockets. Appendix B (section B.5) describes the dimensions and calculation of mass moment of inertia of the carriage sprocket, which was 4.40×10^{-3} kg-m^2.

Motor sprocket. Equation (4.7) was also used to calculate the mass moment of inertia of the drive sprocket. Appendix B (section B.6) describes the dimensions and calculation of the motor sprocket, which was 1.27×10^{-3} kg-m^2.

4.5.3 Torques and motor power

The total mass moment of inertia for the system was calculated based on eq. (4.8):

$$J_M = J_1 + J_2 + J_3 + J_4 + J_5 \tag{4.8}$$

Where,

J_M = total mass moment of inertia (kg-m^2)

J_1 = mass moment of inertia of the carriage (kg-m^2)

J_2 = mass moment of inertia the drive shafts (kg-m^2)

J_3 = mass moment of inertia the drive sprocket (kg-m^2)

J_4 = mass moment of inertia the carriage sprockets (kg-m^2)

J_5 = mass moment of inertia the motor sprocket (kg-m^2)

Hence, J_M was 0.661 kg-m^2. Torque due to the moment of inertia and the draft of the tool should be determined based on eq. (4.9) and eq. (4.10) respectively:

$$T_M = J_M \alpha \tag{4.9}$$

Where,

T_M = torque due to mass moment of inertia of the system (N-m)

$$T_D = F_D R \tag{4.10}$$

Where,

T_D = torque due to the draft force (N-m)

F_D = draft force (N-m)

Previously, it was determined that the angular acceleration was 38.6 rad/s^2. Thus, torque due to the moment of inertia, T_M was 25.52 N-m. It was determined previously that the tool draft was 1700 N and the radius, R of the carriage sprocket was 0.05 m. Therefore, torque due to the draft force, T_D was 85 N-m. The total torque of the system should be the summation of T_M and T_D, which was 110.52 N-m. Torque and power are related by eq. (4.11)

$$P = T \omega \tag{4.11}$$

Where,

P = power of the motor (kW)

T = total torque (N-m)

Given an angular speed of 55.6 rad/s, the motor power required was 6.14 kW.

4.4.4 Motor selection

Based upon the required power of 6.14 kW estimated to overcome the inertia force and the draft force, the motor was selected based on the manufacturer's catalog. An electric motor with 11.19 kW (15 hp) was selected to power the carriage, which gives a safety factor of approximately 1.8.

4.5 Structural analysis

Structural analysis was performed on critical structure members to aid in material selection and to verify the capability of the design. Four structures with critical members were analyzed against known parameters.

- the vertical member of rail-support;
- the vertical member of the soil container frame;
- the vertical adjustment frame of the carriage;
- the carriage body frame.

4.5.1 Rail support

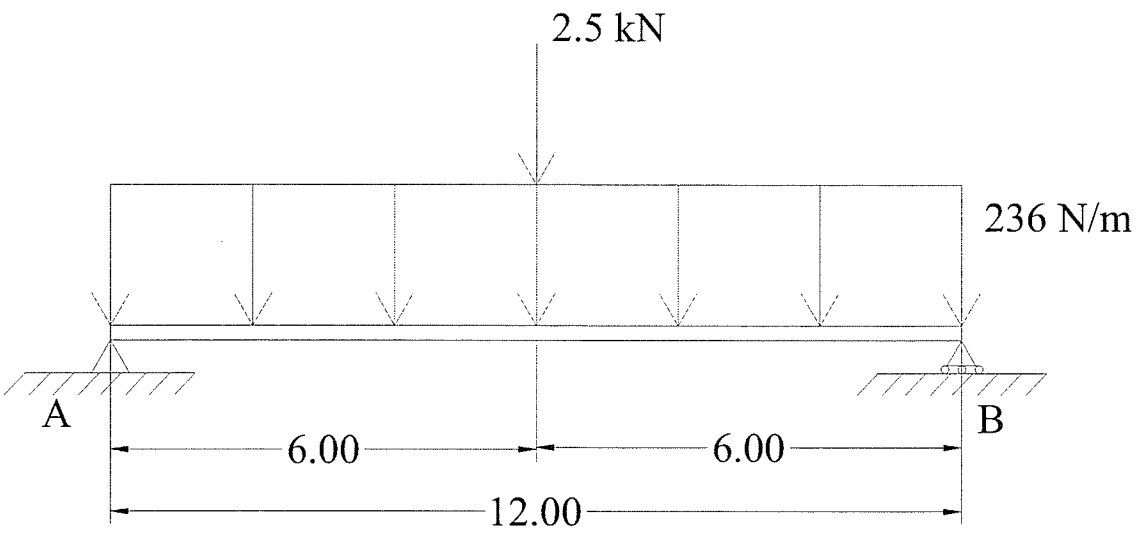

Fig. 4.2 Side view for rail and rail-support positions for design analysis

Rail supports were located at the ends of the rails (I-beams) (Fig. 3.1). For analysis purpose, the rail supports are considered as two supporting points, A and B (Fig. 4.2). The rail support carries load from the rails, which was treated as a distributed load. The cross section area of the I-beam (part No.: sb-rx-1, Appendix D) is 0.003 m^2 and the density of steel ASTM 36 is 7850 kg/m^3 (Muvdi and McNabb 1984). Hence, the value of the distributed load was estimated as 236 N/m. Loads from the carriage assembly were also supported by the rail-support, which was 2.5 kN (section 4.4.2). For worst case scenario, the carriage would be located at the center of the I-beam (Fig. 4.2). The structural design was symmetrical for each side of the soil bin. Therefore, analysis was done only on one side. Based on Fig. 4.2, the vertical reaction force at A and B should be 2.7 kN. There were two vertical support members on each end of the rail-support, so each member took 1.35 kN.

The vertical support members were analyzed in terms of resistance to buckling. They were treated as a free-fixed condition, so that the effective length was twice of the actual length. The critical load of each member was calculated from eq. (4.12)

$$P_e = \frac{1}{4}\frac{\pi^2 E I_v}{L^2} \tag{4.12}$$

Where,

P_e = critical load (kN)

E = modulus of elasticity (kPa)

I_v = area moment of inertia (m^4)

L = length of the member (m)

The vertical support member was a square tubing (Appendix C, C.2). The length of the vertical support member was 0.66 m. From eq. (4.10), the critical load was 19 kN. This critical load was 14 times greater than the load imposed on the member. Hence the rail-support structure was fairly stable with this arrangement and the selected material.

4.6.2 Soil container frame

The result from structural analysis on the vertical member of the rail-support is applicable to the soil container frame, because both components have similar design

configuration to support the vertical load. But, the vertical member of the soil container frame exerted another load acting in lateral direction due to soil in the container (Fig 4.3).

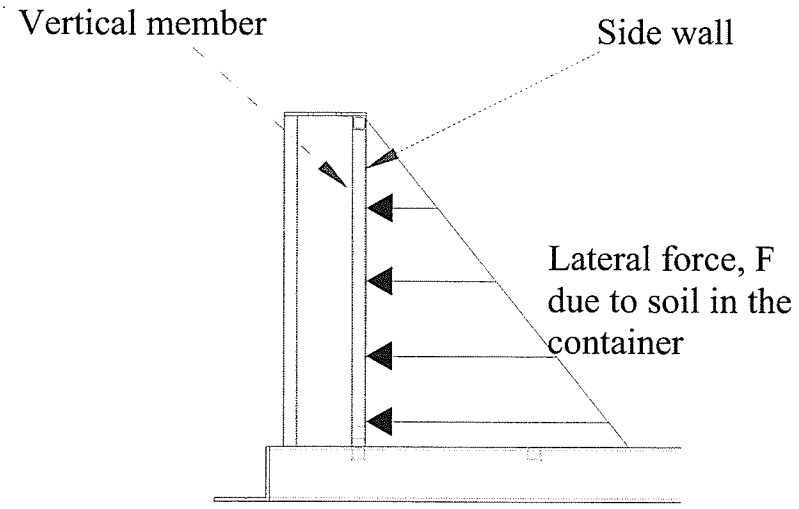

Fig. 4.3 Vertical members of the soil container frame.

There are a number of soil types, and estimating the lateral wall force based on soil types might not be possible. Therefore, only one type of soil, loamy sand, was used for the estimation of the lateral wall force. It was assumed that the Coulomb method (McKyes 1989) would be adequate to define the lateral wall force. The method is described in eq. (4.13):

$$F = \frac{1}{2}\gamma h^2 K_a - c h K_c + \frac{c^2 K_c^2}{2\gamma K_a} \qquad (4.13)$$

Where,

F = soil lateral force per unit length (kN/m)

γ = soil specific weight (kN/m^3)

h = height or depth of the wall (m)

K_a = active earth pressure coefficient (dimensionless)

K_c = active earth pressure coefficient (dimensionless)

c = soil cohesion (kPa)

The active earth pressure coefficients of K_a and K_c can be described by the eq. (4.14):

$$K_c^2 = K_a = \frac{1 - \sin \phi}{1 + \sin \phi} \tag{4.14}$$

where,

ϕ = Soil internal friction angle (^{o})

Rahman and Chen (2001) specified that a loamy sand soil type had the following parameters: $\gamma = 15.35$ kN/m^3, c = 9.23 kPa, and $\phi = 29^o$. As mentioned before, the height (depth) of the soil container wall occupied by soil was chosen as 0.61 m. According to eq. (4.14), one has $K_a = 0.347$ and $K_c = 0.589$. From eq. (4.13), the corresponding soil lateral force for this soil type was F = 0.45 kN/m. Considering a safety factor of 3 for sidewall design (McKyes 1989), the design lateral wall force per unit length was taken as 1.35 kN/m.

The effect from lateral force per unit length was checked for resistance of the vertical members against bending. A unit of soil container frame has 10 vertical members. For analysis purpose, only one vertical member was considered for worst case scenario. The maximum deflection in vertical plane was estimated based on the distributed load on a beam as:

$$v = \frac{F L^4}{30 E I_v} \tag{4.13}$$

Where,

v = deflection (m)

The maximum deflection in vertical plane due to the wall lateral force is 1.52 mm on the tip of the vertical member. If maximum allowable deflection is considered as span/360 (Erdman 1984), the maximum allowable deflection is 1.69 m. In this case, the maximum allowable deflection is greater than the maximum deflection due to soil pressure. Therefore, there should not be any problem with the vertical member design, in terms of deflection.

4.6.3 Vertical adjustment frame of the carriage

The vertical adjustment frame (Fig. 3.1) was analysed for resistance to failure in bending. The bending load is the draft of the tool acting at the mid span of the frame in horizontal direction. Considering a safety factor of 3, the bending load was equal to three times of the anticipated draft force of tool, which was 5100 N. Each side of the frame took up half of the load, so the load for the design was 2550 N. The deflection was determined based upon the superposition method as:

$$v = \frac{F_l L^3}{192 E I_v} \tag{4.14}$$

Where,

F_1 = bending load (N)

The length, L of the frame was 1.13 m. The frame was made from steel angle (Appendix C, section C.3). Based on eq. (4.14), the deflection was 0.85 mm. This is acceptable if the span/360 rule is considered, which states that the maximum allowable deflection is 3.00 mm, for this case.

4.6.4 Carriage body frame

Similar analysis was conducted on the carriage body. But, bending was checked on both vertical and horizontal directions because the carriage body frame was designed to withstand loads from both directions. The deflection was also checked againt the span/360 rule. The length of the member that supports the load was 0.99 m. Considering the system as a fixed support, the maximum bending should occur at the mid span. Based on eq. (4.14), the maximum deflection in horizontal direction was 1.24 mm, while the maximum limit based on the span/360 rule for horizontal deflection was 2.75 mm.

The effect of vertical load was considered based on the weight imposed to the body. The total vertical load was considered to determine the maximum deflection of the carriage body. Assuming the weight of the tool and the vertical adjustment frame were summed up to give a total of 2500 N. For this case, the maximum deflection in vertical

direction was 1.46 mm, while the maximum limit based on the span/360 for vertical deflection was 2.75 mm, which is acceptable for this case.

4.7 Summary

In summary, a detail design process was undertaken to ensure that the proper components were selected. Some components were fabricated in-house, while standard components were purchased. The components fabricated in-house were the soil container, carriage, rail supports, rails, motor end frame, and tensioner end frame. Purchased (standard) parts were the electric motor and other drive components. A list of complete components can be referred to Table A.1 (Appendix A).

CHAPTER 5

DESIGN FEATURE, FABRICATION, ASSEMBLY, AND SOIL BIN CONTROLS

5.1 Model development

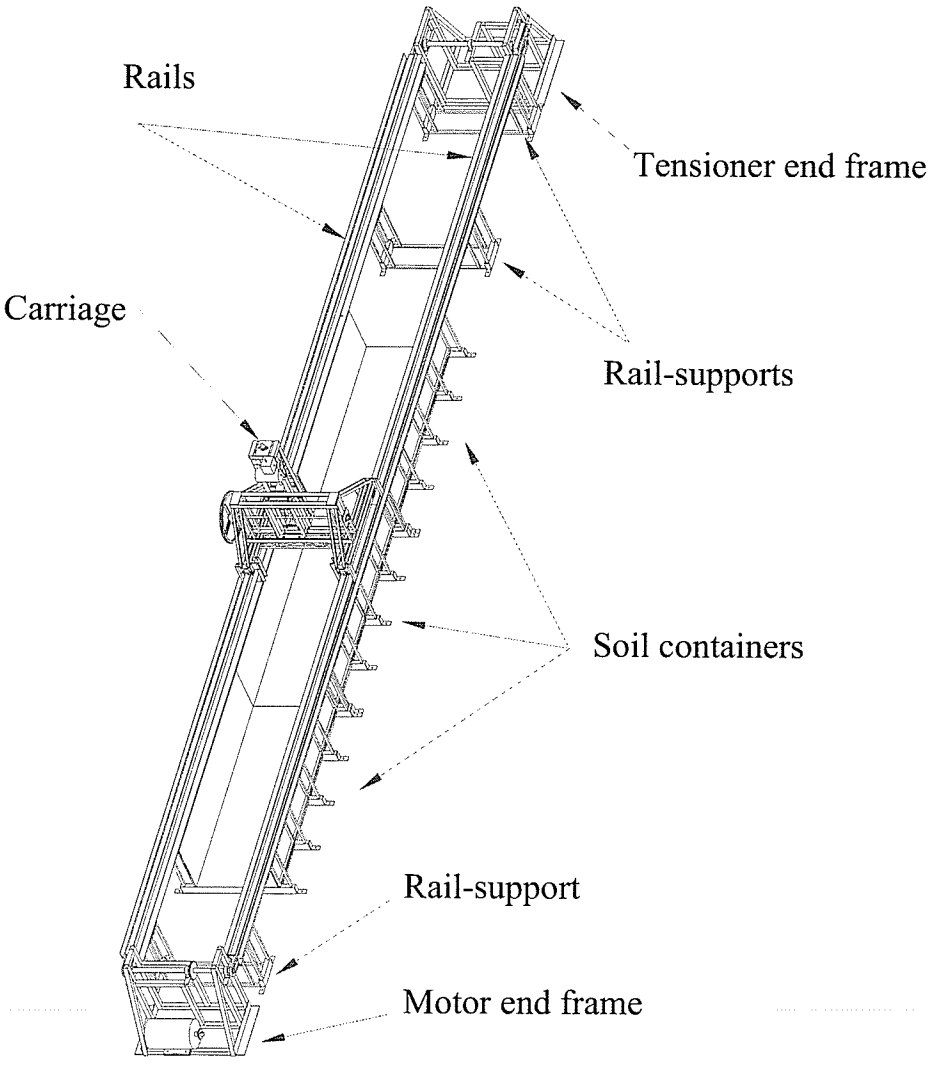

Fig. 5.1 A computer model of the soil bin

Figure 3.1 was refined into a 3-D computer model. The 3-D model was generated after the essential components (as discussed in Chapter 3) had been analyzed and important dimensions have been decided (Chapter 4). Several other factors, such as easy to manufacture and replace, and quick disassembly of components were taken into consideration. The 3-D model had undergone several iterations before a final version was decided for fabrication (Fig. 5.1). The 3-D model was originally constructed in English units. All standard parts (Table A.1), and steel materials were also in English units. Based on Fig. 5.1, detail part drawings (Appendix D) were developed and used for fabrication and assembly.

5.1.1 Soil container

Three units of soil containers were designed and incorporated into the soil bin. Each unit was 2.44 m long (Fig. 5.2), while the dimensions for inner width and depth were as specified in Chapter 4. All units were assembled in longitudinal direction to form a large section. The overall length of the large section was 7.32 m. The container was made up from two parts, a soil box and a frame. The soil box was made from plywood, while the frame was made from steel. The soil box was bolted and reinforced to the frame and bottom floor. The frame members that reinforced the soil box's sidewalls were designed to have a feature for mounting rails on top of it. The frame was bolted to the laboratory concrete floor at five mounting points on each side in longitudinal direction. The mounting points were 0.6 m apart.

During a soil-machine testing, each soil container unit can have different soil type, which makes it possible to test different soil types in test run. This feature is

convenient for experiments that involve performance comparison of a test-tool in different soil types. The soil containers occupied only the constant speed section of the rail. This feature enables quicker soil preparation as the amount of soil used for testing is optimized for the needs to collect data at the constant speed section.

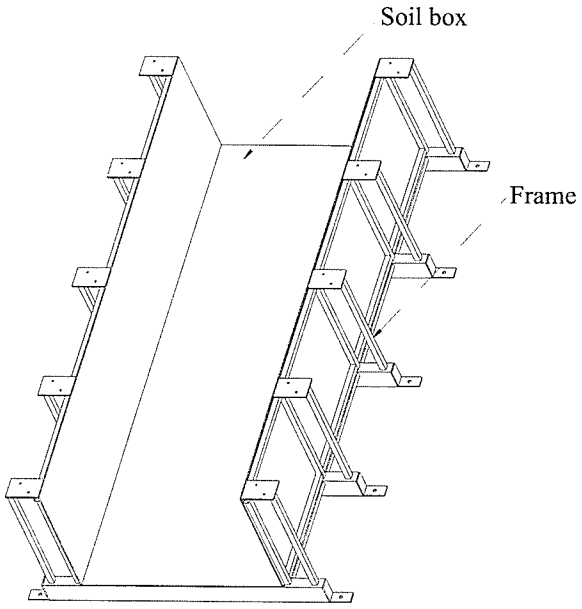

Fig. 5.2 A unit of soil container

5.1.3 Rail

Wide flange steel I-beams were used as the rail base (Fig. 5.3). Two I-beams (each I-beam was 6.1 m long) were connected end to end to form a total length of 12.2 m. The upper part of the I-beams was connected to a steel angle. The lower part of the I-beams was connected to the soil container and rail-supports. An I-beam has two channels. One channel was facing inside the soil bin. The other channel faced outside the soil bin and container chain separator. Chain B (Fig. 3.1) ran within the channel that faced outside the soil bin. A chain separator, attached to the I-beam, was used to separate

the roller chain (chain B) that ran on the upper and lower part within this channel. A chain guard, to prevent direct contact to the roller chain, was bolted to the chain separator.

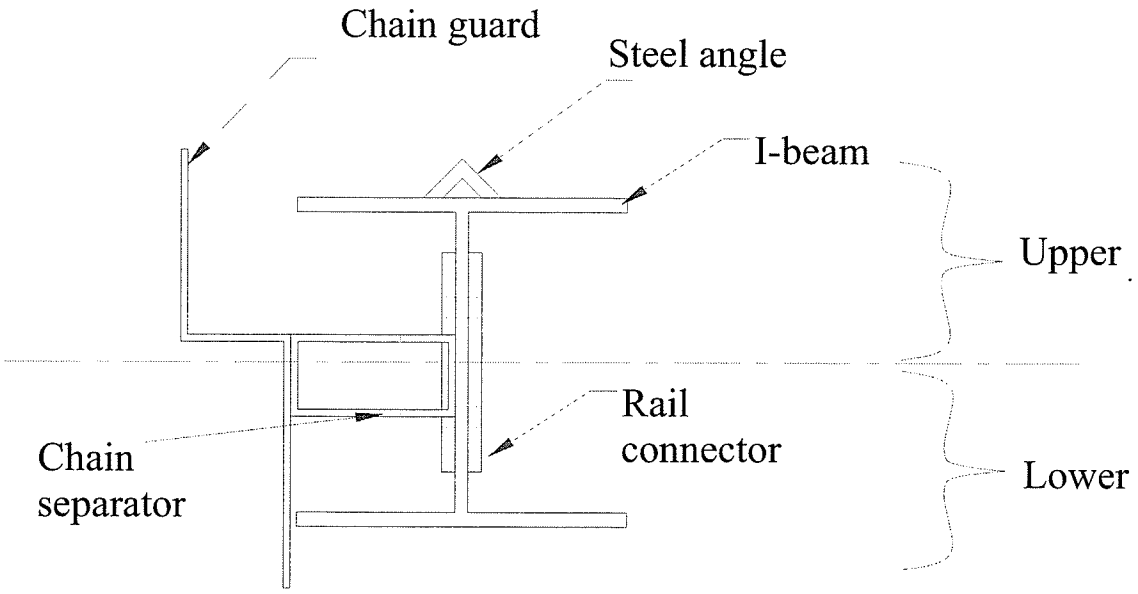

Fig. 5.3 The cross-sectional view of the rail

5.1.2 Rail-support

The soil containers supported a section of 7.32 m of the rail and the remaining section was supported by three rail-supports (Fig. 5.1). The rail-support was made from steel materials (Fig. 5.3). In assembly, all rail-supports were fixed stationary on the floor.

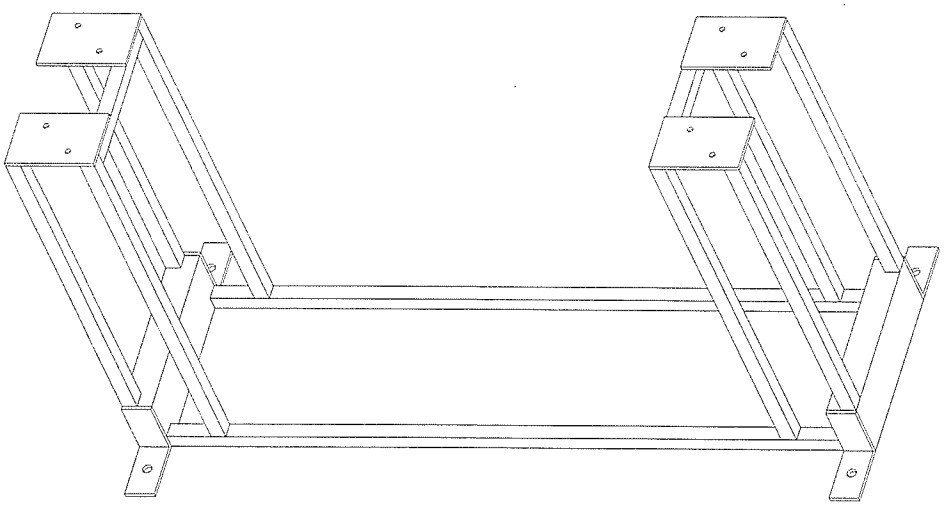

Fig. 5.4 A unit of rail-support

5.1.4 Carriage

The carriage body frame was made from steel materials (Fig. 5.5). It was supported on the rails by four rigid wheels (top rigid wheel), which were installed at four-corners at the bottom of the carriage (two wheels per side). Groovy surface rigid wheels (top rigid wheel) were used so that the carriage motion was restricted to back and forth on a straight path. Furthermore, four rigid wheels (lower wheel) with flat surface that run on the bottom surface of the upper part of the I-beam were used to compensate any net vertical force that would cause tilting. Roller chain B (Fig. 3.1) was connected to the carriage body frame.

A vertical adjustment frame was designed to allow for adjustment of test-tool position along the vertical direction. The frame consisted of an outer and an inner frames. The outer frame served as a cage, while the inner frame slided within the outer frame. The inner frame was connected to a threaded rod. Adjustment in vertical position was

achieved by turning the threaded rod clockwise or counterclockwise. The threaded rod for vertical adjustment was powered by a small electric motor. Normally, a test-tool is mounted to a dynamometer, so the vertical adjustment frame had mounting points to mount the dynamometer.

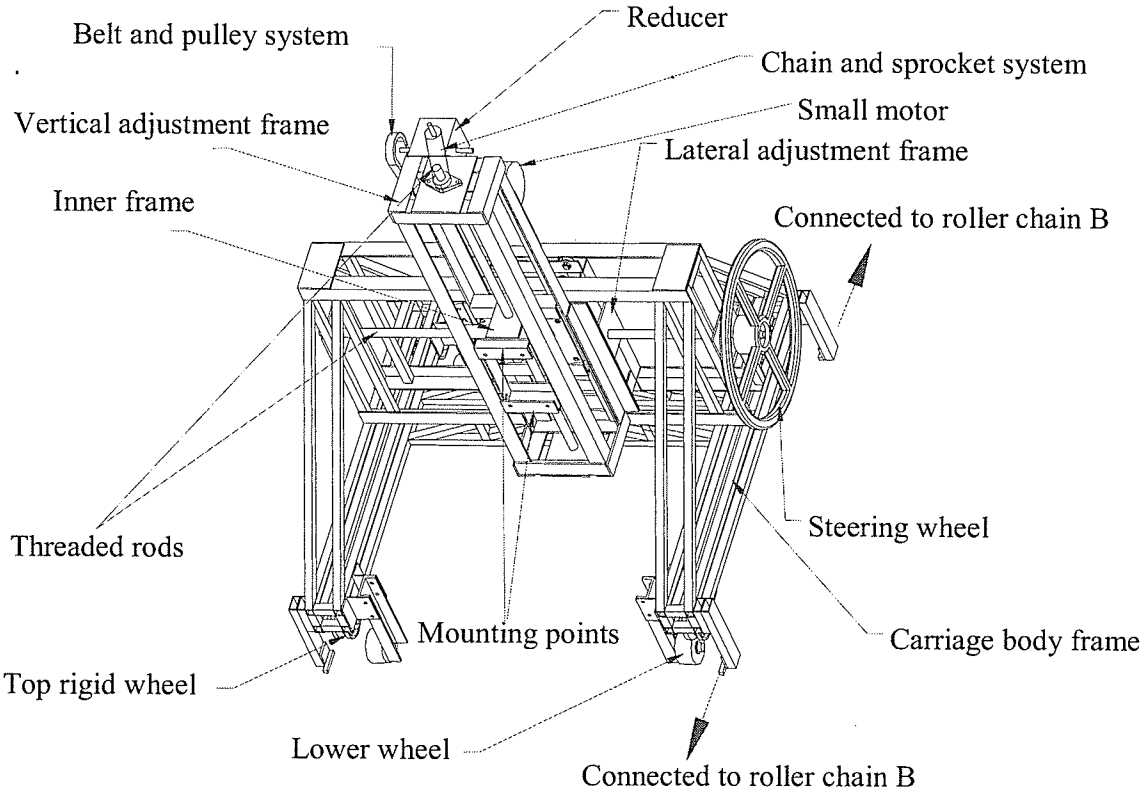

Fig 5.5. Features of the soil bin carriage

The same concept was applied for lateral position adjustment of the test-tool. But the lateral position adjustment was accomplished by manually turning a steering wheel.

The lateral adjustment frame was integrated to the carriage body frame. It slides within the body frame. The vertical adjustment frame was bolted to the lateral adjustment frame.

5.1.5 Motor end frame and tensioner end frame

A motor end frame and a tensioner end frame were designed and fabricated to hold all rotating components for the drive system to tow the carriage. The motor end frame assembly consisted of a drive shaft, pillow bearings, and carriage sprockets, drive sprockets, roller chain A, and an electric motor (Fig. 5.6). The tensioner end frame assembly consisted of a drive shaft, pillow bearings and a chain tensioner on both sides (Fig. 5.7). The frames were located at the ends of the rails and bolted to the floor.

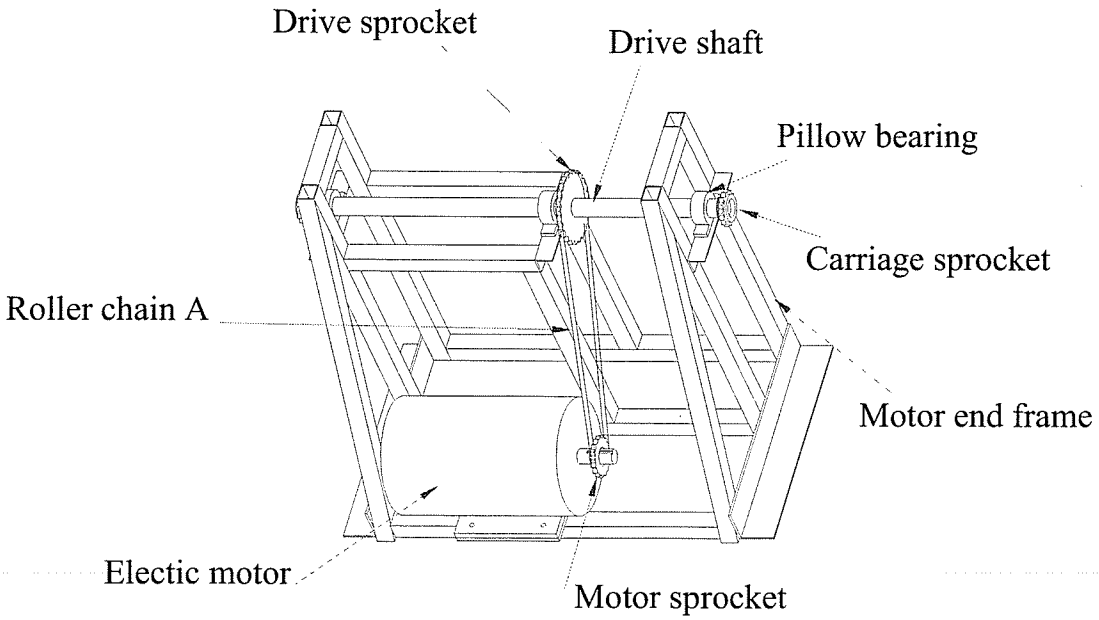

Fig. 5.6 Motor end frame assembly.

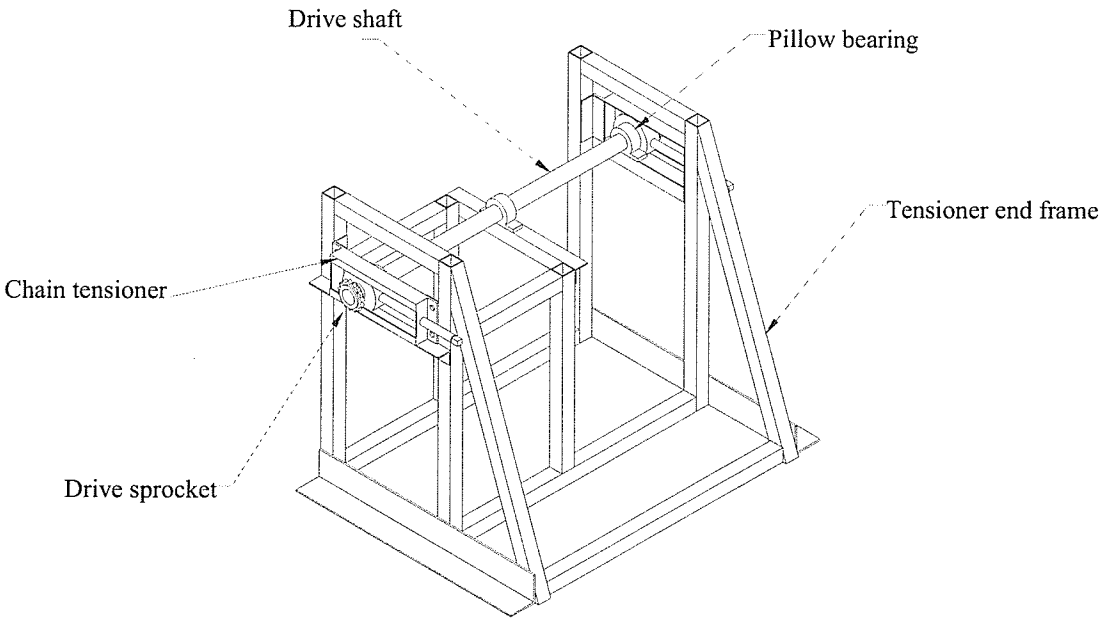

Fig. 5.7 Tensioner end frame assembly

5.2 Soil bin control

A Toshiba TEFC Premium Efficiency EQP III, A.C, 3-phase, 15 hp, and 240 V electric motor was used to tow the carriage. The motor has a maximum speed of 1725 rpm. Based on Chapter 4, the maximum speed required for testing was 531 rpm. The electric motor was equipped with a Toshiba VSD G-11 series, Variable Speed Drive (VSD) control to regulate the motor speed. The electric motor was hard wired to the VSD. The VSD was hard wired to the power supply.

The application of VSD into the soil bin test facility allowed operators to control the test speed easily. The VSD was basically a micro-computer that reads input parameters, specified by the operators. Three input parameters were required, which were the time period, t (s) to accelerate and decelerate, and the maximum intended frequency, f (Hz). The frequency, f indicated the test speed on the VSD display.

Assuming the relationship as linear, the frequency on the VSD display and the motor speed (rpm) are related by eq. (5.1).

$$f = 0.035\ N \tag{5.1}$$

Where,

f = frequency on the VSD display (Hz)

N = motor speed (rpm)

Based on eq. (5.1), if N is 0 rpm, f is 0 Hz. At the maximum motor speed of 1725 rpm, the equivalent f is 60 Hz.

The soil bin will be equipped with limit sensors and a Toshiba Dynamic Braking Resistor (DBR) unit to control the carriage motion. The limit sensors (Topwork Go Switch, non-contact sensor type) and the DBR are to be wired to the VSD controller. The sensors work by sensing the presence of any moving steel component within a distance of 10 mm. In this case, the moving steel component is the carriage. The DBR works to stops the carriage motion. There are two limit sensors. One sensor is located at the intersection of the acceleration and constant speed sections. The other one is located at the intersection of the constant speed and deceleration sections. Moller Control Switches are used to enable only one of the limit sensors to work at one time, either forward or reverse motion. Once the carriage is detected by the sensor, the VSD starts the deceleration mode and engage the DBR to stop the carriage automatically.

5.3 Safety issues

The Canadian Standards Association (CSA) Safeguarding for Machinery (Z43204) was followed for safety consideration in the design. The standard states that all rotating parts and moving parts must be guarded from direct exposure. The parts that were considered for guarding were the sprockets, drive shafts, and motor. Chain guards were installed along the outer sides of the rails to covers the moving roller chains (Fig. 5.3). Sheet metal boxes covered the drive shafts, sprockets, and motor.

5.4 Soil bin assembly

After fabrications of all components, the soil bin was installed in the laboratory (Fig. 5.8 (a), (b), (c), (d), and (e)). Three units of soil containers were assembled in the longitudinal direction and fixed to the laboratory floor. The rails were assembled to the mounting plates on top of the soil container. The free ends of the rail were supported by rail-supports. A laser aligner was used to ensure straightness in lateral and longitudinal directions. Several shim plates were inserted underneath the soil container and rail supports to the level the surface before the components were bolted to the floor. The carriage was put on top of the rails. The center of four rigid wheels was aligned to the center of the steel angle on top of the rail to ensure straightness. Roller chain B was connected to the carriage. Roller chain A was used to connect the drive shaft to the motor shaft. Chain tension was controlled by adjusting the position of the chain tensioner at the tensioner end of the soil bin.

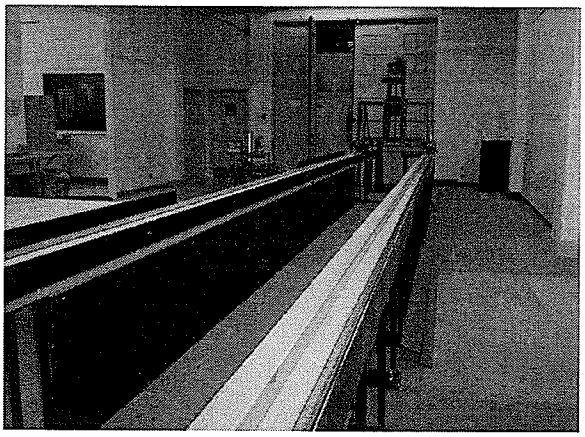

Fig. 5.8 (a) Soil bin assembly

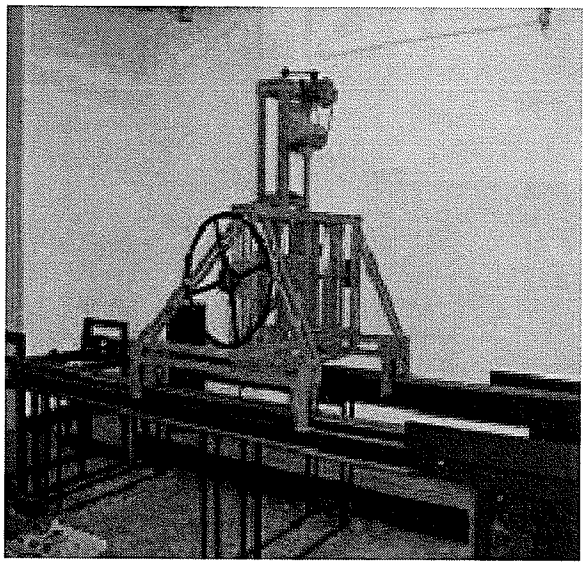

Fig. 5.8 (b) Soil bin carriage

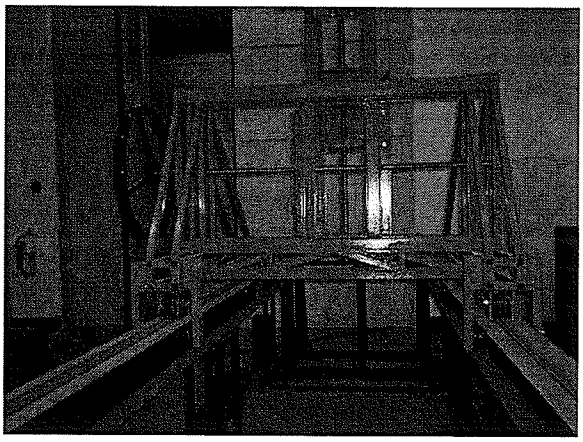

Fig. 5.8 (c) Carriage on top of the rail

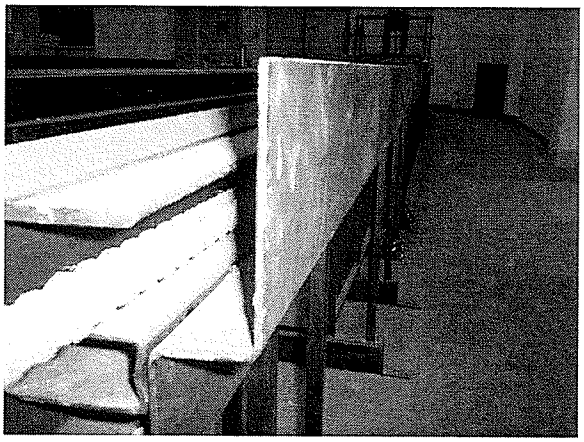

Fig. 5.8 (d) Chain B, the rail assembly, and chain guard

Fig. 5.8 (e) Chain B connection to the carriage

CHAPTER 6

CONCEPTUAL DESIGN OF A THREE-DIRECTIONAL DYNAMOMETER AND A SINGLE WHEEL TESTER

6.1 Introduction

The soil bin is a versatile test facility for soil-machine studies. One can add variety of instruments to the soil bin for any specific test objectives. One of the major interests in soil-machine studies is measuring the forces of test-tools, because those forces reflect the performance of the tools in terms of power requirement. Another major interest in soil-machine studies is measuring the traction force and the level of compaction due to wheel traffic. A dynamometer is a useful instrument to measure the forces of test-tools. Similarly, a single wheel tester is an instrument to measure forces of soil-wheel interaction.

6.2 Three-directional dynamometer

6.2.1 Motivation and intention

Normally, three forces (horizontal, vertical, and lateral) and six moments exist during a soil-tool interaction test. Among the three forces, draft force, which occurs along the horizontal axis, is the most critical force. A 3-directional dynamometer to

measure forces in all three directions is needed for the soil bin. The intention of this study was to complete a conceptual design of a 3-directional dynamometer.

6.2.2 Design criteria

The dynamometer should be able to measure forces in all the aforementioned three directions. It should minimize the undesired effects of moments. Weight of the dynamometer should not increase the load on the carriage significantly. Thus the dynamometer should be compact and lightweight.

6.2.3 Forces and moments of a test tool

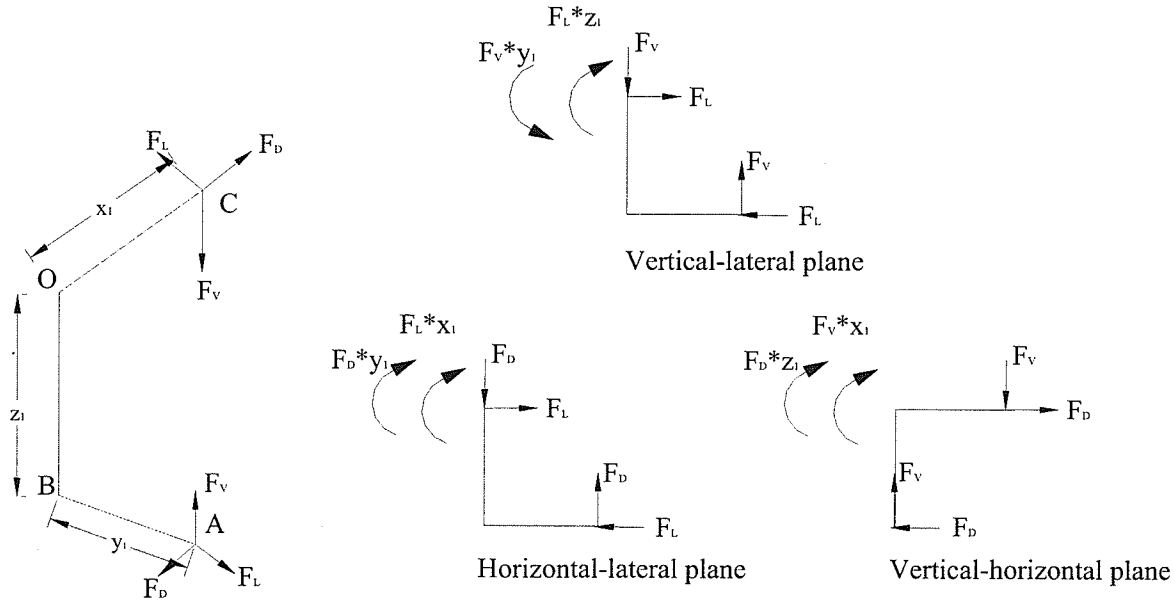

Fig. 6.1 Forces and moments of a test tool

Figure 6.1 describes the forces and moments of a test tool (Godwin et al. 1993). Point O is the origin of the coordinate system (0, 0, 0). Point A is the position of the tool tip, with a coordinate of (x_1, y_1, z_1) from the origin. Point B is an offset distance below the origin (0, 0 z_1), which represents the way a tool is mounted to an implement. Point C is the interface between the tool and the dynamometer, which is located (x_1, 0, 0) from the origin. During a test, the tool tip at point A is experiencing a draft force (F_D) that occurs along the x-axis, vertical force (F_V) along the y-axis and lateral force (F_L) along the z-axis. The forces at point A can be replaced by the equivalent forces and moments system at point C. The reaction forces are equal but in opposite direction at point C. The moments at points C are $F_V * y_1$ and $F_L * z_1$, acting along the axis of the draft force in vertical-lateral plane; $F_D * y_1$ and $F_L * x_1$ acting along the axis of the vertical force in horizontal-lateral plane; and $F_D * z_1$ and $F_V * x_1$ acting along the lateral force axis in vertical-horizontal plane.

6.2.4 Design analysis

The key to measure forces and minimize moments lies on the selection of proper load cells and the arrangement of the load cells in the dynamometer. The selected load cells are Michigan Scientific, Model TR3D-A-1, pancake type (Fig. 6.2). The cost for each load cell is US$ 2100. Each load cell can measure forces up to 4.5 kN. Assuming the maximum draft is 1700 N (Rahman and Chen 2001), the dynamometer has a safety factor of 10, which ensures measurement without damaging the load cells.

Error! Unknown switch argument.
Fig. 6.2 The three directional load cell (Michigan Scientific)

Four load cells are arranged symmetrically (Fig. 6.3). On average, each load cell should take up only a quarter of the total force (e.q. 6.1).

$$F_{D(1)} = F_{D(2)} = F_{D(3)} = F_{D(4)} = \frac{1}{4}F_D$$
$$F_{V(1)} = F_{V(2)} = F_{V(3)} = F_{V(4)} = \frac{1}{4}F_V \qquad (6.1)$$
$$F_{L(1)} = F_{L(2)} = F_{L(3)} = F_{L(4)} = \frac{1}{4}F_L$$

Where,

$F_{D(1)}$, $F_{D(2)}$, $F_{D(3)}$, and $F_{D(4)}$ = draft force at load cell 1, 2, 3, and 4 respectively (N)

$F_{V(1)}$, $F_{V(2)}$, $F_{V(3)}$, and $F_{V(4)}$ = vertical force at load cell 1, 2, 3, and 4 respectively (N)

$F_{L(1)}$, $F_{L(2)}$, $F_{L(3)}$, and $F_{L(4)}$ = lateral force at load cell 1, 2, 3, and 4 respectively (N)

Summation of all forces from all load cells gives the total values of draft, vertical and lateral forces. The moments due to the draft, vertical, and lateral forces are compensated by the load cells. The summation of moments due to location of each load is canceled by the symmetrical arrangement. Equation 6.2 describes the summation of forces and eq. (6.3) describes the summation of moments at the dynamometer.

$$
\begin{aligned}
F_D &= F_{D(1)} + F_{D(2)} + F_{D(3)} + F_{D(4)} \\
F_V &= F_{V(1)} + F_{V(2)} + F_{V(3)} + F_{V(4)} \\
F_L &= F_{L(1)} + F_{L(2)} + F_{L(3)} + F_{L(4)}
\end{aligned} \tag{6.2}
$$

$$
\begin{aligned}
&2F_{V(1)}*y_2 - 2F_{V(2)}*y_2 + 2F_{V(4)}*y_2 - 2F_{V(3)}*y_2 = 0 \\
&2F_{L(3)}*z_2 + 2F_{L(4)}*z_2 - 2F_{L(1)}*z_2 - 2F_{L(2)}*z_2 = 0 \\
&2F_{D(1)}*z_2 - 2F_{D(4)}*z_2 + 2F_{D(2)}*z_2 - 2F_{D(3)}*z_2 = 0 \\
&2F_{D(2)}*y_2 + 2F_{D(3)}*y_2 - 2F_{D(1)}*y_2 - 2F_{D(4)}*y_2 = 0
\end{aligned} \tag{6.3}
$$

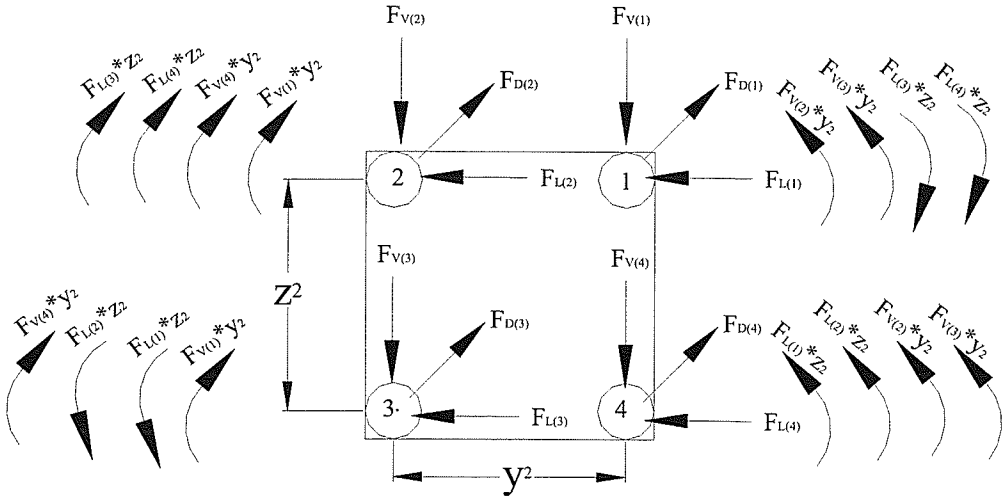

Fig. 6.3 Load cells arrangement in the dynamometer

6.2.5 Dynamometer construction

The dynamometer frame is made of two aluminum plates, sandwiching the load cells between them (Fig. 6.4). Aluminum would be a better choice of material because of the lightweight properties. One face of the plate is attached to the test tool through a tool

plate. The other face of the plate is integrated to the carriage (carriage plate). Four placement holes are bored at the four corners of each plate. Each placement hole has an opening to allow cables protruding out from the load cells and be connected to a signal conditioner. The load cells are installed exactly in those placement holes. The load cells are restrained firmly in the placement hole by bolting four M8 x 1.25 threaded holes of the load cells to the carriage plate. Each load cell has a threaded hole M12 x 1.75 facing the tool plate. This hole should be used to mount the test tool.

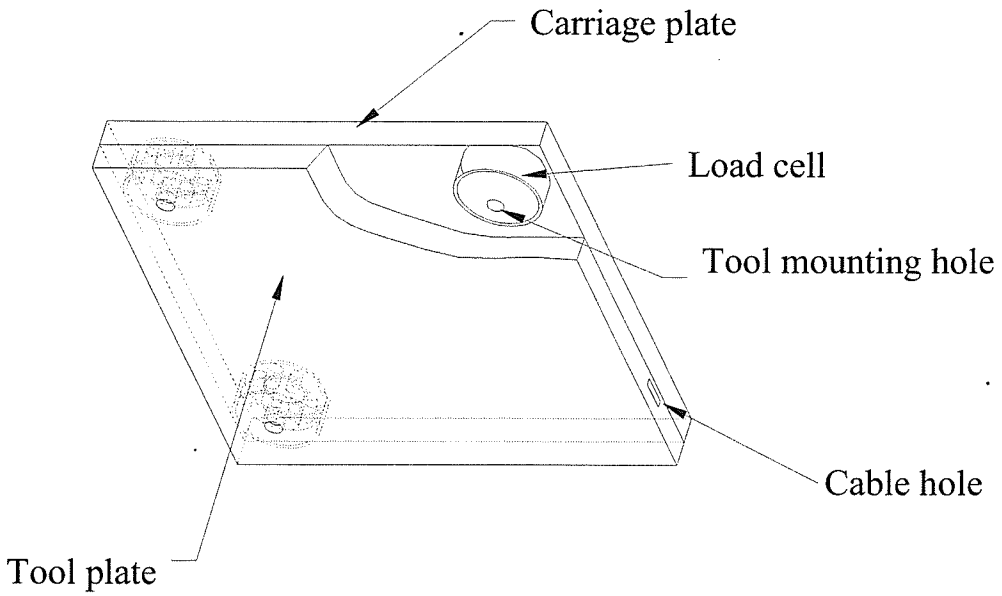

Fig. 6.4 The dynamometer frame and location of load cells

6.3 Single wheel tester

6.3.1 Motivation and intention

A wheel can be treated as either a rigid wheel or pneumatic tires. For pneumatic tires, it is better to study the effect of a pneumatic tire on soil with a single wheel tester, instead of deriving the results from other methods, such as cone index and soil triaxial test. It is because the interface of soil-tire interaction is complex. The ground contact area may be represented by different modes, such as rectangular or ellipse mode. The soil-tire interaction is also affected by vertical loading, tire inflation pressure and mechanical properties of the soil. The intention of this study was to complete a conceptual design of a simple single wheel tester for soil-tire studies in the soil bin.

6.3.2 Design criteria

The single wheel tester should fit into the soil bin. The test wheel diameter and width are dependent upon the size of the soil bin. The possible tire size can be determined by using Clark and Liljedahl (1968) method. The objective of the single wheel tester is to measure the braking torque of a tire. The braking torque can be defined as the minimum torque required to overcome the motion resistance and produced motion. Therefore, the single wheel tester can be placed stationary on the soil bin. The braking torque should be tested against various vertical load levels. Thus, the single wheel tester should have the capability to vary the vertical load.

6.3.4 Apparatus description

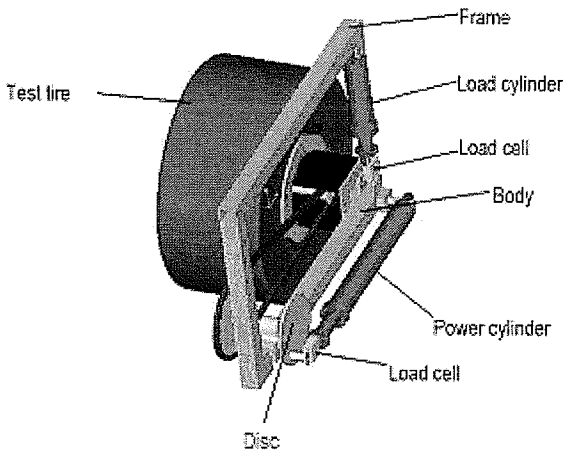

Fig. 6.5 Single wheel tester frame

The wheel tester consists of several subassemblies (Fig. 6.5). The first subassembly is the tire assembly. A test-tire is assembled to a hub. The hub is assembled to a body. A sprocket is connected to the body to receive torque and to rotate the test tire. The second subassembly is the power assembly. A power hydraulic cylinder is connected to the body at one end. The other end of the power hydraulic cylinder is assembled to a disc, which is located at the end of the body. A shaft connects the disc and a sprocket on the opposite side of the body. A chain is used to connect this sprocket to another sprocket at the test tire. This connection allows for input transmission to the test tire. The third subassembly is the vertical load assembly. A load hydraulic cylinder is connected from one end of the frame to one end of the body. The hydraulic cylinder can be set to provide various loading conditions to the test tire. A load cell is assembled between the load cylinder and the body, which measures the amount load imposed to the test tire. Another

load cell is assembled between the body and the frame, which measures the potential traction force of a given test tire on a given soil condition.

6.3.3 Design consideration and analysis

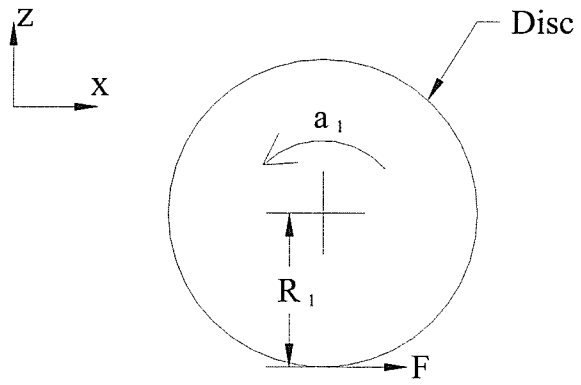

Fig. 6.6 Forces equilibrium on a disc

The single wheel tester is powered by a hydraulic cylinder, which is connected to a disc. The rotation of the disc causes rotation on a sprocket on the opposite site of the body. Fig. 6.6 describes the forces and moment on the disc. For simplicity, the design analysis is considered in two dimensional, in horizontal and vertical directions. The forces of interest in a soil-wheel analysis are the wheel loads that occurs on the vertical axis, and the traction force that acts along the horizontal direction. The force equilibrium in horizontal direction on the disc is described in eq. (6.1):

$$F_x = m\, a_x = 0 \qquad (6.1)$$

Where,

F_x = horizontal force (N)

m = mass of the disc (kg)

a_x = acceleration in horizontal direction (m/s^2)

Based on the equation, the disc does not move in horizontal direction. The force equilibrium in vertical direction is described by eq. (6.2):

$$F_z = m\, a_z = 0 \tag{6.2}$$

Where,

F_z = vertical force (N)

a_z = acceleration in vertical direction (m/s^2)

The disc also does not move in vertical direction. The moment about the center of the disc or at point O can be calculated by eq. (6.3):

$$\begin{aligned} F\, R_1 &= I\, \alpha_1 \\ &= \left[\frac{1}{2} m R_1^2\right] \alpha_1 \\ \alpha_1 &= \frac{2\, F}{m\, R_1} \end{aligned} \tag{6.3}$$

Where,

F = force supplied by the power cylinder (N)

I = mass moment of inertia of the disc (kg-m^2)

α_1 = the angular acceleration of the disc (rad/s^2)

R_1 = the distance from the center of the disc to the location of power cylinder attachment (m)

The angular acceleration α_1 is transferred to the sprocket on the other side of the body. Assuming both the sprocket besides the disc and the sprockets at the test tire are the same size, the angular acceleration should be the same for all sprockets and disc.

$$\alpha_1 = \alpha_2 = \alpha_3 \tag{6.4}$$

Where,

α_2 = the angular acceleration of the sprocket (rad/s^2)

α_3 = the angular acceleration of the sprocket at the test tire (rad/s^2)

Equations 6.1, 6.2 and 6.3 are useful to describe how the power cylinder provides power to rotate the test tire on a test soil.

Vertical load on the test tire is provided by a hydraulic cylinder. But the position of the cylinder may not be exactly at vertical position. Therefore, the geometry of the fix frame assembly is analyzed to find the correct angle of the vertical load (Fig. 6.7).

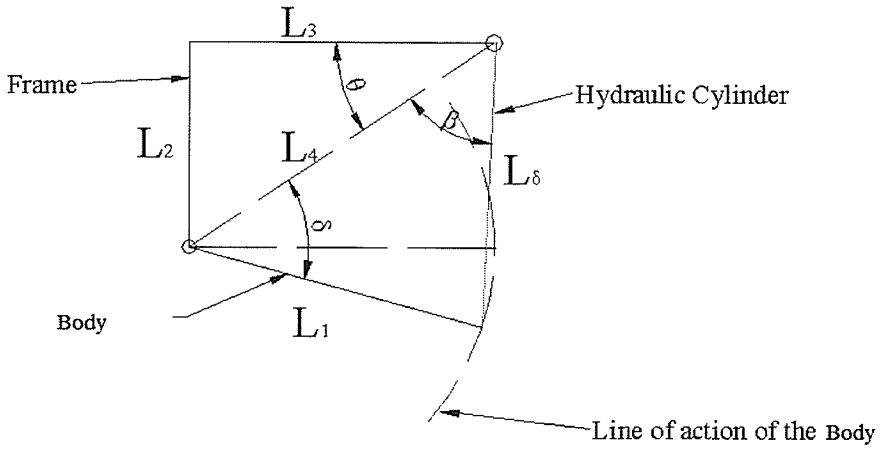

Fig. 6.7 Geometry of the test frame

The length of the load cylinder, L_δ varies along with the load setting, which is directly proportional to the load set on the hydraulic cylinder. Therefore, L_δ is measured directly from the tester. Angle δ is the angle from the body to an imaginary line L_4 from the lower corner of the frame to the upper corner of the frame, and is solvable by applying triangle rule:

$$L_4=\sqrt{L_2^2+L_3^2} \tag{6.5}$$

Where,

L_2 = the vertical length of the frame (m)

L_3 = the horizontal length of the frame (m)

If L_1 is the length of the body, which is a known value, L_δ is solved by cosine rule (eq. 6.6), which is used to determine δ:

$$L_\delta^2 = L_1^2 + L_4^2 - 2\,L_1\,L_4(\cos\delta)$$

therefore:

$$\cos\delta = \frac{L_\delta^2 - (L_1^2 + L_4^2)}{-2\,L_1\,L_4} \qquad (6.6)$$

$$\delta = \cos^{-1}\left(\frac{L_\delta^2 - (L_1^2 + L_4^2)}{-2\,L_1\,L_4}\right)$$

Then, angle β is determined by using sine's rule:

$$\frac{\sin\beta}{L_4} = \frac{\sin\delta}{L_\delta}$$

$$\beta = \sin^{-1}\left(L_4\frac{\sin\delta}{L_\delta}\right) \qquad (6.7)$$

The force interaction at the tire, which is the main interest of a soil-tire study, can be determined once the geometry of the frame in action has been determined. Figure 6.6 shows the general case of force equilibrium system in a soil-tire system. Load F_δ from the vertical hydraulic cylinder consists of a horizontal and vertical components. The components of F_δ can be determined by eq. (6.8):

$$F_{\delta x} = F_\delta\,\cos(\theta + \delta)$$
$$F_{\delta y} = F_\delta\,\sin(\theta + \delta) \qquad (6.8)$$

Therefore, the force equilibrium in horizontal direction is described eq. (6.9):

$$F_{mr} - F_{gt} - F_{\delta x} = 0 \qquad (6.9)$$

Where,

F_{mr} = soil resistance (N)

F_{gt} = gross traction force (N)

The force equilibrium in vertical direction is described in eq. (6.10):

$$F_{mr} - F_{\delta z} - W = 0 \qquad (6.10)$$

Where,

W = weight of the test tire and the frame (N)

The summation of moment about the wheel center:

$$T - F_{mr}(r_t) = I\,\alpha_3 \qquad (6.11)$$

Where,

r_t = torque radius of the wheel (m)

T = the braking torque (N-m)

In most cases, the unknown parameters are F_{mr} r_t and F_{gt}. In this design, these parameters can be determined from the single wheel tester. Based on these parameters, further tractive performance can be analyzed for a given test tire and a soil condition.

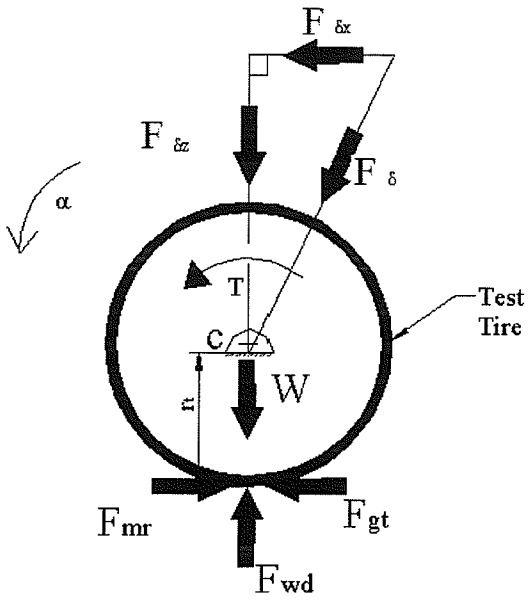

Fig. 6.6 Forces on a test-tire

CHAPTER 7

CONCLUSION

The indoor soil bin test facility developed in this study has several unique features. The soil bin has three small units of soil container for testing up to three different soil types in a test run. The combined units of soil containers were designed to occupy only the effective length section. Thus, quicker soil processing is possible. The soil bin was designed to test a soil-engaging tool at a maximum speed of 2.78 m/s, that is the common speed limit of actual operations on field. For that maximum speed, the effective length was designed for 6 m, which was adequate for collecting data for soil-machine interaction studies.

The soil bin utilizes a VSD control, which enables researchers to vary the test speed easily. The carriage was designed with adjustable mounting tool frame features. Thus, the test-tool can be adjusted in lateral and vertical directions. Safety of operation was considered based upon CSA standards. Thus, all moving and rotating parts were covered adequately to prevent injuries by direct contact.

The fundamental components were fabricated and assembled in a temporary site prior to the installation in the actual intended site. It is expected that the soil bin should be able to aid soil-machine interaction studies as long as the soil bin is operated within the specified speed.

The conceptual designs of a three-directional dynamometer and a single wheel tester were also discussed. The dynamometer is capable of measuring tool forces in all three directions. The load cells and their symmetrical arrangement in the dynamometer are capable of minimizing moments. The dynamometer is light and compact, which makes it suitable for indoor soil bin testing. The single wheel tester is a simple instrument for studying soil-tire interaction in the soil bin. The device can be used to measure the braking torque to induce motion at various vertical loads. Both the dynamometer and single wheel tester can be constructed in the future to extend the testing capability of the soil bin.

REFERENCES

Alcock, R and V. Wittig. 1992. An empirical method of predicting traction. *Journal of Terramechanics* 29 (4-5): 381-394.

Burt, E. C., C. A. Reaves, A. C. Bailey and W. D. Pickering. 1980. A machine for testing tractor tires in soil bins. *Transactions of the ASAE* 23 (3): 546-547, 552.

Cannilas, E. C and V. M. Salokhe. 2002. A decision support system for compaction assessment in agricultural soil. *Soil & Tillage Research* 65 (2): 221-230.

Carmen, K. 2002. Compaction characteristics of towed wheels on clay loam in a soil bin. *Soil & Tillage Research* 65 (1): 37-43.

Chen, Y and X. Ren. 2002. High performance tool for liquid manure injection. *Soil & Tillage Research* 67 (1): 75-83.

Chen, Y. 2002. A liquid manure injection tool adapted to different soil conditions. *Transaction of the ASAE* 45 (6): 1729-1736.

Chen, Y., N. B. McLaughlin and S. Tessier. 2005. Double extended octagonal ring (DEOR) drawbar dynamometer. CSAE Paper 05-059. Winnipeg, Manitoba, Canada. June 26-29, 2005.

Chen, Y., S. Tessier and B. Irvine. 2004. Drill and crop performance as affected by different drill configurations for no till seeding. *Soil & Tillage Research* 77 (2): 147-155.

Clark, S. J and J. B Liljendahl. 1969. Model studies of single, dual and tandem wheels. *Transactions of the ASAE* 12: 240-245.

Clark, S. J and J. B. Liljedahl. 1968. Soil bins, artificial soils and scale model testing. *Transactions of the ASAE* 11 (2): 198-202.

Durant, D. M., J. V. Perumpral and C. S. Desai. 1980. Soil bin test facility for soil-tillage tool interaction studies. *Soil & Tillage Research* 1: 289-298.

Erdman, A. G. 1984. *Mechanism Design: Analysis and Synthesis*. Prentice Hall: New York.

Gill, W. R and G. E. V. Berg. 1968. *Soil Dynamics in Tillage and Traction, Agricultural Handbook No. 316*. Washington D. C. Government Printing Office.

Godwin, R. J. 1975. An extended octagonal ring transducer for use in tillage studies. *Journal of Agricultural Engineering Research*. 20 (4): 347-352.

Godwin, R. J., G. Spoor and J. Kilgour. 1980. The design and operation of a simple low cost soil bin. *Journal of Agricultural Engineering Research* 25 (1): 57-66.

Gu, Y., R. L. Kushwaha, G. C. Zoerb. 1991. Cross sensitivity analysis of extended octagonal ring (EOR) transducer. Paper No. 91-3542. St. Joseph, MI: ASAE.

Hammer, G. L., N. Nichols and C. Mithell. 2000. *Applications of Seasonal Climate Forecasting in Agricultural and Natural Ecosystems: the Australian Experience*. Dordrecht; Boston: Kluver Academic Publishers.

Harrison, W. L. Jr. 1961. Soil bins and instrumentation for research and engineering application. SAE Paper No. 408B. Milwaukee, WI: SAE.

Hendriadi, M and V. M. Solakhe. 2002. Improvement of a power tiller cage wheel for use in swampy peat soil. *Journal of Terramechanics* 39(2): 55-70.

Hoag, D. L and R. R. Yoerger. 1975. Analysis and design of load rings. *Transactions of the ASAE* 19: 995-1000.

Jayasuria, H. P. W and V. M. Salokhe. 2003. A method for obtaining three-dimensional soil profile failure used in modeling traction tool interaction. *Biosystems Engineering* 86 (3): 363-373.

Kirisci, V., B. S. Blackmore, R. J Godwin and J. Blake. 1993. Design and calibration of three different three-point linkage dynamometers. ASAE/CSAE Paper No. 93-1009. St. Joseph, MI: ASAE.

Kiss, P. 2003. Rolling radii of a pneumatic tire on deformable soil. Biosystems Engineering 85 (2): 153-161.

Kuczewski, J and E. Piotrowska. 1998. An improved model for forces on narrow soil cutting tines. *Soil & Tillage Research* 46: 231-239.

Liu, J. 2005. *Study of Tillage Tool-Soil-Crop Residue Interaction*. Department of Biosystems Engineering, University of Manitoba, Canada.

Liu, J., D. Lobb and Y. Chen. 2002. Design features of a high-speed soil-bin to facilitate research on soil-tillage kinematics. 45th Annual Manitoba Soil Science Society Meeting. February 5-6, 2002 Winnipeg, MB, Canada.

McKyes, E. 1985. *Soil Cutting and Tillage*. Elsavier: Amsterdam.

McKyes, E. 1989. *Agricultural Engineering Soil Mechanics*. Elsavier: Amsterdam.

McLaughlin, N. B, S. Tessier and A. Guilbert. 1998. Improved double extended octagonal ring drawbar transducer for 3-D force measurement. *Canadian Agricultural Engineering*. 40: 257-264.

MMSW. 2002. Monthly Meteorological Summary for Winnipeg, Manitoba.

Muvdi, B. B and J. W. McNabb. 1984. *Engineering Mechanics of Materials 2nd edition*. Macmillan Publishing Co: NY.

Onwualu, A. P and K. C. Watts. 1989. Development of a soil bin test facility. ASAE Paper No.13 89-1106. St. Joseph, MI: ASAE.

Rahemen, H and R. Singh. 2004. Steering forces on undriven tractor wheel. *Journal of Terramechanics* 40 (3): 161-178.

Rahman, S and Y. Chen. 2001. Laboratory investigation of cutting forces and soil disturbance resulting from different manure incorporation tools in a loamy sand soil. *Soil & Tillage Research* 58 (1): 19-29.

Rahman, S., Y. Chen, K. Buckley and W. Akinremi. 2004. Slurry distribution in soil as influenced by slurry application micro-rate and injection tool type. *Biosystems Engineering* 89 (4): 495-504.

Ram, R. B and B. S. Pathak. 1978. Tractive efficiency of soil under simple traction device. *Journal of Agricultural Engineering Research* 23 (2): 141-150.

Shikanai, T., K. Hashiguchi, Y. Nohse, M. Ueno and T. Okayasu. 2000. Precise measurement of soil deformation and fluctuation in drawbar pull for steel and rubber coated rigid wheels. *Journal of Terramechanics* 37: 21-39.

Shmulevich, I., D. Ronai and D. Wolf. 1996. A new field single wheel tester. *Journal of Terramechanics* 33 (3): 133-141.

Siemens, J. C and J. A. Weber. 1964. Soil bin for model studies on tillage tools and traction devices. *Journal of Terramechanics* 1 (2): 56-67.

Sowers, G. F. 1964. Shallow foundations. Chapter 6, *Foundation Engineering*. Edited by G. A. Leonards. McGraw Hill Book Co. New York.

Stafford, J. V. 1979. A versatile high-speed soil tank for studying soil and implement interaction. *Journal of Agricultural Engineering Research* 24 (1): 57-66.

Taniguchi, T., J. T. Makanga, K. Ohtomo and T. Kishimoto. 1999. Draft and soil manipulation by a moldboard plow under different forward speed and body attachments. *Transactions of the ASAE* 42 (6): 1517-1521.

Tessier, S., A. Guilbert, N. McLaughlin and D. Tremblay. 1992. A double EOR drawbar pull transducer for 3-D force measurement. Paper No. 92-406. Winnipeg, MB: CSAE.

Upadhyaya, S. K., J. Mehlshau, D. Wulfson and J. L. Glancey. 1986. Development of a unique, mobile, single wheel traction testing machine. *Transaction of the ASAE* 29 (5): 1243-1246.

Wanji, S., T. Hiroma, Y. Ota and T. Kataoka. 1997. Prediction of wheel performance by analysis of normal and tangential stress distributions under the wheel-soil interface. *Journal of Terramechanics* 34(3): 165-186.

Watyotha, C., D. Gee-Clough and V. M. Salokhe. 2001. Effects of circumferential angle, lug spacing and slip on lug wheel forces. *Journal of Terramechanics* 38: 1-14.

Zoerb, G. C., N. G. Musonda and R. L. Kushwaha. 1983. A combined drawbar pin and force transducer. *Canadian Agricultural Engineering* 25: 157-161.

Zoz, F. M and R. D. Grisso. 2003. Traction and tractor performance. ASAE Lecture Series No. 913C0403. St. Joseph, MI: ASAE.

APPENDIX A

Table A.1 Bill of materials

Desciption	Part No.					status
soil bin assembly	sb					fabricate
soil container assembly	sb	sc				fabricate
soil container frame	sb	sc	1			fabricate
floor tubing	sb	sc	1	1		fabricate
wall tubing in	sb	sc	1	2		fabricate
wall tubing out	sb	sc	1	3		fabricate
lower wall tubing	sb	sc	1	4		fabricate
floor tubing out	sb	sc	1	5		fabricate
lower wall tubing in	sb	sc	1	6		fabricate
floor tubing in	sb	sc	1	7		fabricate
upper wall tubing	sb	sc	1	8		fabricate
rail plate	sb	sc	1	9		fabricate
floor mount	sb	sc	1	10		fabricate
soil container box	sb	sc	2			fabricate
wall	sb	sc	2	1		fabricate
floor	sb	sc	2	2		fabricate
rail assembly assembly	sb	rx				
rail base	sb	rx	1			fabricate
top rail	sb	rx	2			fabricate
connecting plate	sb	rx	3			fabricate
chain seperator	sb	rx	4			fabricate
chain guard	sb	rx	5			fabricate
rail support frame	sb	rs				fabricate
floor tubing in	sb	rs	1			fabricate
floor tubing out	sb	rs	2			fabricate
wall tubing out	sb	rs	3			fabricate
top wall tubing	sb	rs	4			fabricate
wall tubing in	sb	rs	5			fabricate
rail plate	sb	rs	6			fabricate
floor mount	sb	rs	7			fabricate
motor end frame assembly	sb	mf				fabricate

Desciption	Part No.					status
motor end frame	sb	mf	1			fabricate
floor tubing	sb	mf	1	1		fabricate
vertical tubing	sb	mf	1	2		fabricate
top tubing	sb	mf	1	3		fabricate
support	sb	mf	1	4		fabricate
base	sb	mf	1	5		fabricate
mid vertical tubing	sb	mf	1	6		fabricate
mid lateral tubing	sb	mf	1	7		fabricate
support tubing	sb	mf	1	8		fabricate
electric motor	sb	mf	2			standard
drive shaft	sb	mf	3			fabricate
drive sprocket	sb	mf	4			standard
chain # 80	sb	mf	5			standard
pillow bearing	sb	mf	6			standard
carriage sprocket	sb	mf	7			standard
motor sprocket	sb	mf	8			standard
tensioner end frame assembly	sb	tf				fabricate
tensioner end frame	sb	tf	1			fabricate
floor tubing	sb	tf	1	1		fabricate
vertical tubing	sb	tf	1	2		fabricate
top tubing	sb	tf	1	3		fabricate
bearing support	sb	tf	1	4		fabricate
bearing support	sb	tf	1	5		fabricate
vertical tubing	sb	tf	1	6		fabricate
top tubing	sb	tf	1	7		fabricate
floor mount	sb	tf	1	8		fabricate
tensioner mount	sb	tf	1	9		fabricate
support tubing	sb	tf	1	10		fabricate
drive shaft	sb	tf	2			fabricate
pillow bearing	sb	tf	3			standard
chain tensioner	sb	tf	4			standard
carriage sprocket	sb	tf	5			standard
carriage assembly	sb	cg				fabricate

Desciption	Part No.					status
carriage body frame	sb	cg	1			fabricate
center tubing	sb	cg	1	1		fabricate
center support	sb	cg	1	2		fabricate
center vertical support	sb	cg	1	3		fabricate
side frame tubing	sb	cg	1	4		fabricate
mid support tubing	sb	cg	1	5		fabricate
vertical mid support tubing	sb	cg	1	6		fabricate
angle base	sb	cg	1	7		fabricate
top plate	sb	cg	1	8		fabricate
center top tubing	sb	cg	1	9		fabricate
side rod tubing	sb	cg	1	10		fabricate
spacer	sb	cg	1	11		fabricate
chain connector	sb	cg	1	12		fabricate
small spacer	sb	cg	1	13		fabricate
chain mount	sb	cg	1	14		fabricate
side cage tubing	sb	cg	1	15		fabricate
rear support tubing	sb	cg	1	16		fabricate
front support tubing	sb	cg	1	17		fabricate
left front chain connector	sb	cg	1	18		fabricate
horizontal adj frame asm	sb	cg	2			fabricate
horizontal adj frame	sb	cg	2	1		fabricate
main cage	sb	cg	2	1	1	fabricate
top cage	sb	cg	2	1	2	fabricate
rod plate	sb	cg	2	1	3	fabricate
mid cage	sb	cg	2	1	4	fabricate
mount	sb	cg	2	1	5	fabricate
nut	sb	cg	2	1	6	standard
roller bearing assembly	sb	cg	2	2		standard
roller bearing	sb	cg	2	2	1	standard
bolt	sb	cg	2	2	2	standard
nut	sb	cg	2	2	3	standard
spacer	sb	cg	2	2	4	standard
vertical adj frame assembly	sb	cg	3			fabricate

Desciption	Part No.					status
outer frame	sb	cg	3	1		fabricate
side frame	sb	cg	3	2		fabricate
lateral side frame	sb	cg	3	3		fabricate
end tubing	sb	cg	3	4		fabricate
mount	sb	cg	3	5		fabricate
inner cage	sb	cg	3	6		fabricate
rod plate	sb	cg	3	7		fabricate
inner vertical cage	sb	cg	3	8		fabricate
inner side cage	sb	cg	3	9		fabricate
tool mount	sb	cg	3	10		fabricate
reducer plate	sb	cg	3	11		fabricate
motor plate	sb	cg	3	12		fabricate
roller bearing assembly	sb	cg	3	13		standard
roller bearing	sb	cg	3	13	1	standard
bolt	sb	cg	3	13	2	standard
nut	sb	cg	3	13	3	standard
spacer	sb	cg	3	13	4	standard
nut	sb	cg	3	14		standard
steering wheel	sb	cg	4			standard
chain and sprocket assembly	sb	cg	5			standard
dynamometer	sb	cg	6			conceptual
lower wheel assembly	sb	cg	7			standard
flat surface rigid wheel	sb	cg	7	1		standard
wheel holder	sb	cg	7	2		fabricate
bracket	sb	cg	7	3		fabricate
horizontal threaded rod	sb	cg	8			standard
vertical threaded rod	sb	cg	9			standard
reducer	sb	cg	10			standard
belt and pulley assembly	sb	cg	11			standard
electric motor	sb	cg	12			standard
chain hook bracket	sb	cg	13			fabricate
rod bearing	sb	cg	14			standard
top rigid wheel assembly	sb	cg	15			fabricate
groovy rigid wheel	sb	cg	15	1		standard

Desciption	Part No.					status
bracket	sb	cg	15	2		fabricate
chain # 60	sb	cg	16			standard

APPENDIX B

B.1 Electric motor

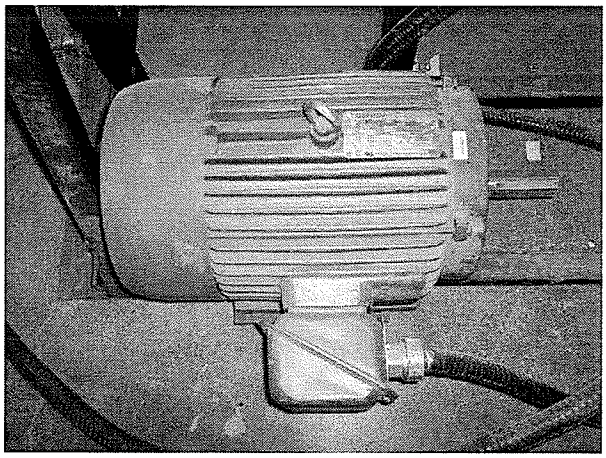

Fig. B.1 Electric motor, sb-mf-2

Part No.: sb-mf-2

Model: Toshiba EQP III TEFC Premium Efficiency 254T

Electrical: A.C, 3-phase, 240 V

Maximum speed: 1725 rpm

Power: 11.19 kW (15 hp)

Quantity: 1

B.1.1 Variable Speed Drive control

Model: Toshiba TOSVERT VF-S11

Electrical: A.C, 3-phase, 240 V

Power: 11.19 kW (15 hp)

Quantity: 1

B.2 Drive sprocket

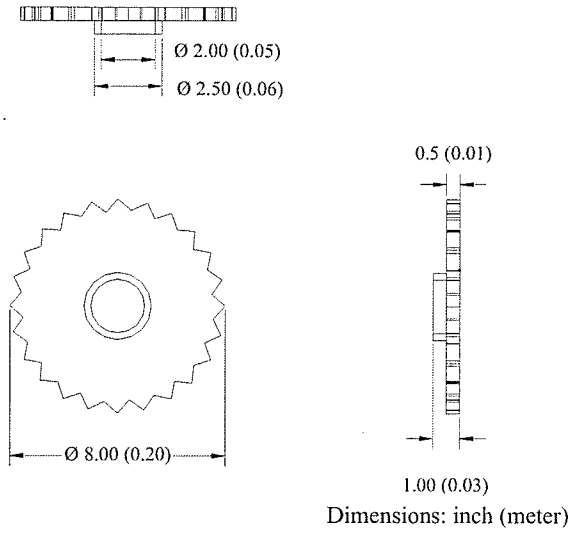

Fig. B.2 Major dimensions of the drive sprocket

Part No.: sb-mf-4

Number of teeth: 24

Quantity: 1

Mass moment of inertia for one unit:

Apply eq (4.7)

Density, $\rho = 7850$ kg/m^3.

$$J=\frac{\pi}{2}(0.01)(7850)\left[(\frac{0.20}{2})^4-(\frac{0.05}{2})^4\right]$$
$$+\frac{\pi}{2}(0.02)(7850)\left[(\frac{0.06}{2})^4-(\frac{0.05}{2})^4\right]$$
$$=\underline{1.23 \times 10^{-2}}\ \text{kg-m}^2$$

B.3 Chain # A

Part No.: sb-mf-5

Chain type = Roller chain, ASA# 80.

# of strand = single strand.

Mass per unit length = 2.607 kg/m.

Chain length = 0.610 m.

Total mass = 1.59 kg.

Quantity = 1.

B.4 Pillow bearing

Part No.: sb-mf-6 and sb-tf-3

Bore size: 2 in (0.05 m)

Quantity: 6

B.5 Carriage sprocket

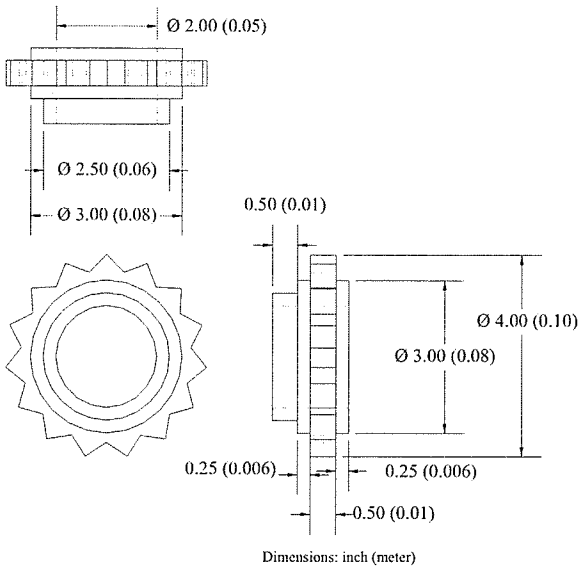

Fig. B.3 Major dimensions of the carriage sprocket

Part No.: sb-mf-7 and sb-tf-5

Number of teeth: 15

Quantity: 4

Mass moment of inertia for one unit:

Apply eq (4.7)

Density, $\rho = 7850\ kg/m^3$.

$$J=\frac{\pi}{2}(0.006)(7850)\left[(\frac{0.08}{2})^4-(\frac{0.05}{2})^4\right]$$
$$+\frac{\pi}{2}(0.01)(7850)\left[(\frac{0.10}{2})^4-(\frac{0.05}{2})^4\right]$$
$$+\frac{\pi}{2}(0.006)(7850)\left[(\frac{0.08}{2})^4-(\frac{0.05}{2})^4\right]$$
$$+\frac{\pi}{2}(0.01)(7850)\left[(\frac{0.06}{2})^4-(\frac{0.05}{2})^4\right]$$
$$= 1.10 \times 10^{-3} \text{ kg-m}^2$$

Mass moment of inertial for four units:

$$J = \underline{4.40 \times 10^{-3} \text{ kg-m}^2}.$$

B.6 Motor sprocket

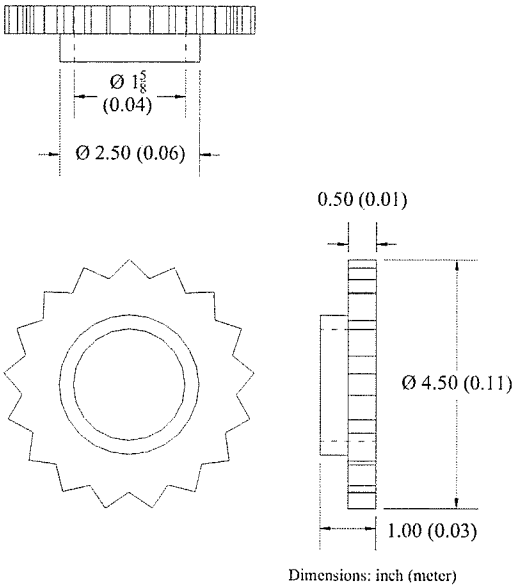

Fig. B.4 Major dimensions of the motor sprocket

Part No.: sb-mf-8

Number of teeth: 17

Quantity: 1

Mass moment of inertia for one unit:

Apply eq (4.7)

Density, $\rho = 7850$ kg/m^3.

$$J=\frac{\pi}{2}(0.01)(7850)\left[(\frac{0.11}{2})^4-(\frac{0.04}{2})^4\right]$$
$$+\frac{\pi}{2}(0.02)(7850)\left[(\frac{0.06}{2})^4-(\frac{0.04}{2})^4\right]$$
$$=\underline{1.27 \times 10^{-3}}\ \text{kg-m}^2$$

B.7 Chain tensioner

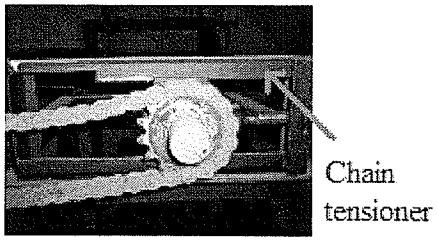

Fig. B.5 Chain tensioner, sb-tf-4

Part No.: sb-tf-4

Quantity: 2

B.8 Nut for threaded rod

Part No.: sb-cg-2-1-6 and sb-cg-3-14

Inner thread diameter: 1.0 in (0.025 m)

Note: the nut for threaded rod should match with a threaded rod with 5 threads/in.

Quantity: 2

B.9 Roller bearing

Part No.: sb-cg-2-2-1 and sb-cg-3-13-1

Inner bore: 5/8 in.

Quantity: 32

B.10 Bolt, nut and spacer for roller bearing

Part No.: sb-cg-2-2-2 and sb-cg-3-13-2 (bolt)

Thread diameter: 5/8 in

Quantity: 32

Part No.: sb-cg-2-2-3 and sb-cg-3-13-3 (nut)

Inner thread diameter: 5/8 in

Quantity: 32

Part No.: sb-cg-2-2-4 and sb-cg-3-13-4 (spacer)

Inner diameter: 5/8 in

Quantity: 64

B.11 Streering wheel

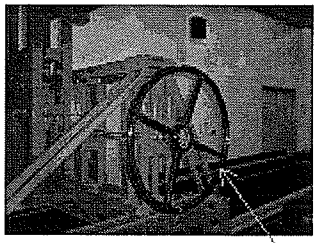

Fig. B.6 Steering wheel to adjust tool position in lateral direction

Part No.: sb-cg-4

Quantity: 1

B.12 Flat surface rigid wheel

Part No.: sb-cg-7

Wheel diameter: 3 in (0.0762 m)

Wheel width: 2 in (0.05 m)

Quantity: 4

B.13 Threaded rod

Part No.: sb-cg-8 (horizontal)

Length: 50 in (1.3 m)

Thread diameter: 1 in (0.0254 m)

Note: 5 threads/in

Quantity: 1

Part No.: sb-cg-9 (vertical)

Length: 60 in (1.5 m)

Thread diameter: 1 in (0.0254 m)

Note: 5 threads/in

Quantity: 1

B.14 Reducer and small electric motor

Part No.: sb-cg-10 (reducer)

Reduction ratio: 60:1

Quantity: 1

Part No.: sb-cg-12 (small motor)

Power: 1/10 hp

Electrical: Single phase, 240 V

Speed: 1725 rpm

Quantity: 1

B.15 Flange bearing

Part No.: sb-cg-14

Inner bore: 0.5 in (0.0127 m)

Quantity: 4

B.16 Groovy rigid wheel

Part No.: sb-cg-15-1

Diameter: 4 in (0.10 m)

Width: 2.5 in (0.06 m)

Quantity: 4

B.17 Chain # B

Part No.: sb-cg-16

Chain type = Roller chain, ASA# 60.

# of strand = single strand.

Mass per unit length = 1.624 kg/m.

Chain length = 24.40 m.

Total mass = 39.62 kg.

Quantity = 2.

APPENDIX C

C.1 Drive shaft

Part No.: sb-mf-3 and sb-tf-2

Quantity: 2

Mass moment of inertia for one unit:

Apply eq. (4.6)

$$J=\frac{\pi}{2}\ (1.26)\ (7850)\ (\frac{0.05}{2})^4 = 6.07 \times 10^{-3}\ \text{kg-m}^2$$

Mass moment of inertia for two units:

$$J = \underline{1.82 \times 10^{-2}}\ \text{kg-m}^2.$$

C.2 Square tubing

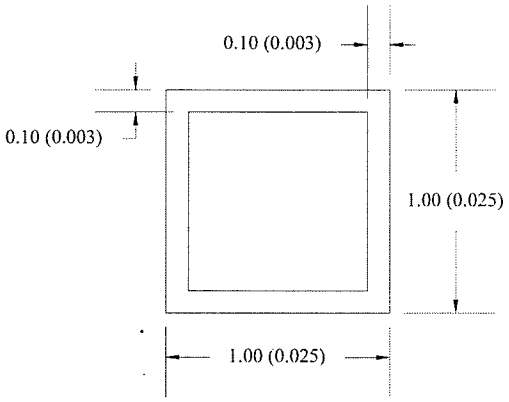

Dimensions: inch (meter)

Fig. C.1 Cross sectional dimensions of a square steel tubing

Material: Steel ASTM 36

$E = 200 \times 10^6$ kPa

Density, $\rho = 7850$ kg/m^3

Cross sectional area, $A_c = 2.32 \times 10^{-4}$ m^2

Area moment of inertia, $I_v = 2.05 \times 10^{-8}$ m^4

C.3 Steel angle

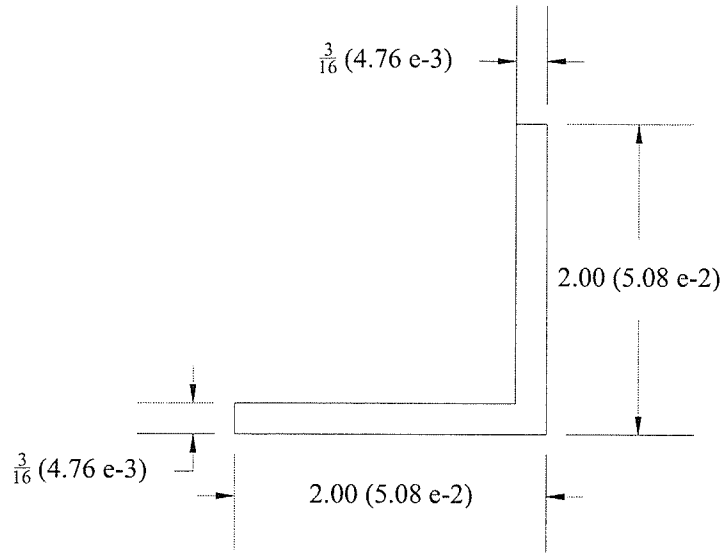

Dimensions: inch (meter)

Fig. C.2 Cross sectional dimensions of a steel angle

Material: Steel ASTM 36

$E = 200 \times 10^6$ kPa

Density, $\rho = 7850$ kg/m^3

Cross sectional area, $A_c = 4.61 \times 10^{-4}$ m^2

Area moment of inertia, $I_v = 1.13 \times 10^{-7}$ m^4

APPENDIX D

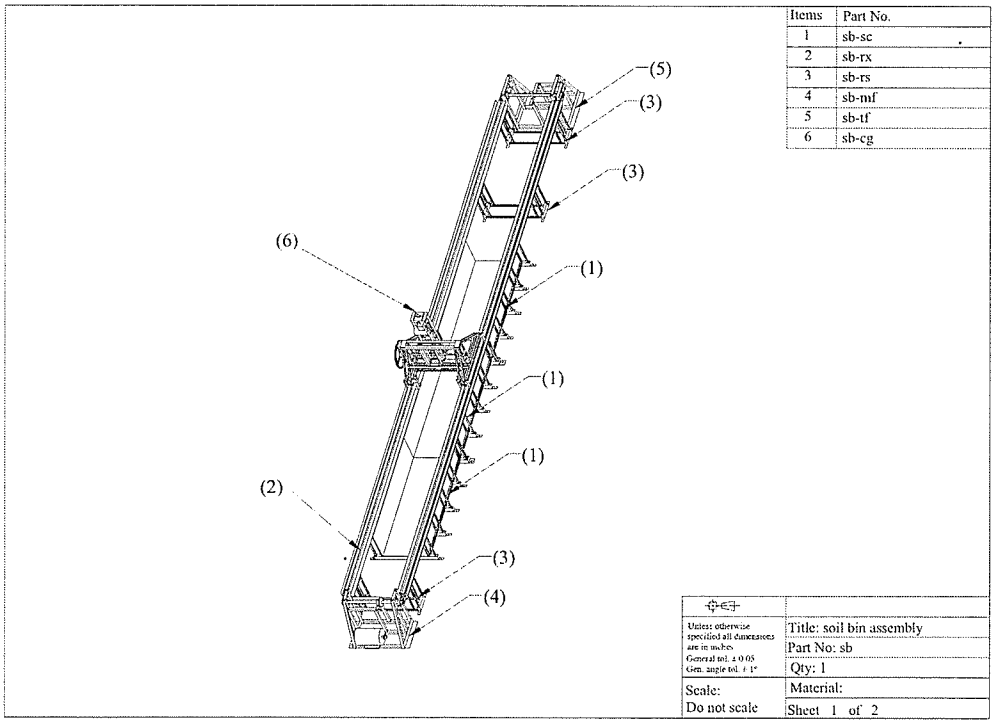

Fig. D. 1 Soil bin assembly components

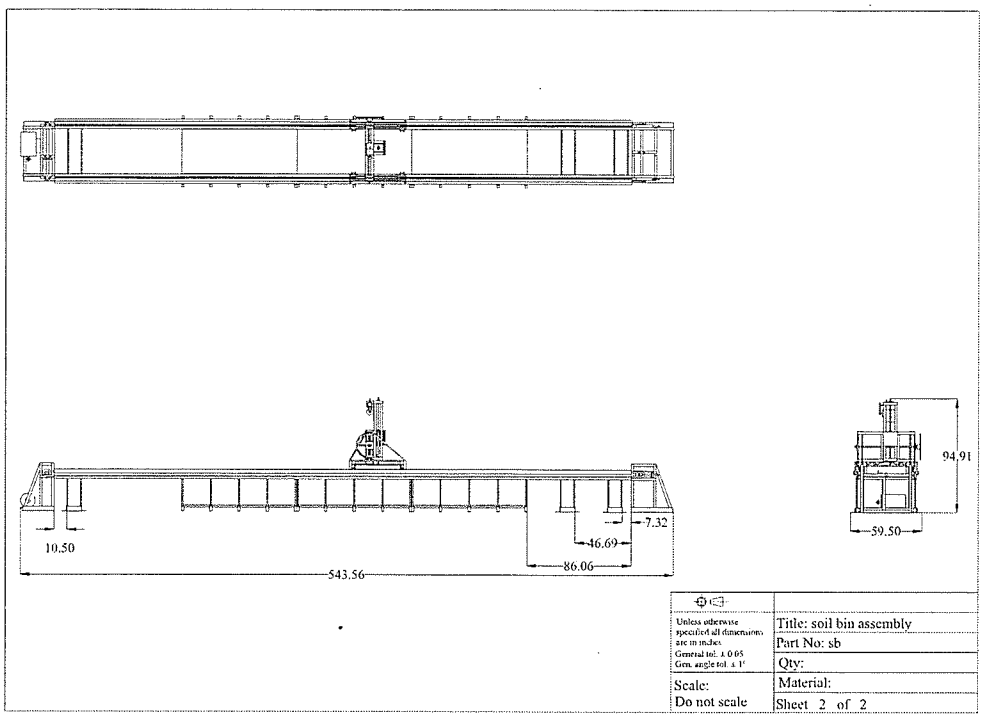

Fig. D. 2 Soil bin assembly dimensions

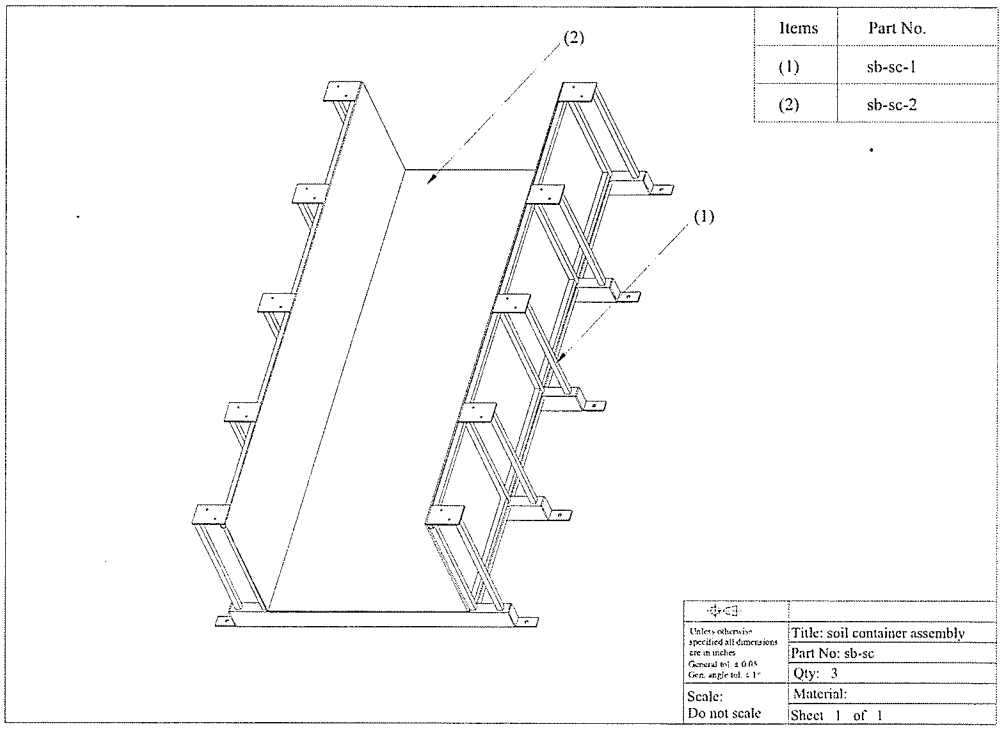

Fig. D. 3 Soil container assembly components

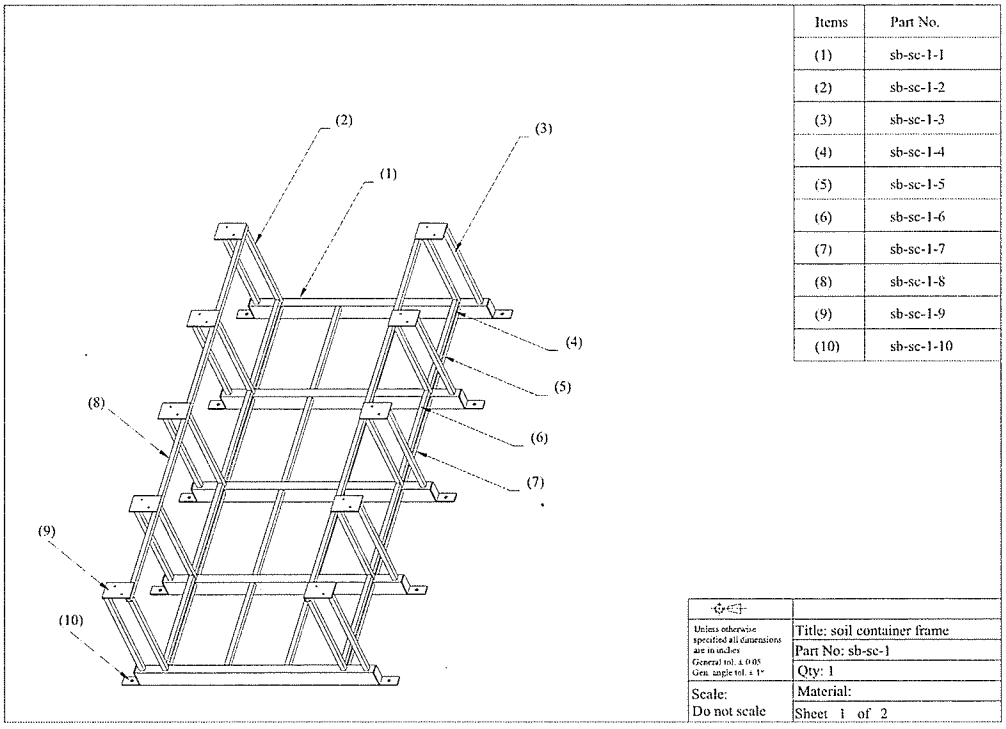

Fig. D. 4 Soil container frame members

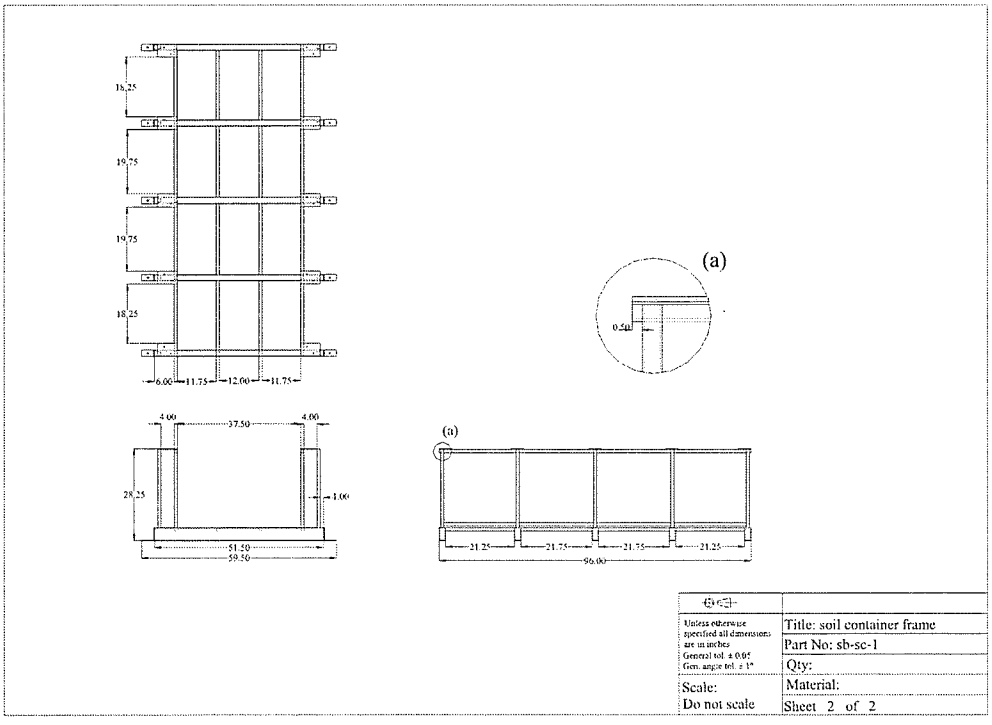

Fig. D. 5 Soil container frame dimensions

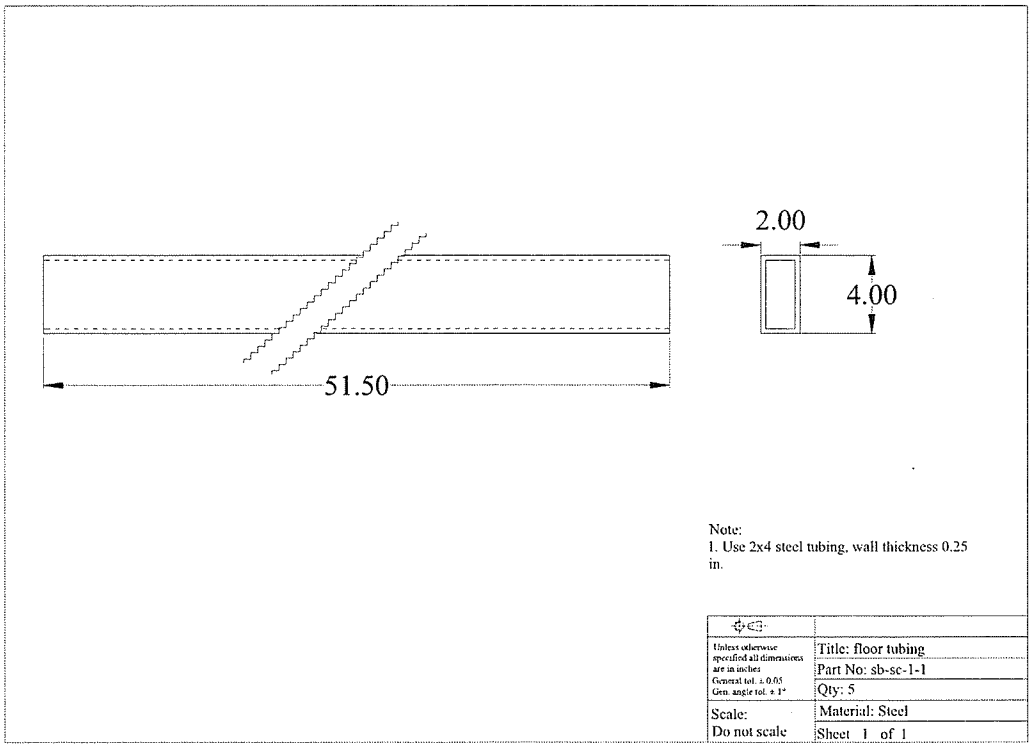

Fig. D. 6 Detail dimensions, sb-sc-1-1

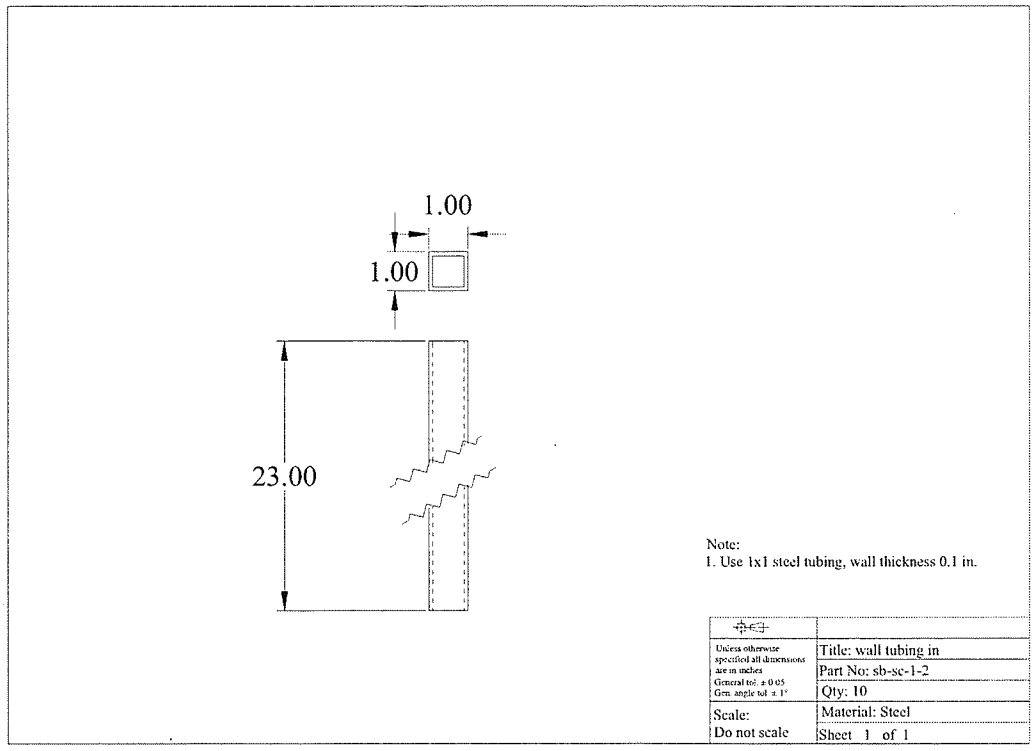

Fig. D. 7 Detail dimensions, sb-sc-1-2

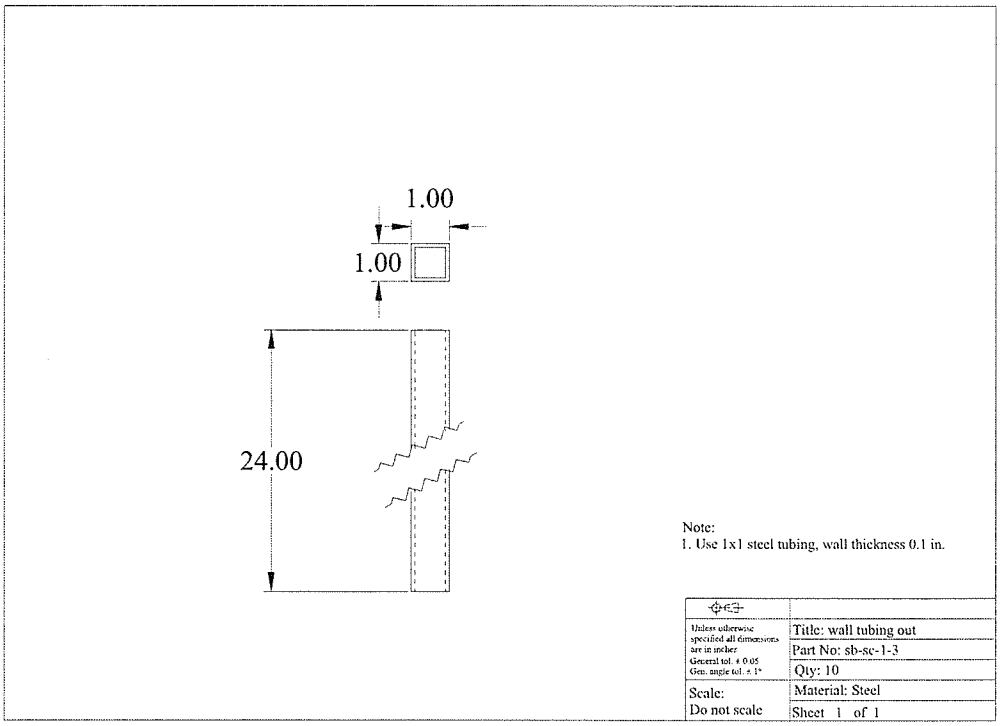

Fig. D. 8 Detail dimensions, sb-1-3

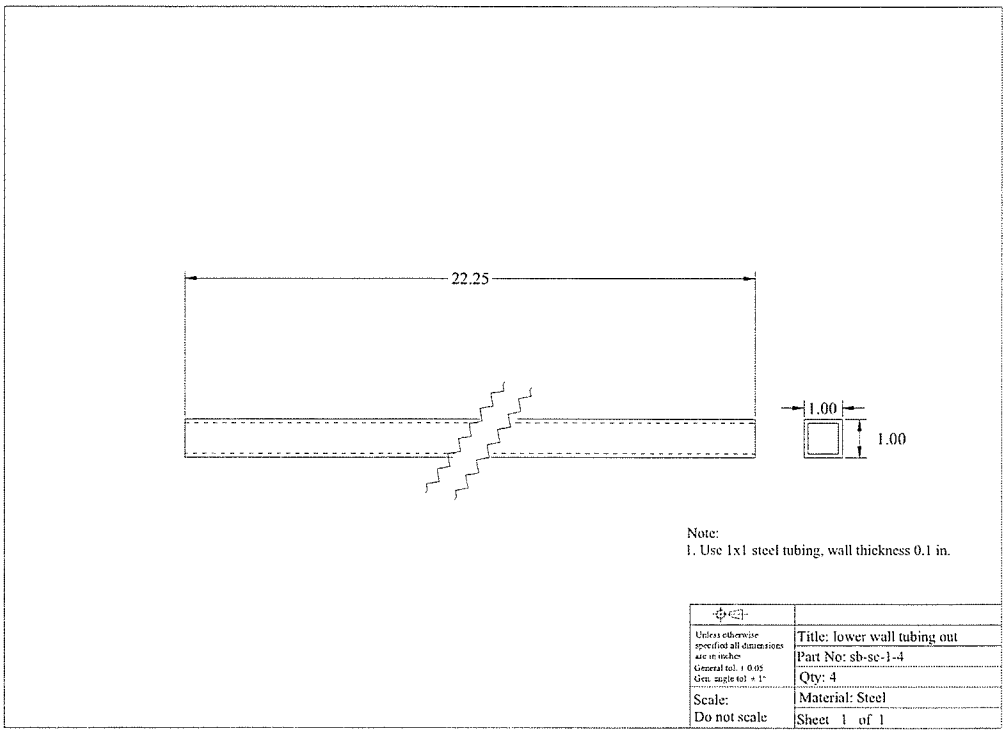

Fig. D. 9 Detail dimensions, sb-sc-1-4

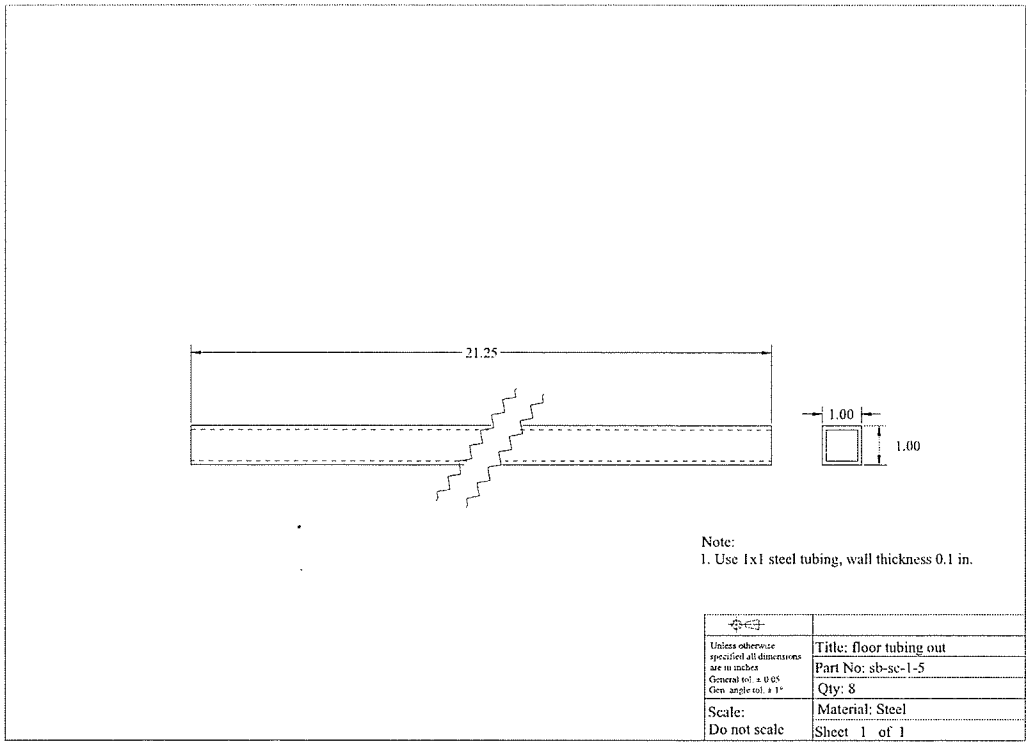

Fig. D. 10 Detail dimensions, sb-sc-1-5

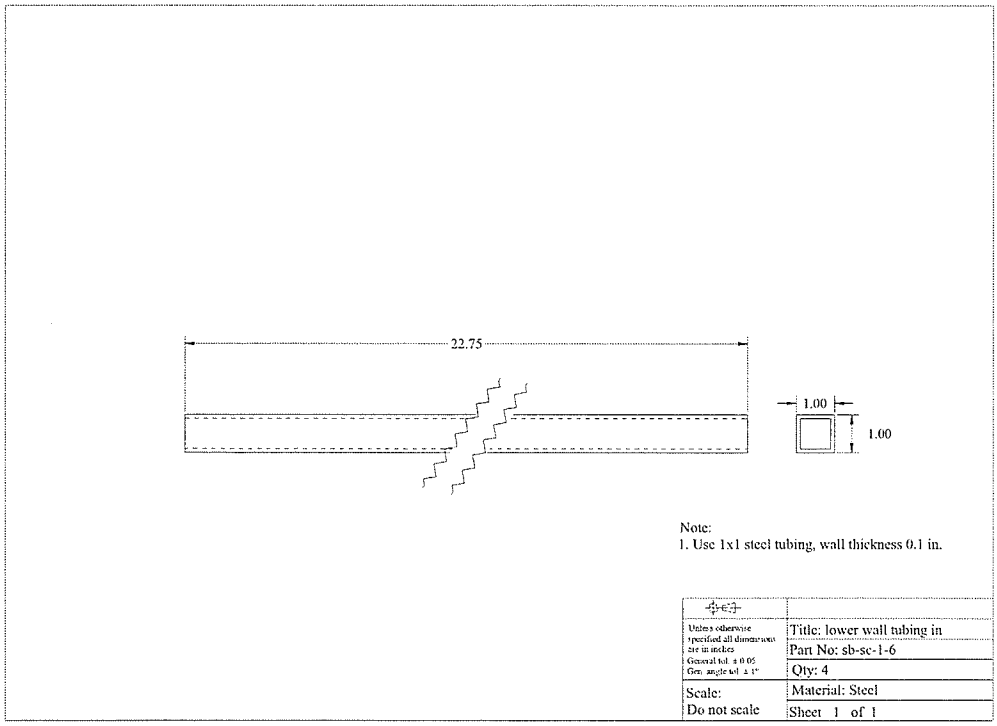

Fig. D. 11 Detail dimensions, sb-sc-1-6

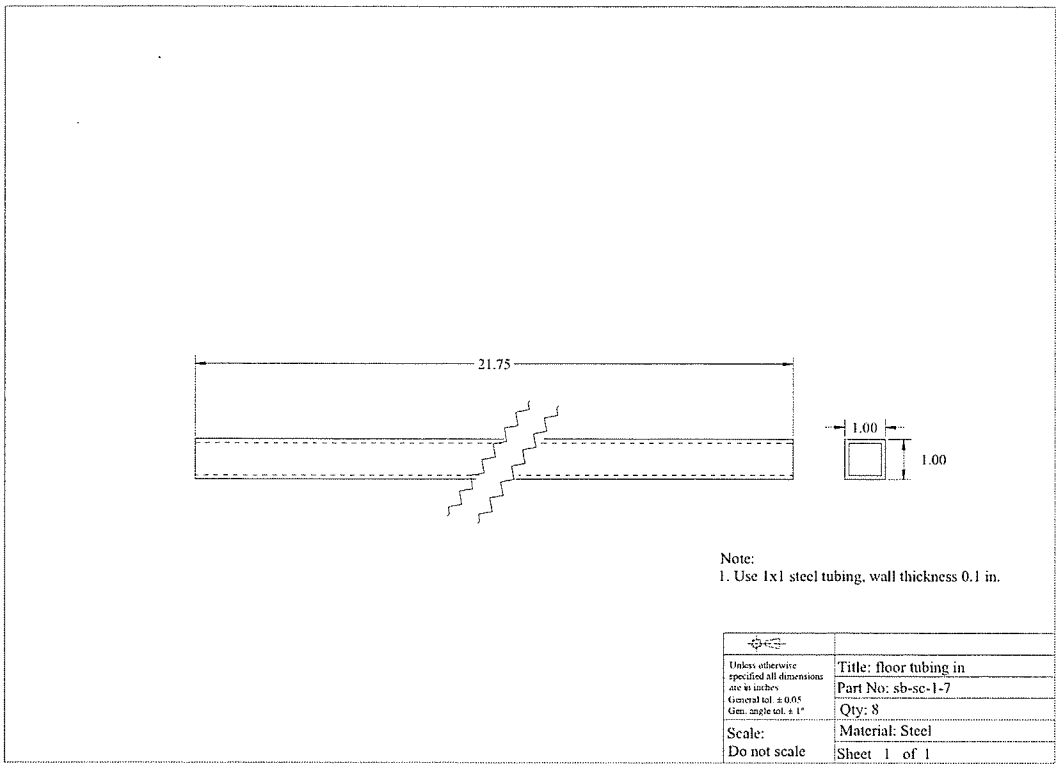

Fig. D. 12 Detail dimensions, sb-sc-1-7

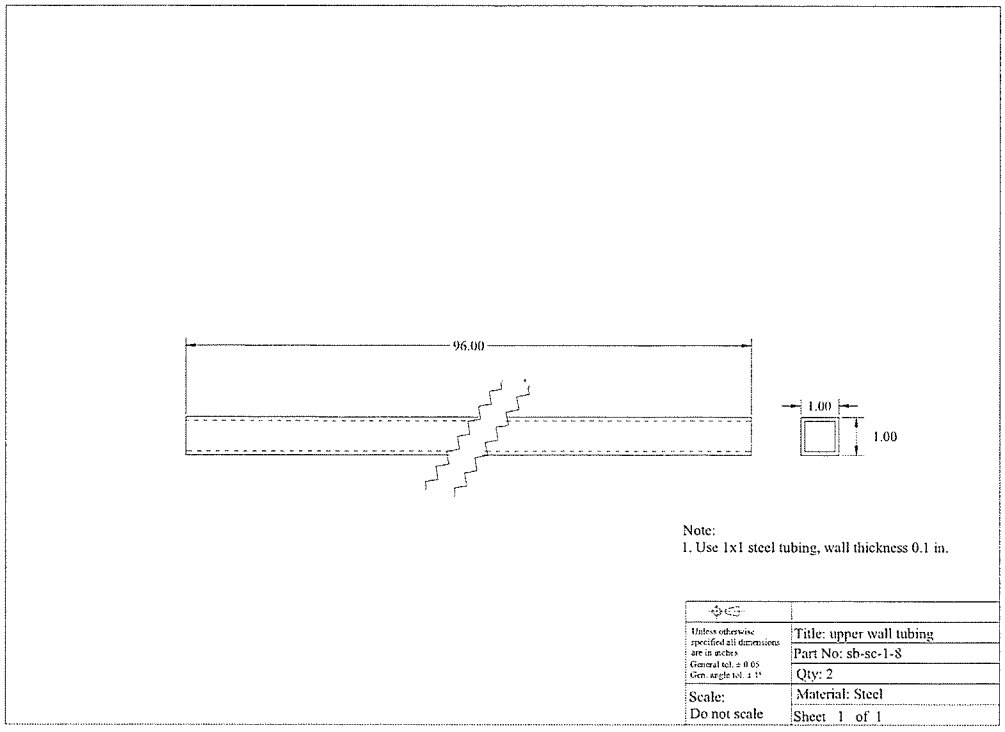

Fig. D. 13 Detail dimensions, sb-sc-1-8

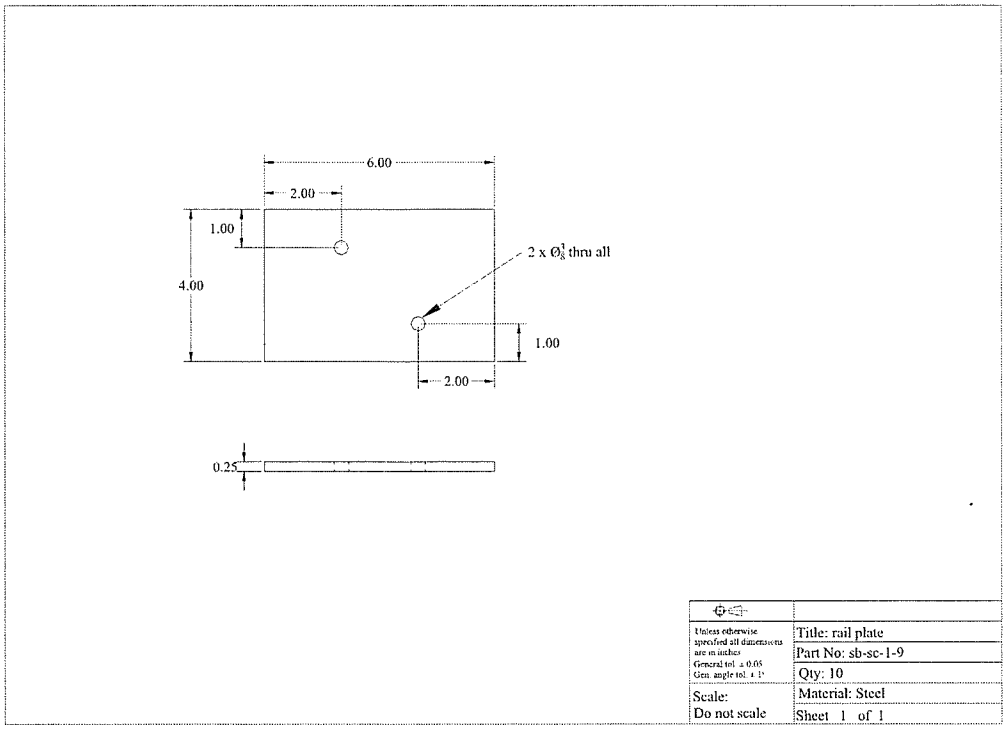

Fig. D. 14 Detail dimensions, sb-sc-1-9

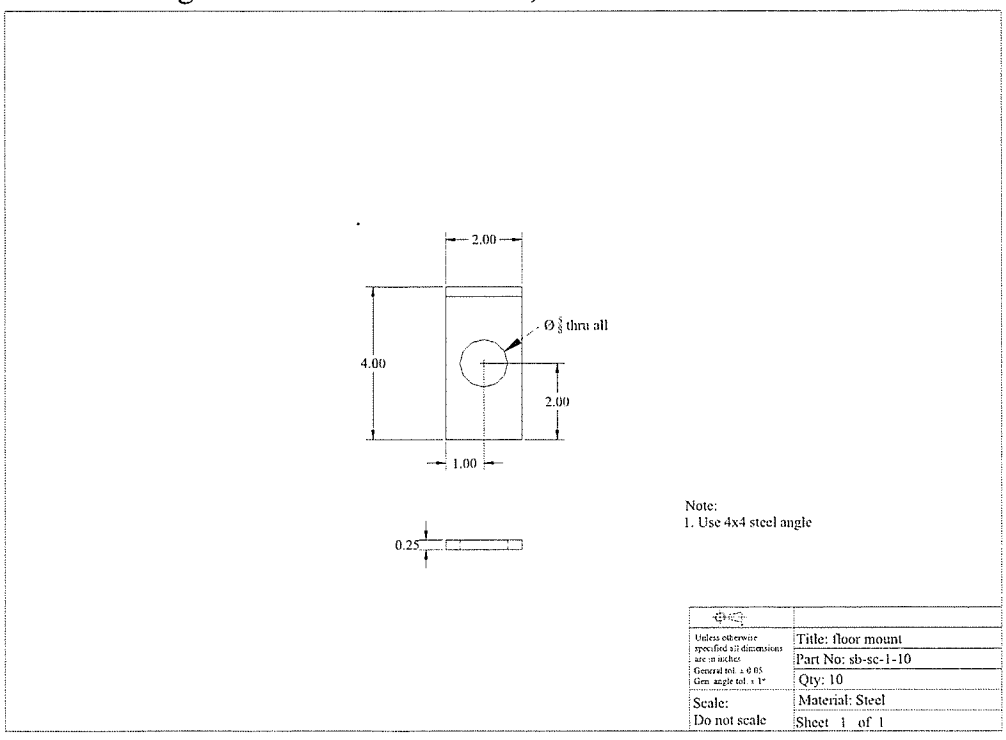

Fig. D. 15 Detail dimensions, sb-sc-1-10

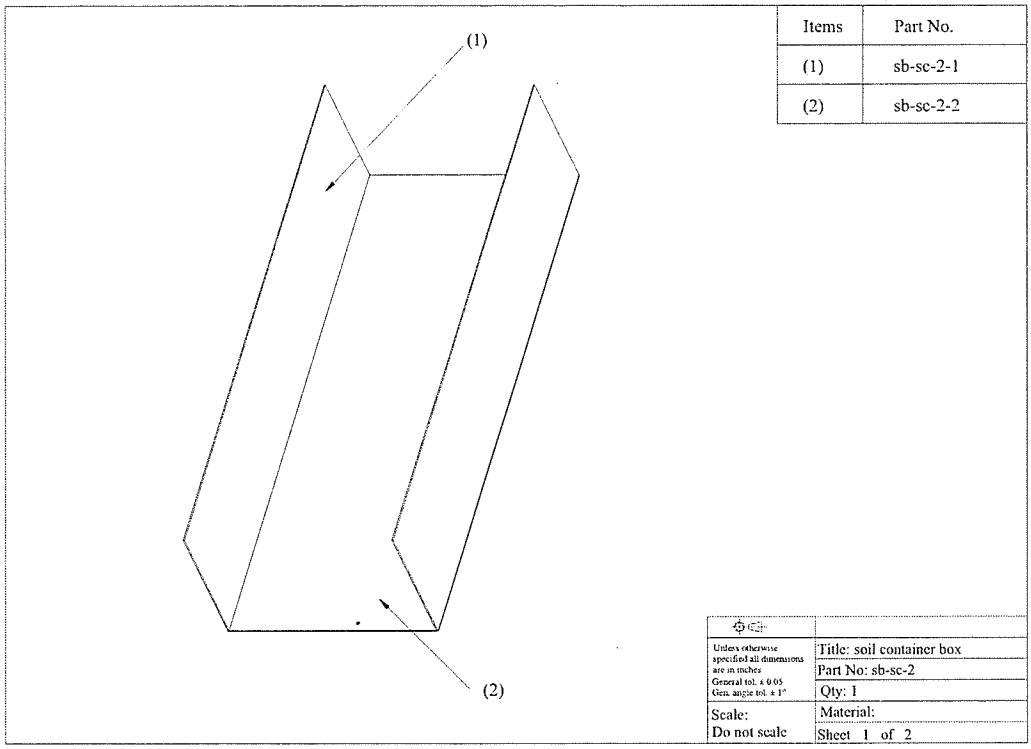

Fig. D. 16 Soil container box members

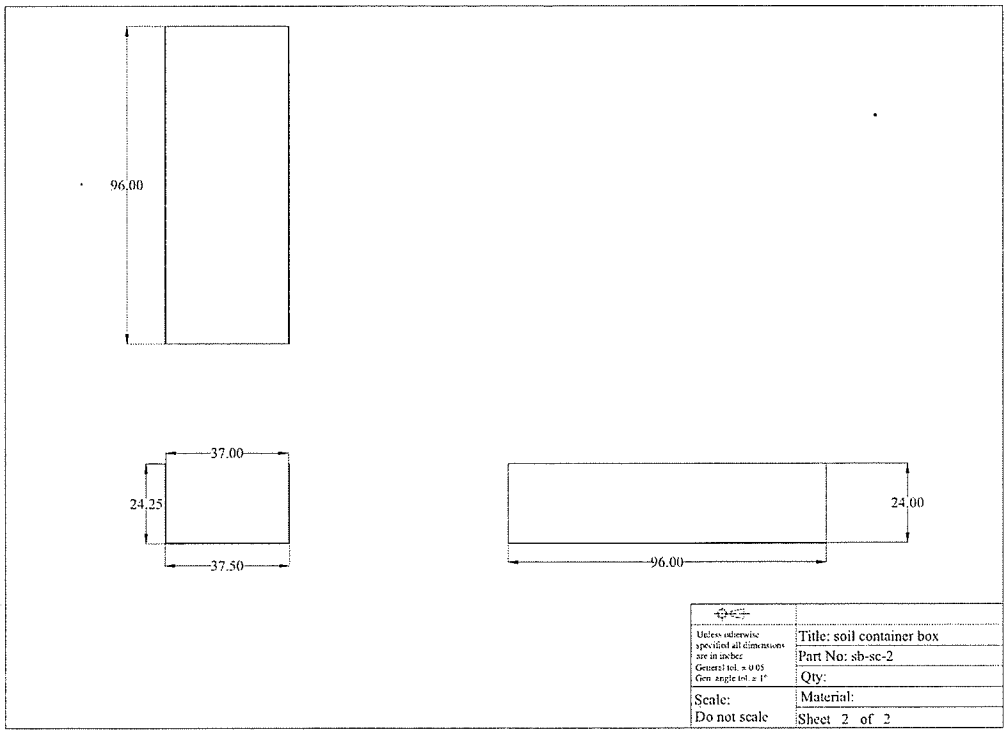

Fig. D. 17 Soil container box dimensions

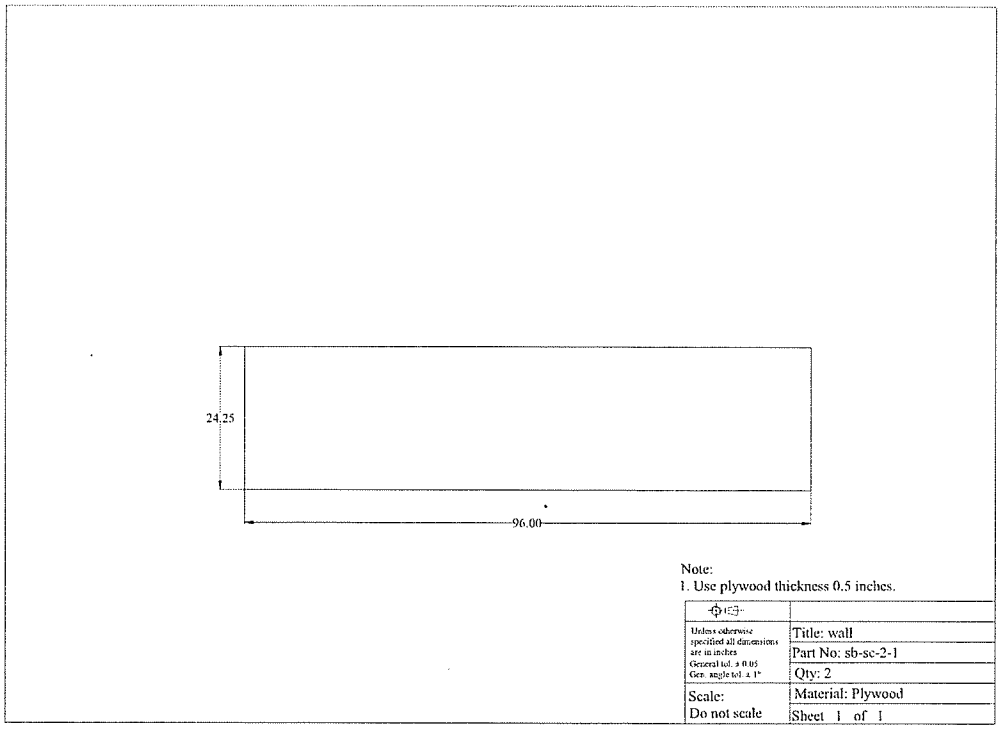

Fig. D. 18 Detail dimensions, sb-sc-2-1

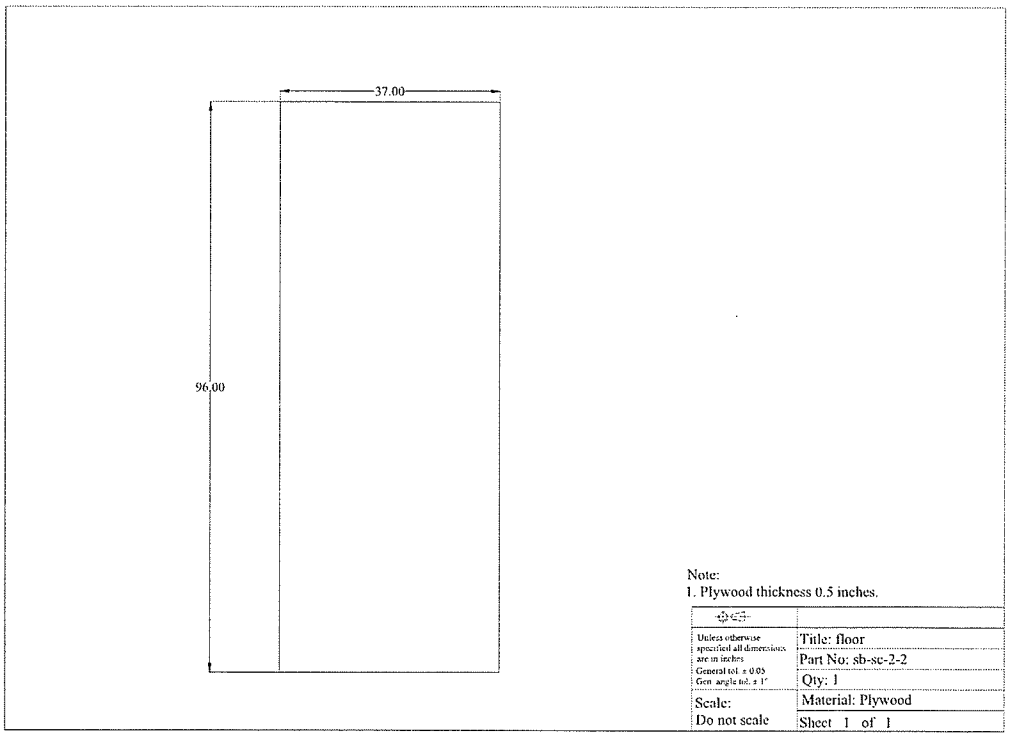

Fig. D. 19 Detail dimensions, sb-sc-2-2

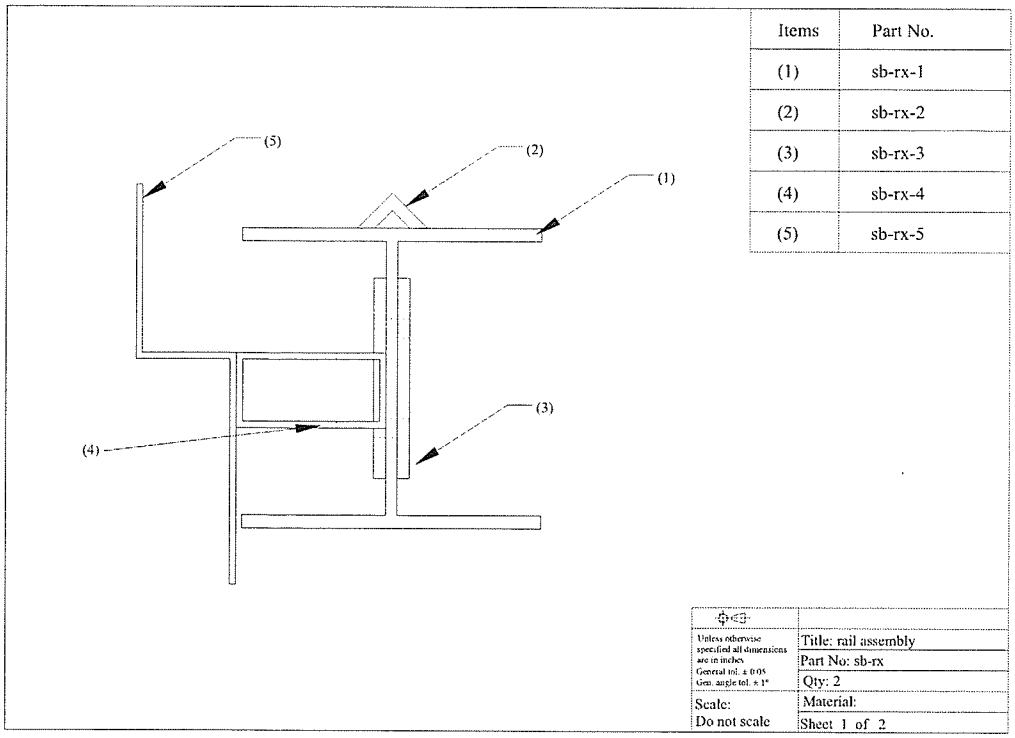

Fig. D. 20 Rail assembly components

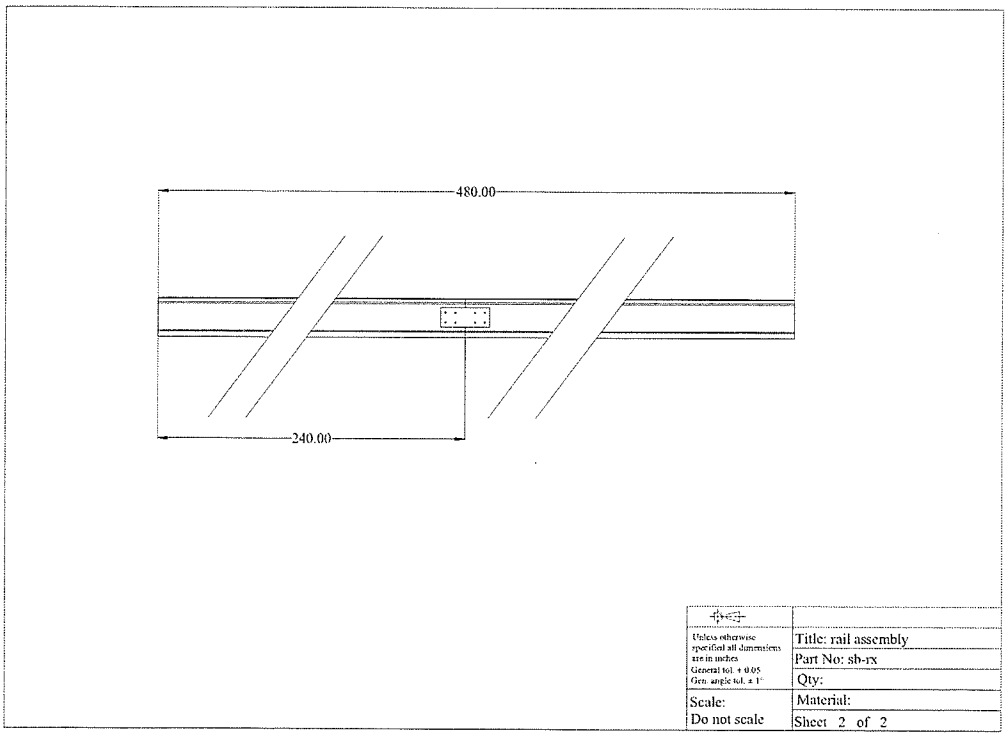

Fig. D. 21 Rail assembly dimensions

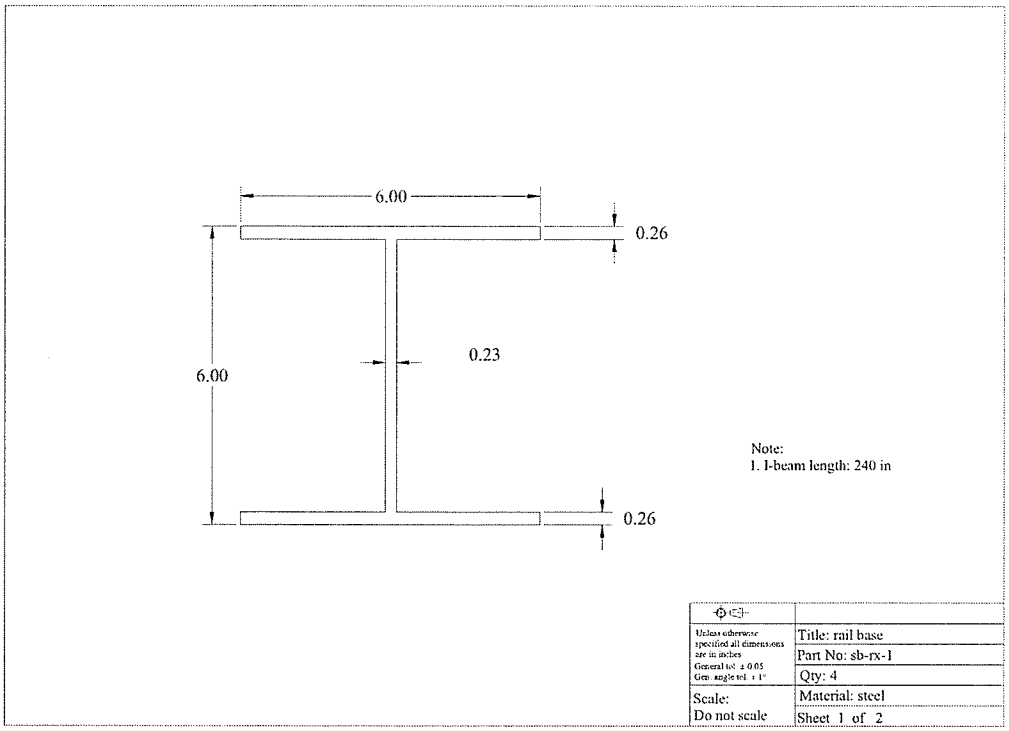

Fig. D. 22 Detail dimensions, sb-rx-1

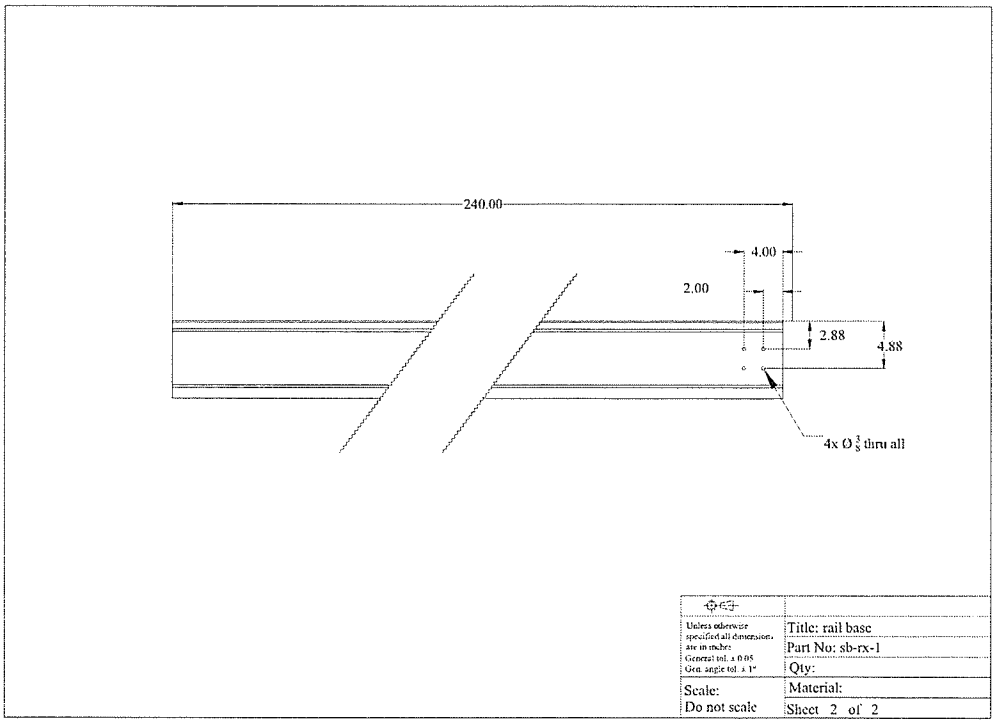

Fig. D. 23 Detail dimensions, sb-rx-1 (side view)

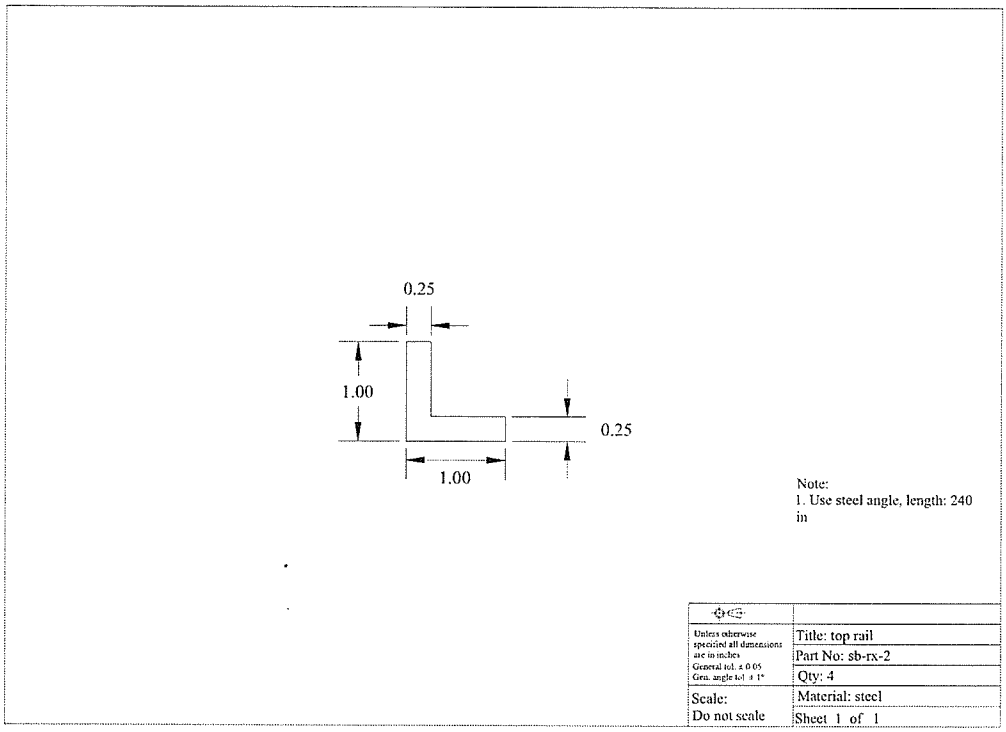

Fig. D. 24 Detail dimensions, sb-rx-2

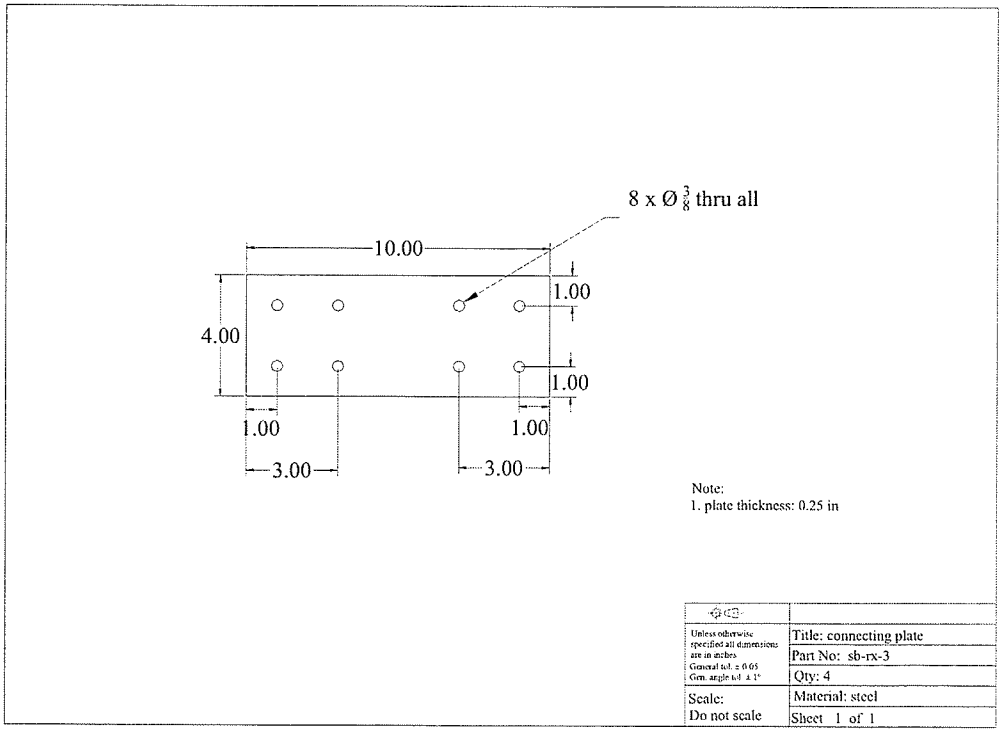

Fig. D. 25 Detail dimensions, sb-rx-3

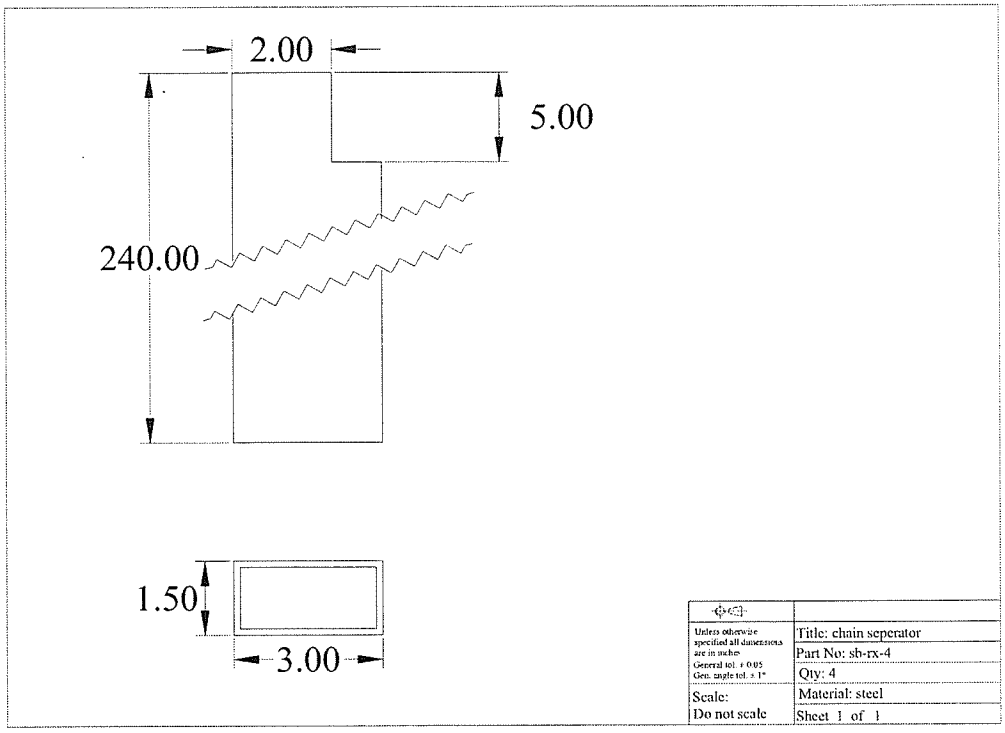

Fig. D. 26 Detail dimensions, sb-rx-4

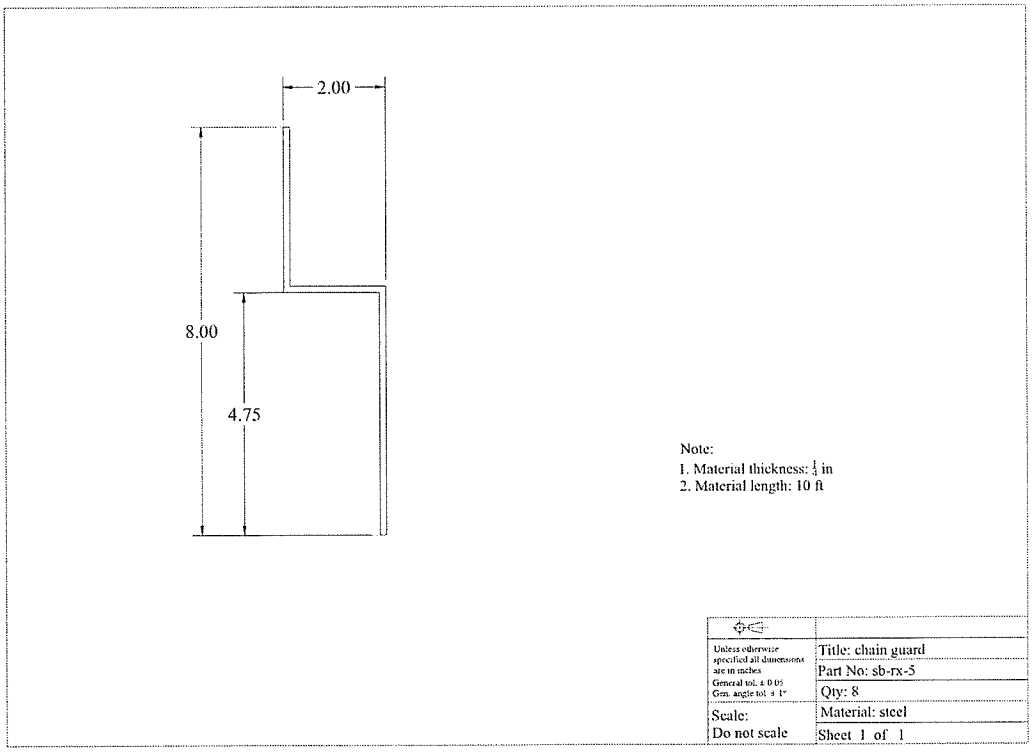

Fig. D. 27 Detail dimensions, sb-rx-5

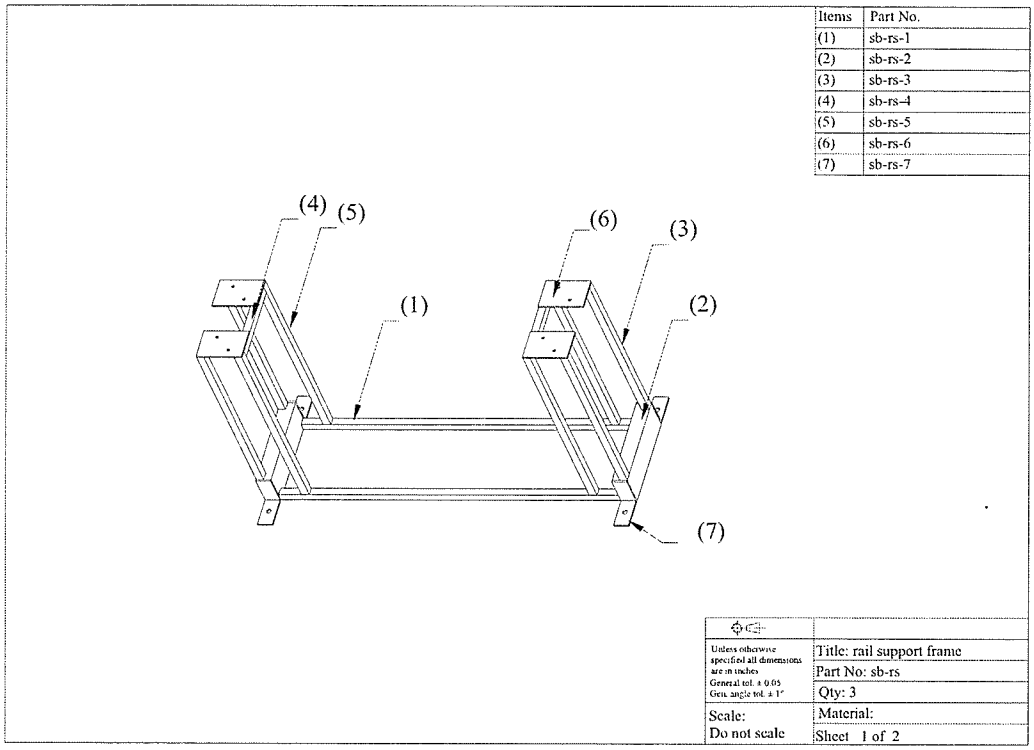

Fig. D. 28 Rail support frame members

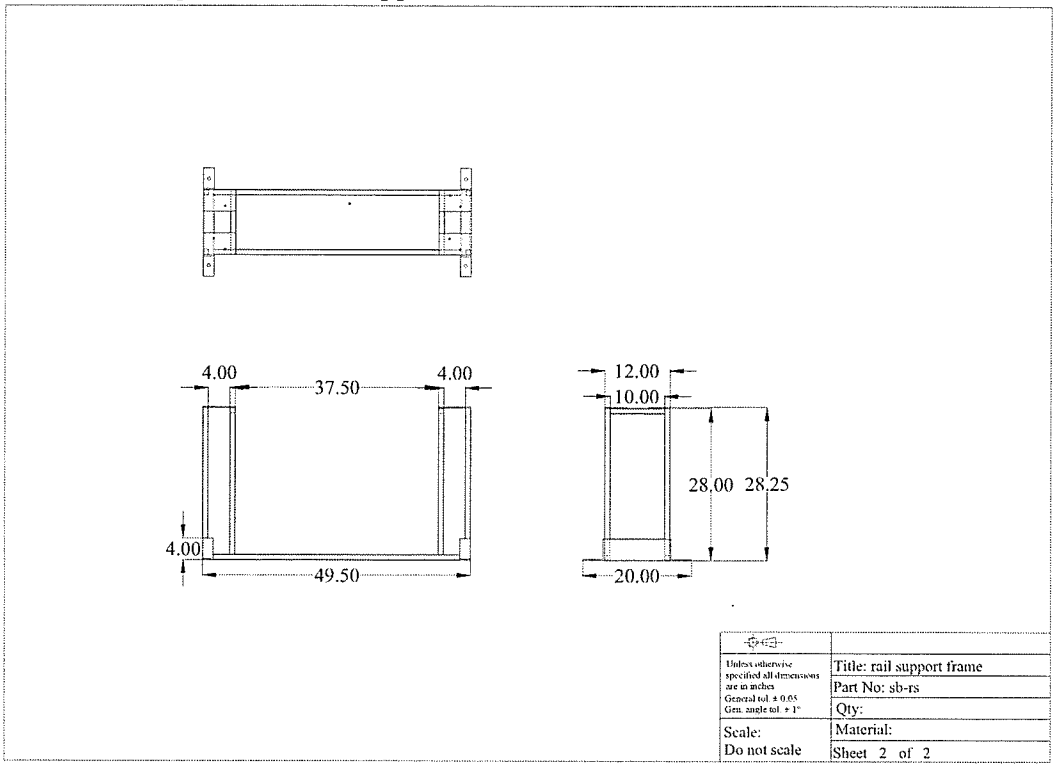

Fig. D. 29 Rail support frame dimensions

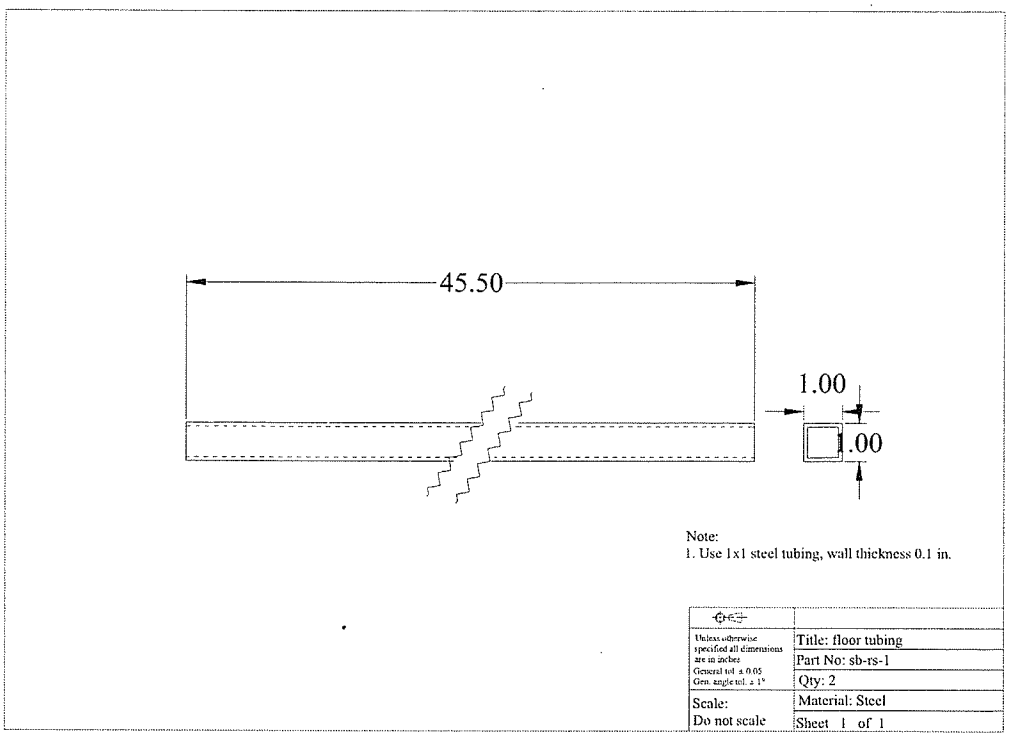

Fig. D. 30 Detail dimensions, sb-rs-1

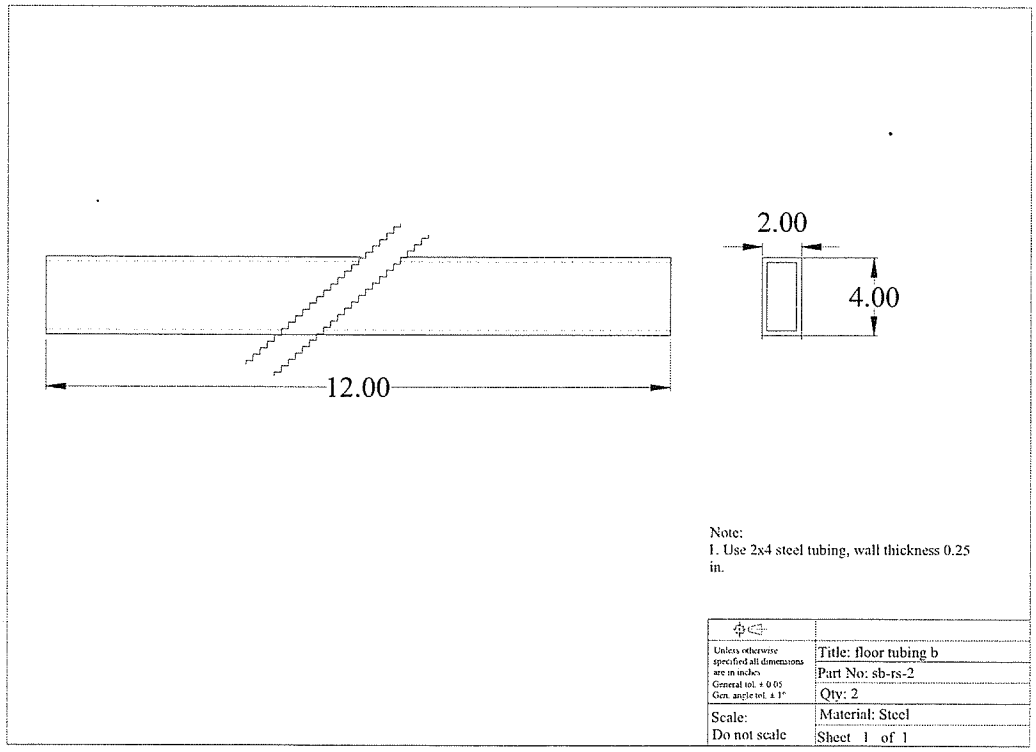

Fig. D. 31 Detail dimensions, sb-rs-2

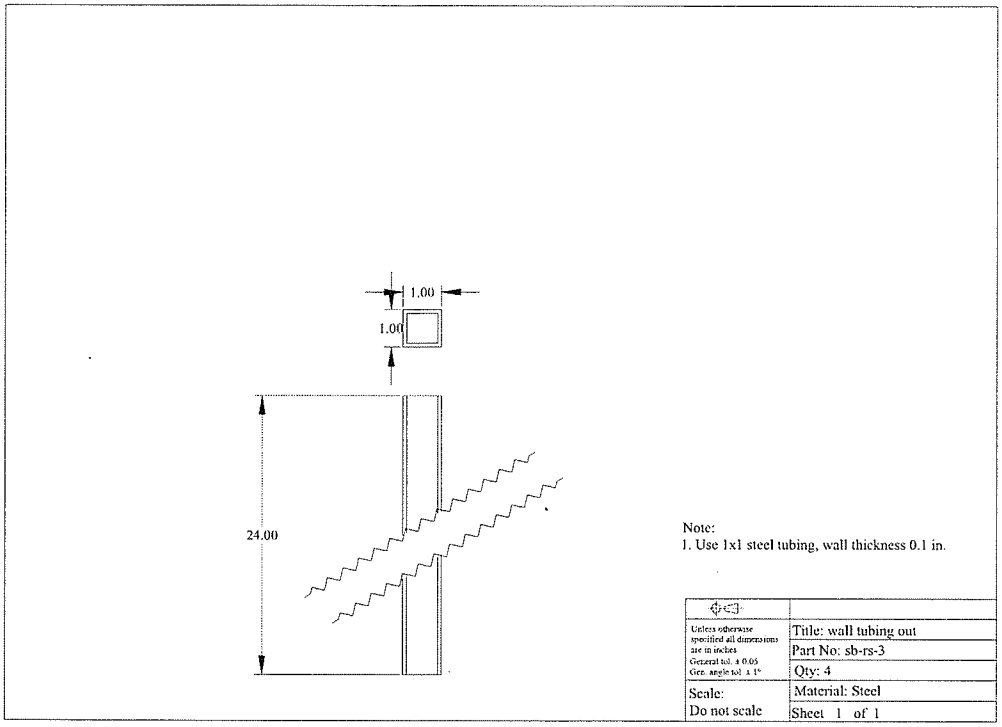

Fig. D. 32 Detail dimensions, sb-rs-3

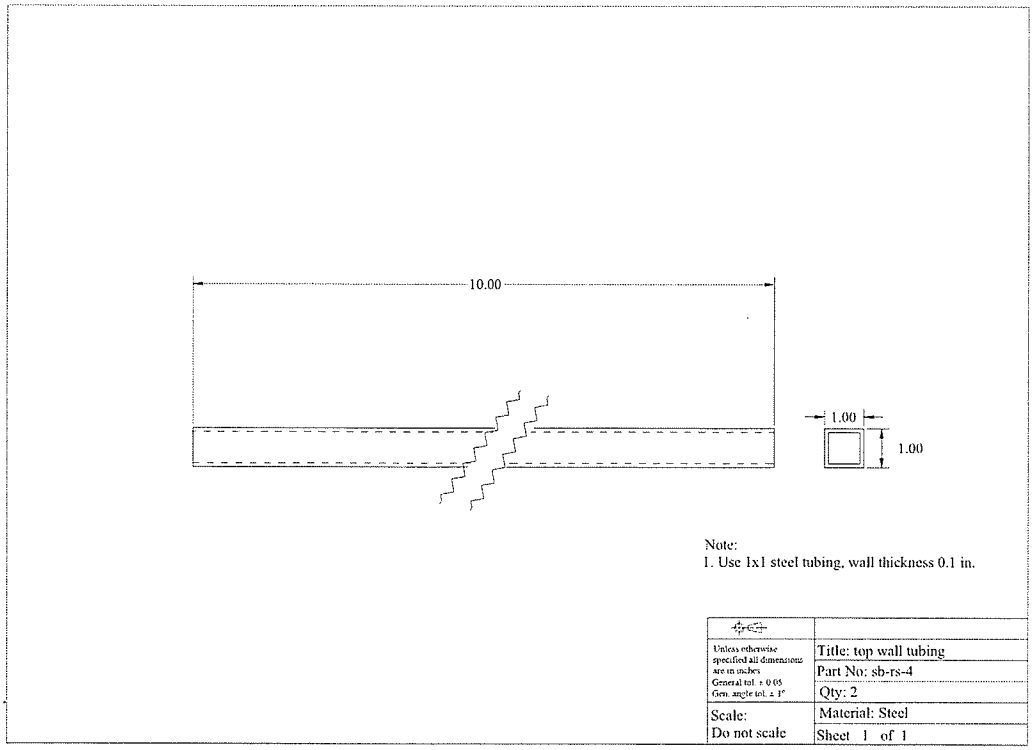

Fig. D. 33 Detail dimensions, sb-rs-4

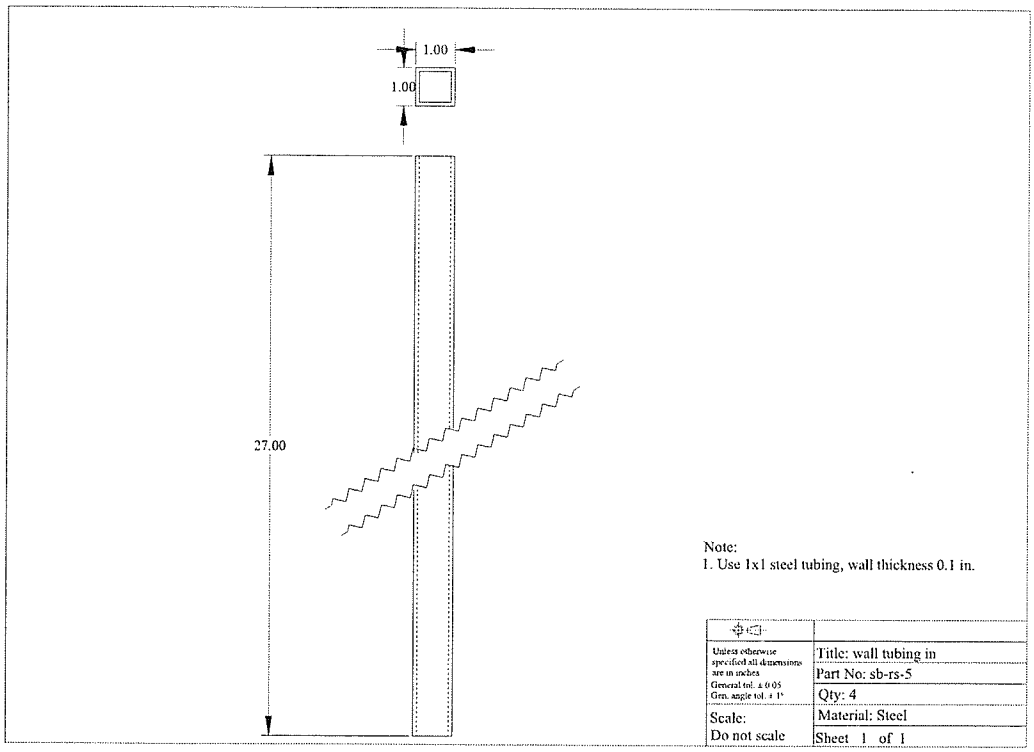

Fig. D. 34 Detail dimensions, sb-rs-5

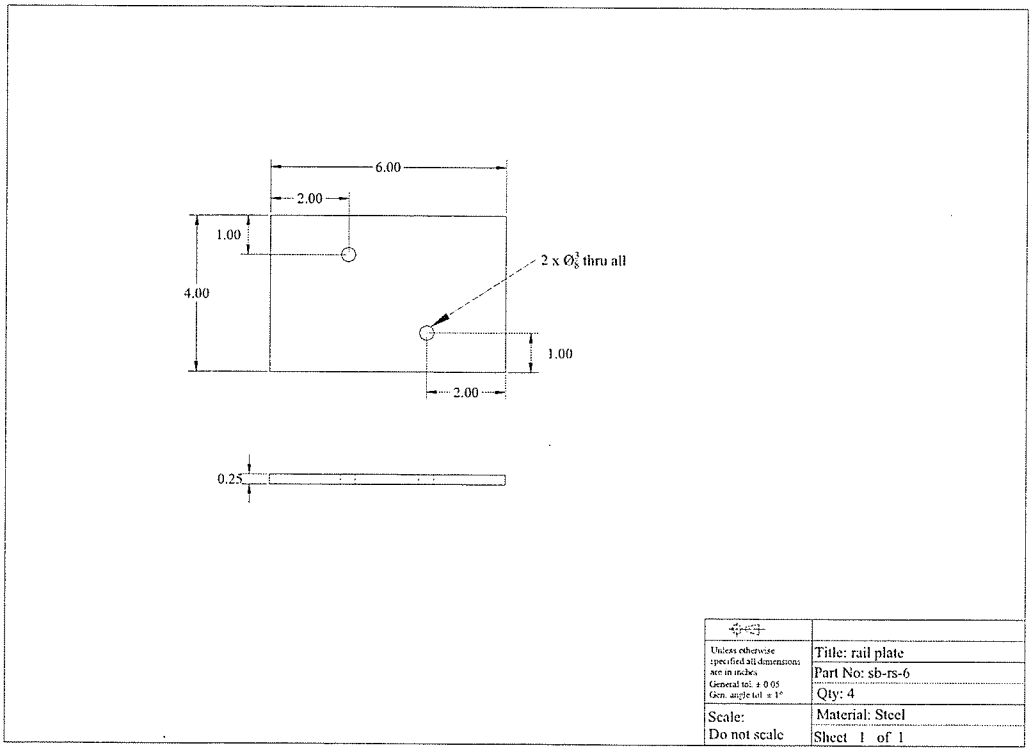

Fig. D. 35 Detail dimensions, sb-rs-6

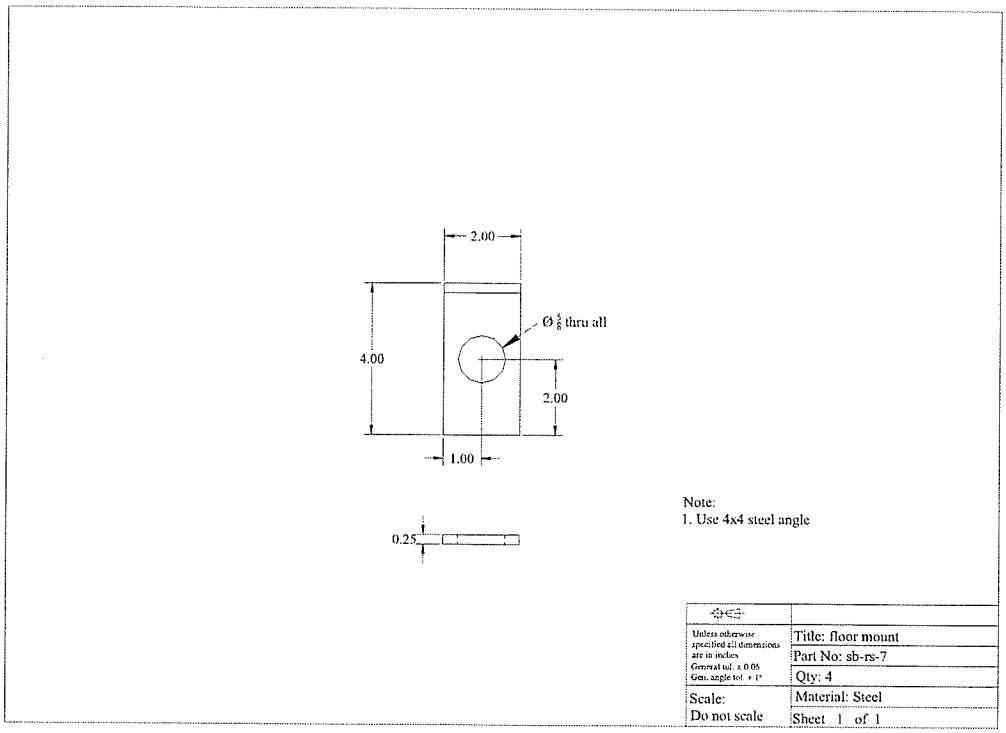

Fig. D. 36 Detail dimensions, sb-rs-7

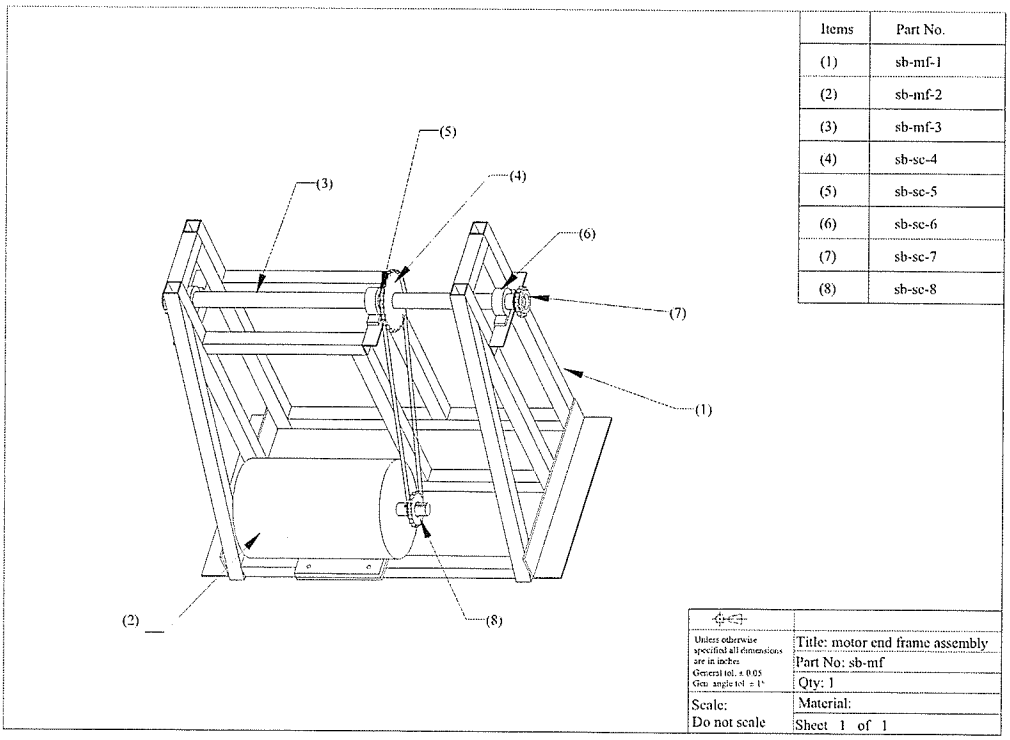

Fig. D. 37 Motor end frame assembly components

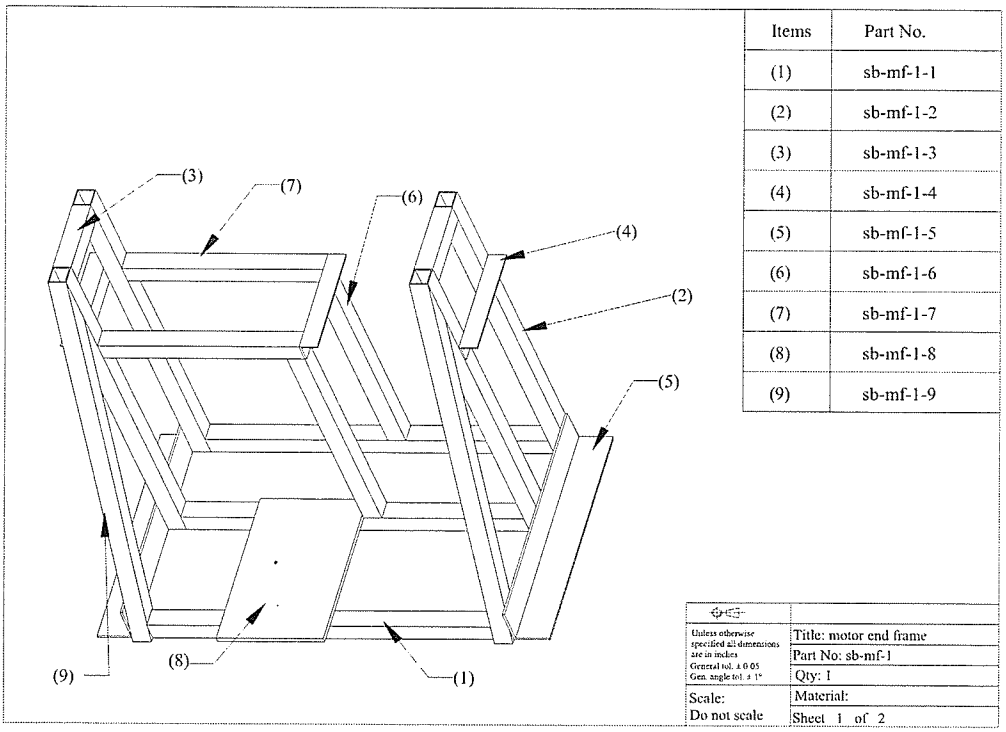

Fig. D. 38 Motor end frame members

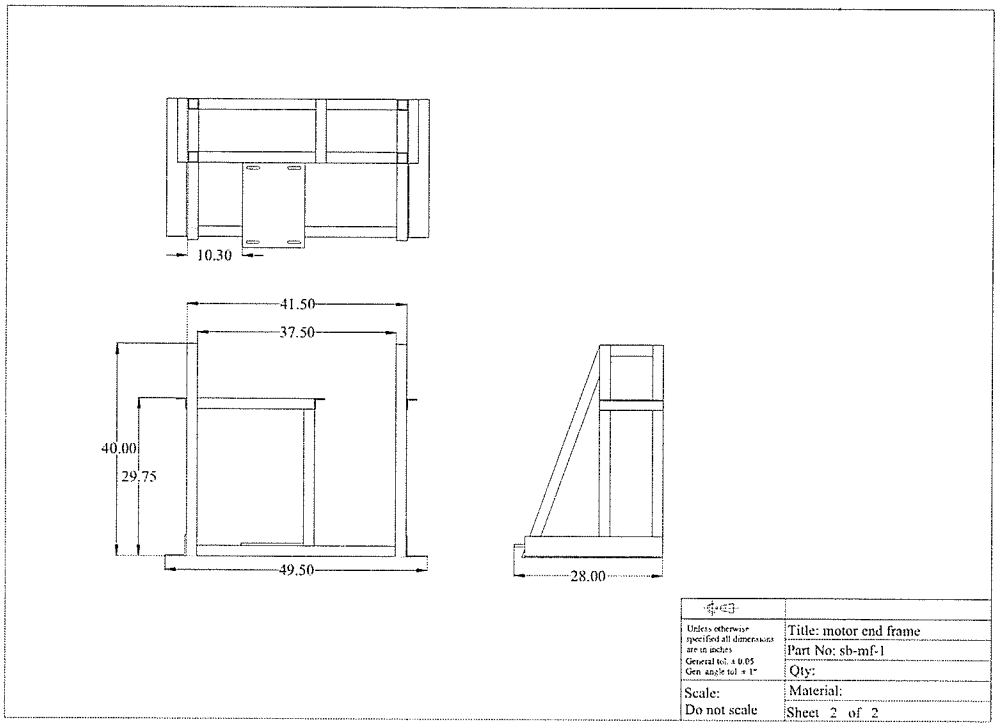

Fig. D. 39 Motor end frame dimensions

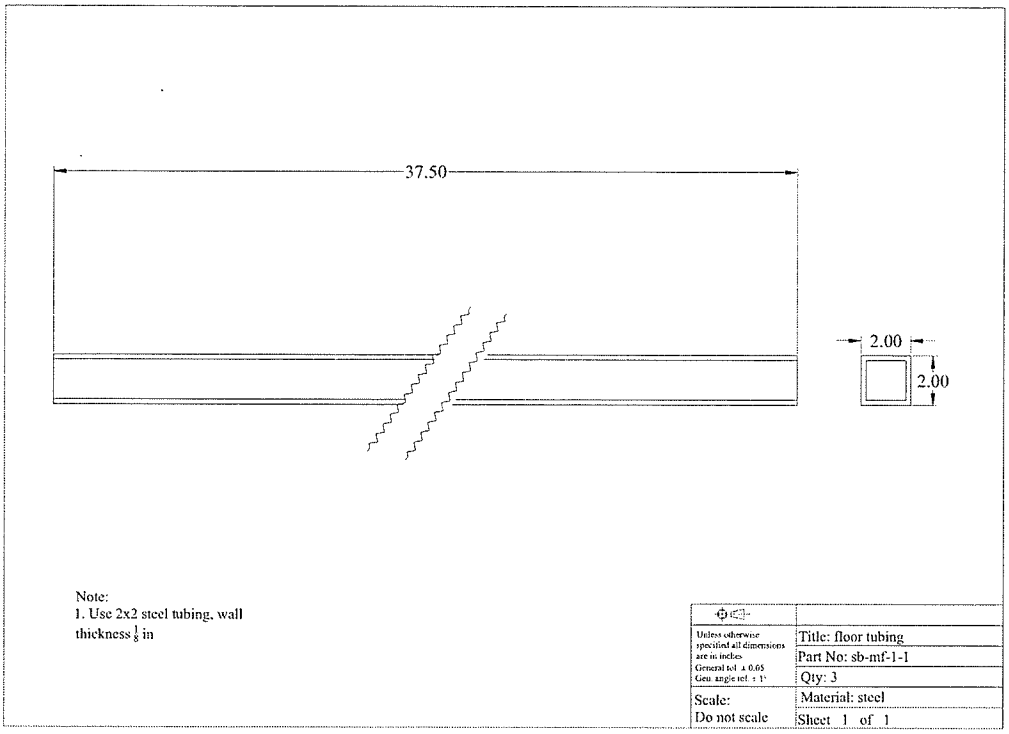

Fig. D. 40 Detail dimensions, sb-mf-1-1

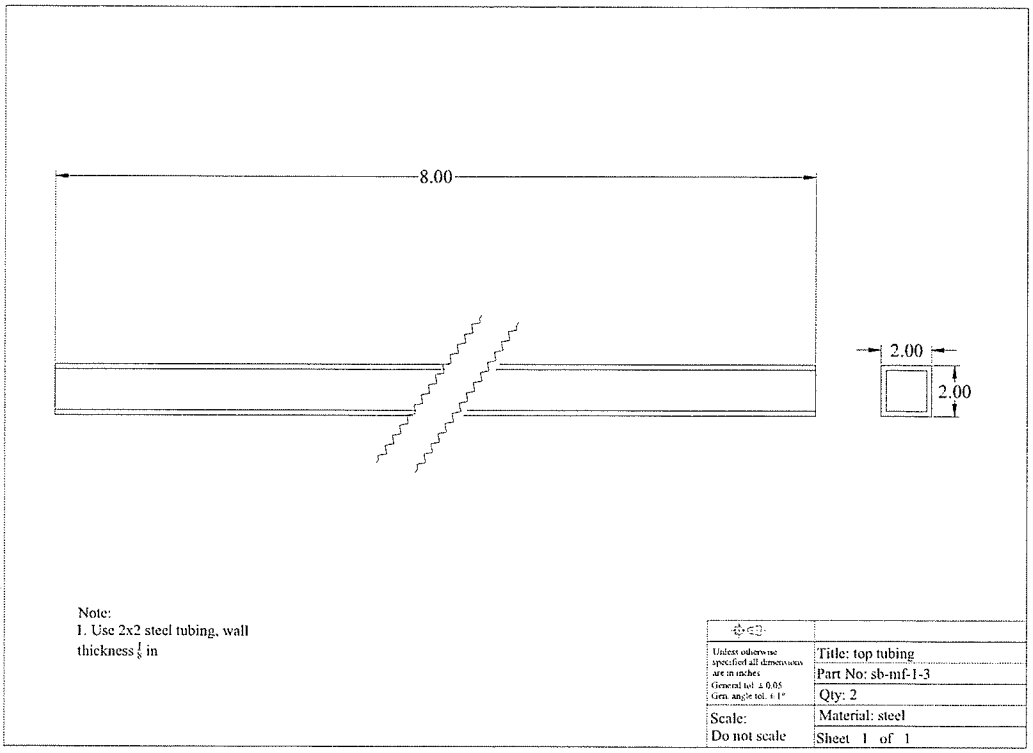

Fig. D. 41 Detail dimensions, sb-rs-1-3

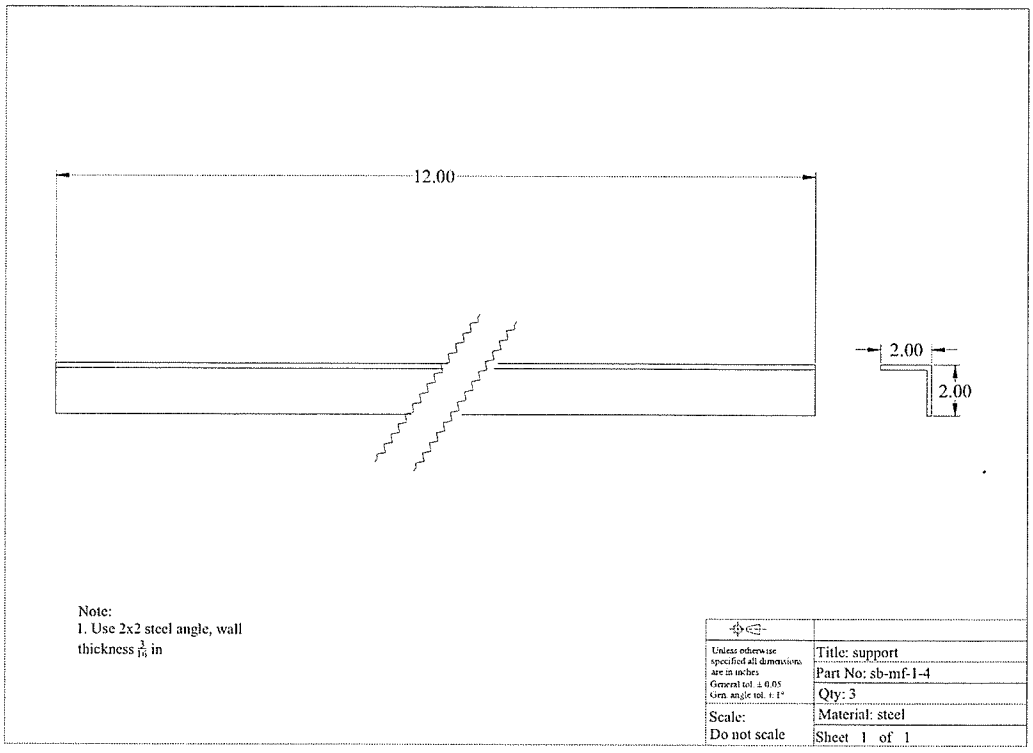

Fig. D. 42 Detail dimensions, sb-rs-4

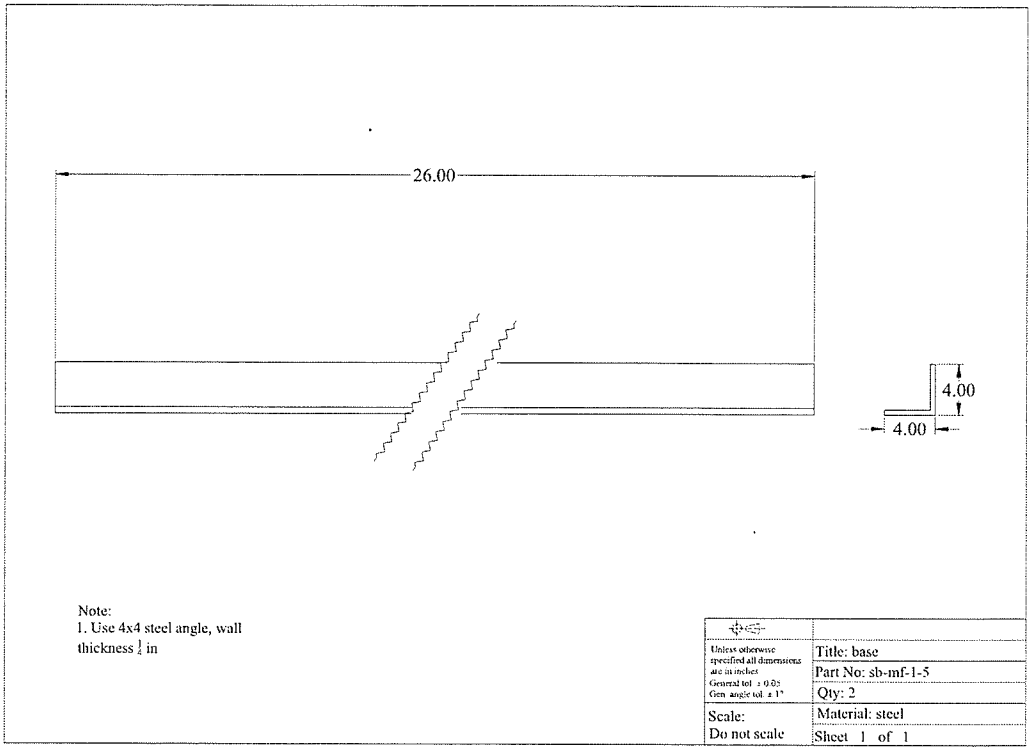

Fig. D. 43 Detail dimensions, sb-rs-1-5

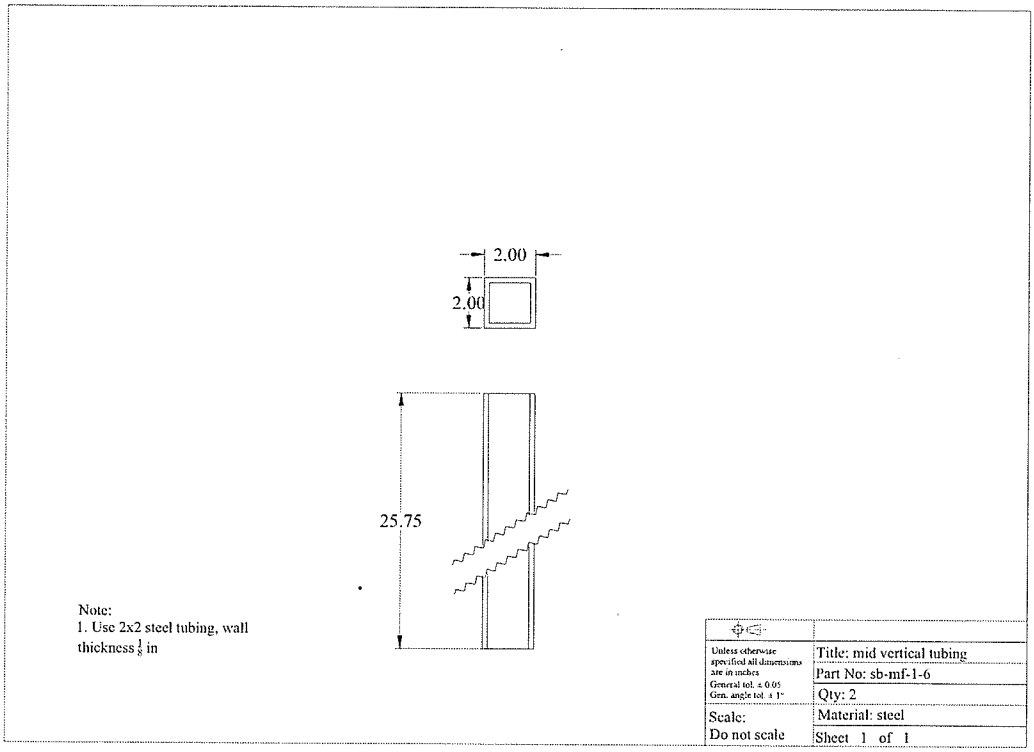

Fig. D. 44 Detail dimensions, sb-rs-1-6

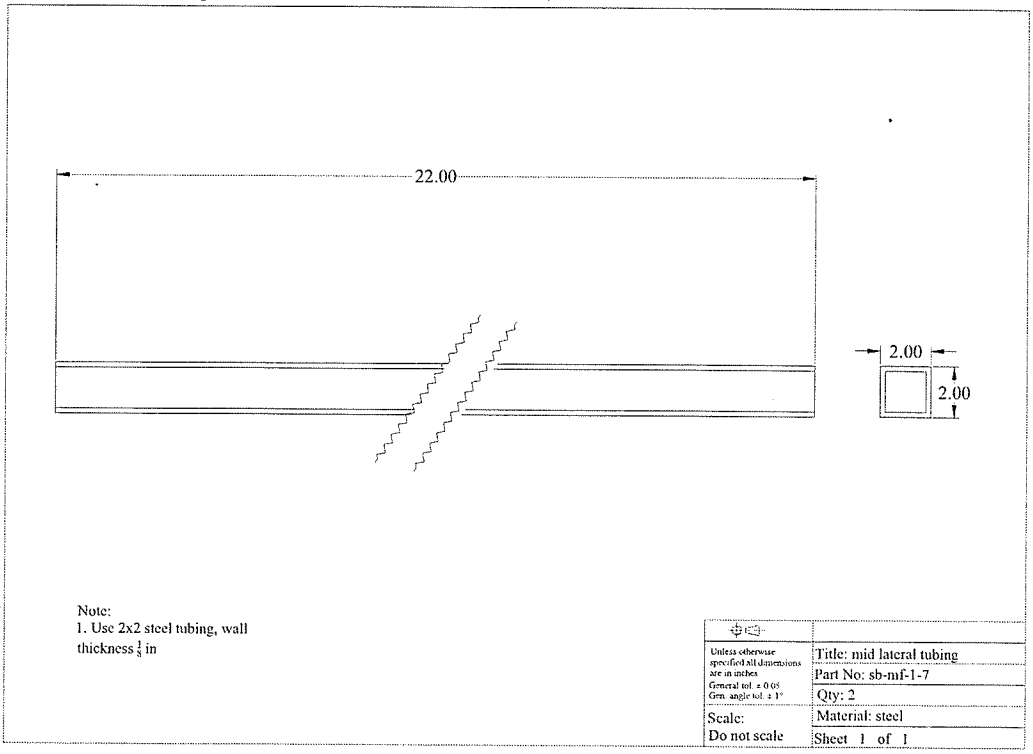

Fig. D. 45 Detail dimensions, sb-rs-1-7

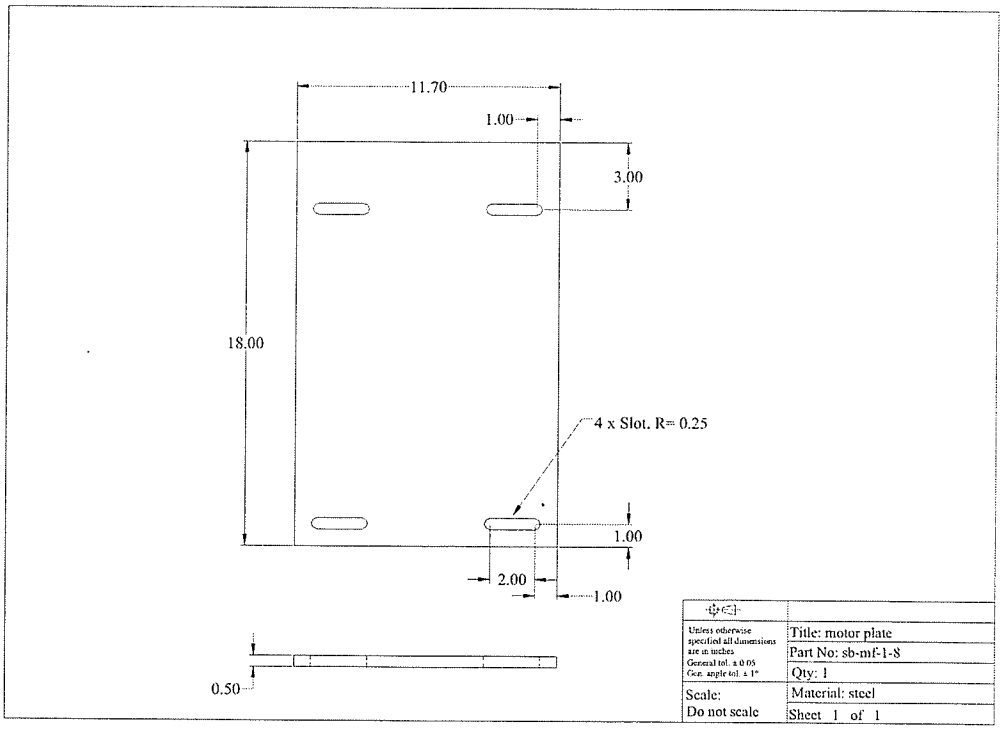

Fig. D. 46 Detail dimensions, sb-rs-1-8

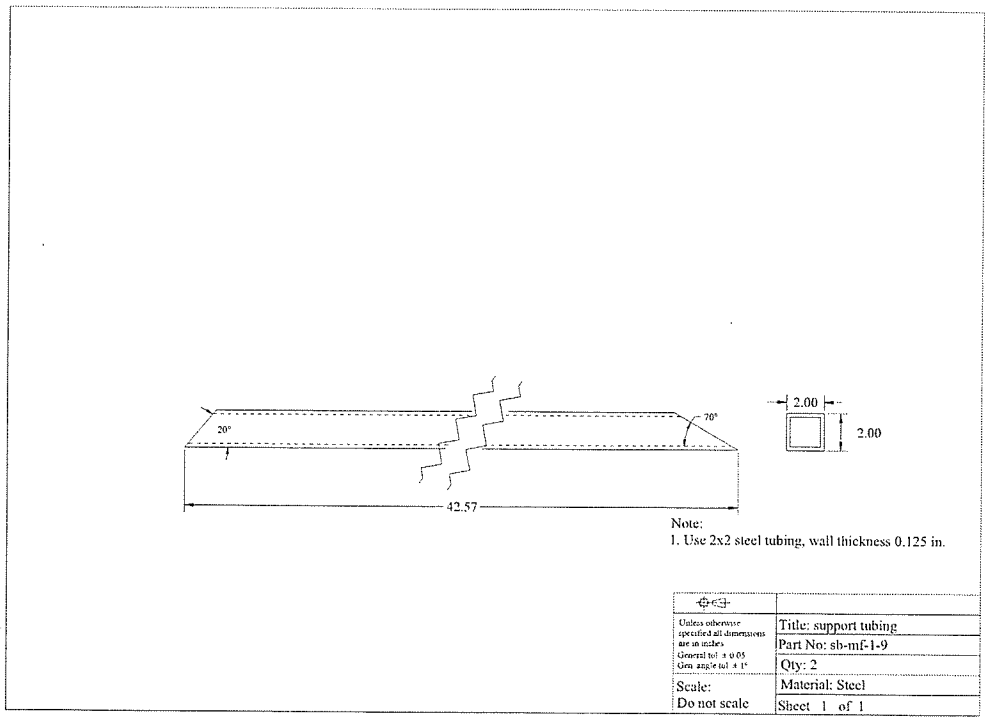

Fig. D. 47 Detail dimensions, sb-rs-1-9

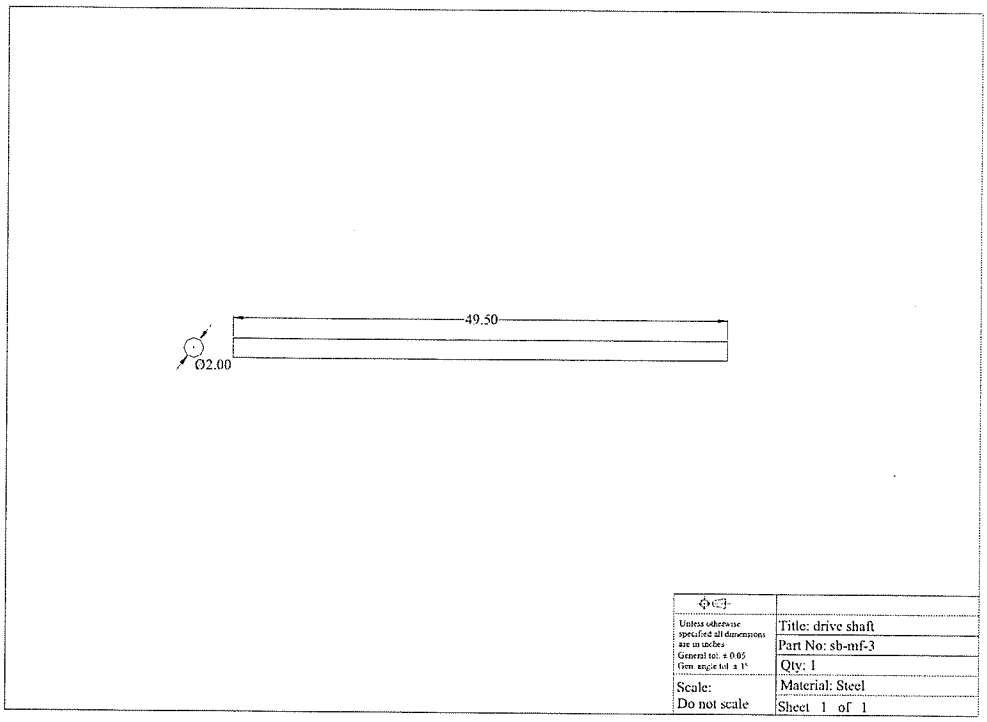

Fig. D. 48 Detail dimensions, sb-mf-3

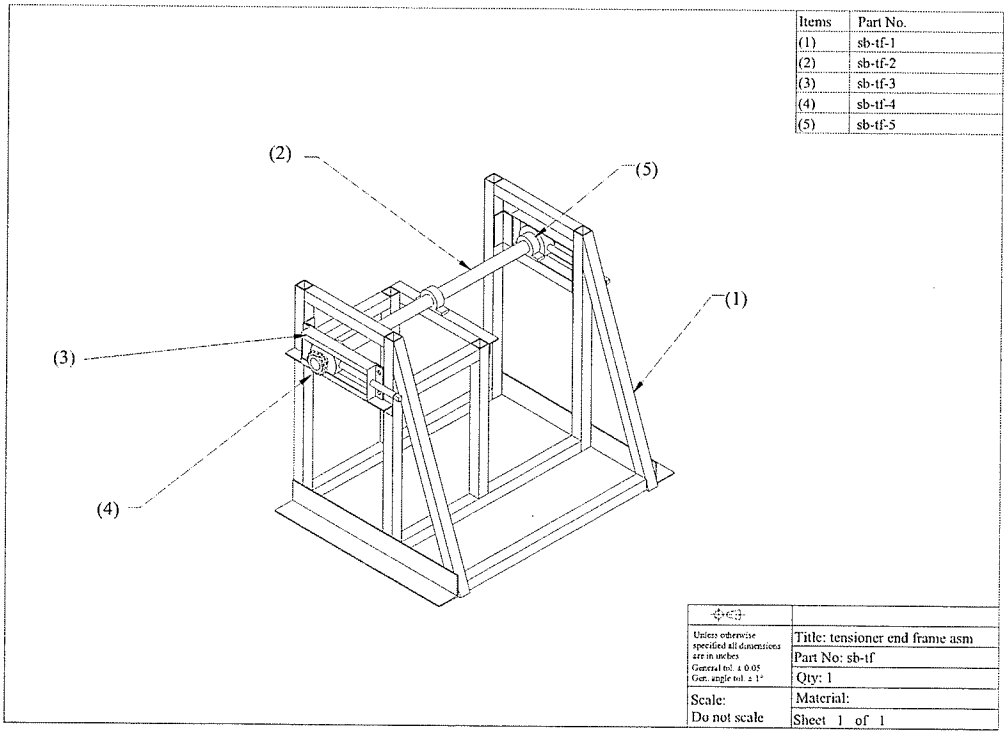

Fig. D. 49 Tensioner end frame assembly components

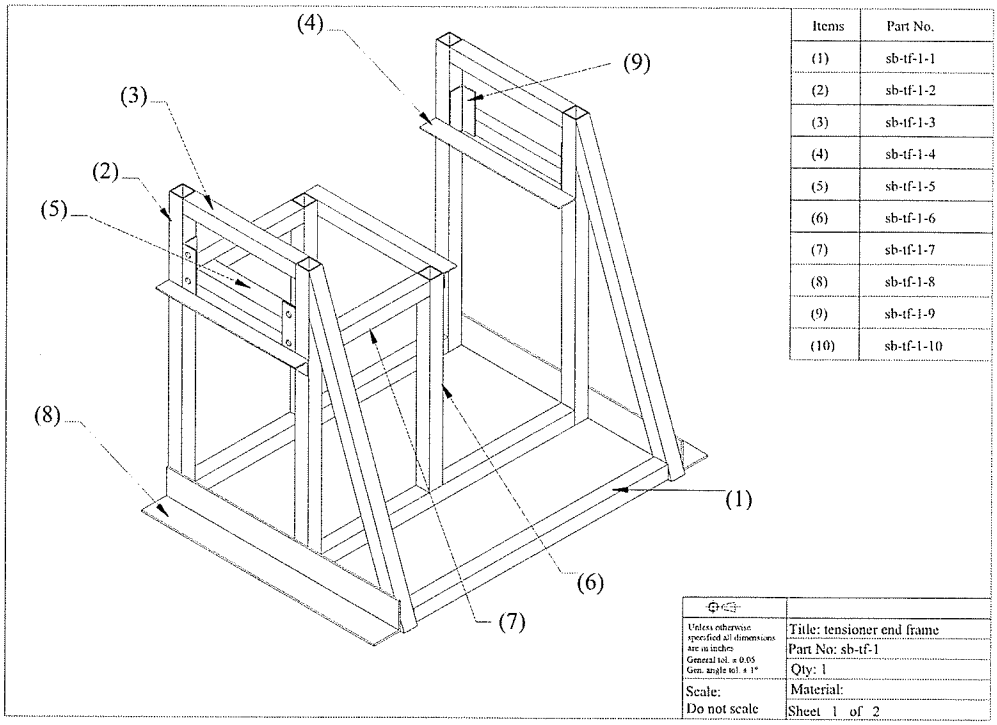

Fig. D. 50 Tensioner end frame members

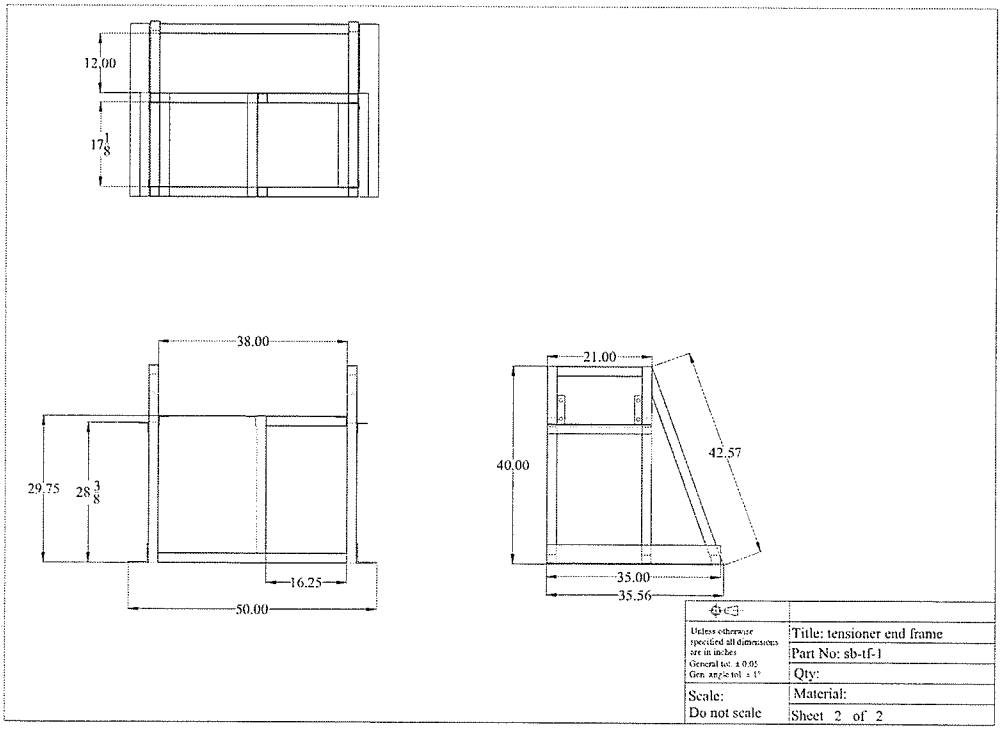

Fig. D. 51 Tensioner end frame dimensions

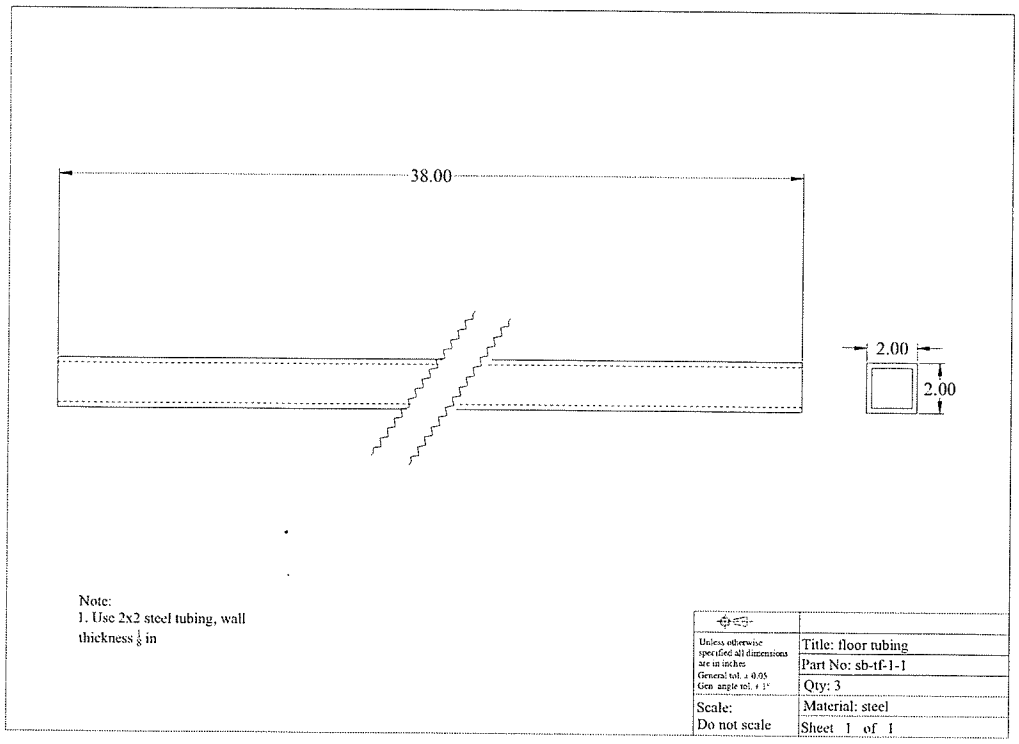

Fig. D. 52 Detail dimensions, sb-tf-1-1

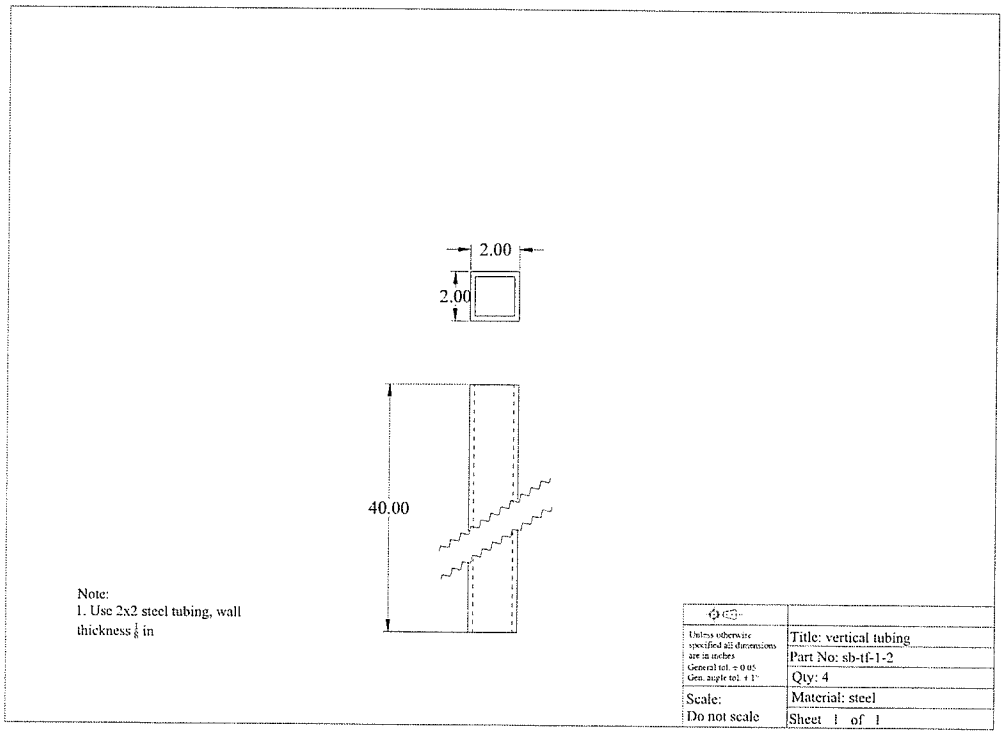

Fig. D. 53 Detail dimensions, sb-tf-1-2

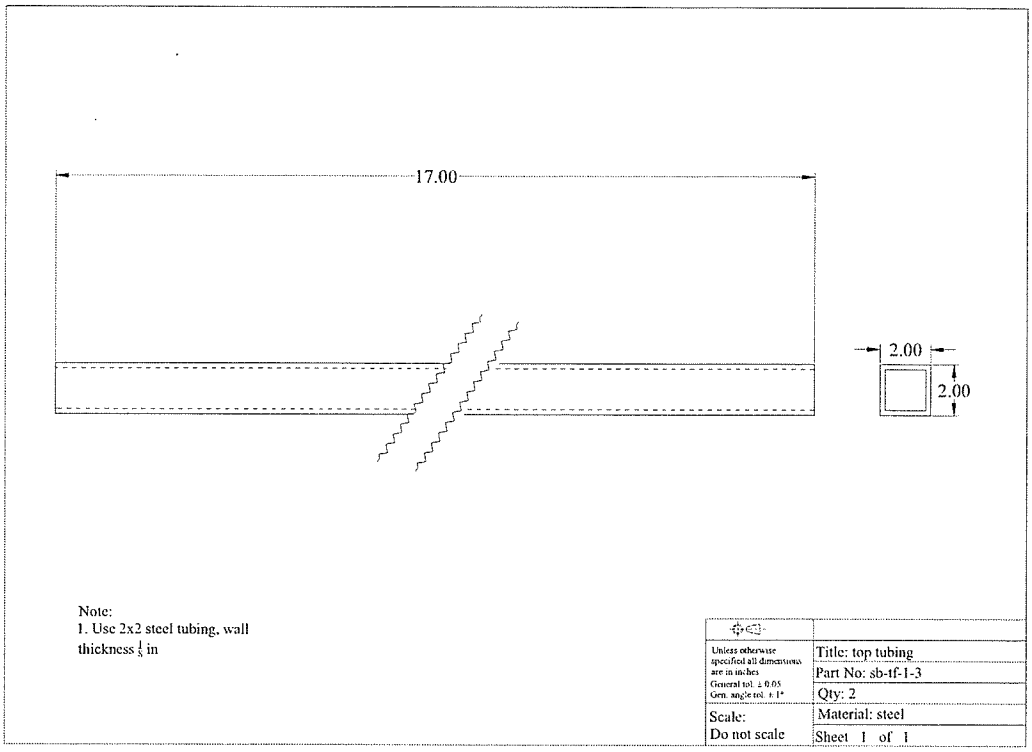

Fig. D. 54 Detail dimensions, sb-tf-1-3

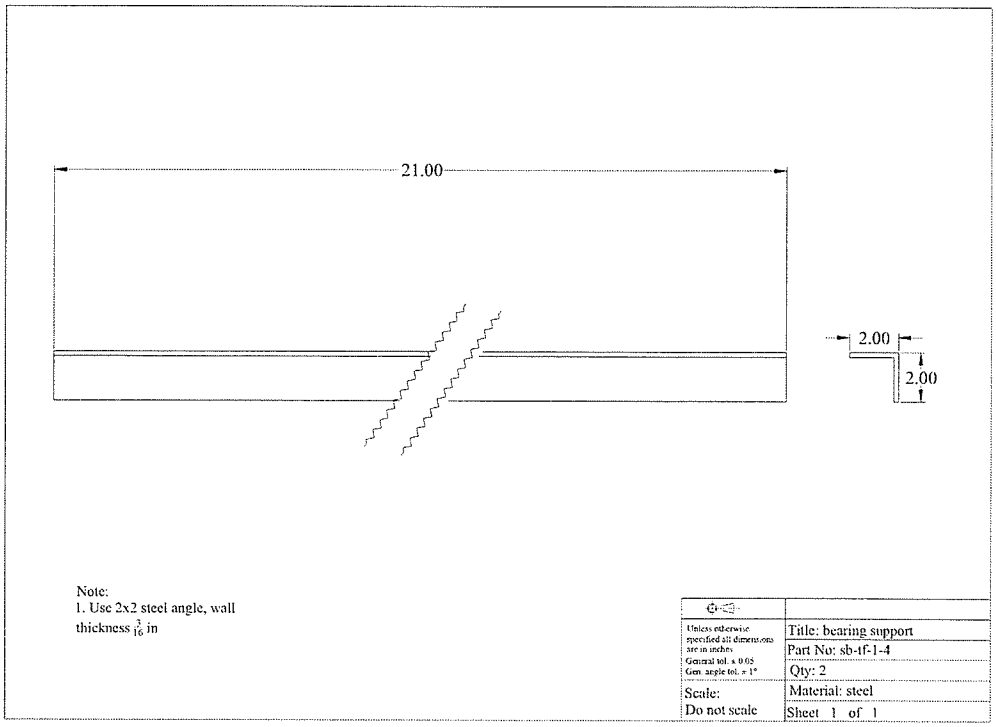

Fig. D. 55 Detail dimensions, sb-tf-1-4

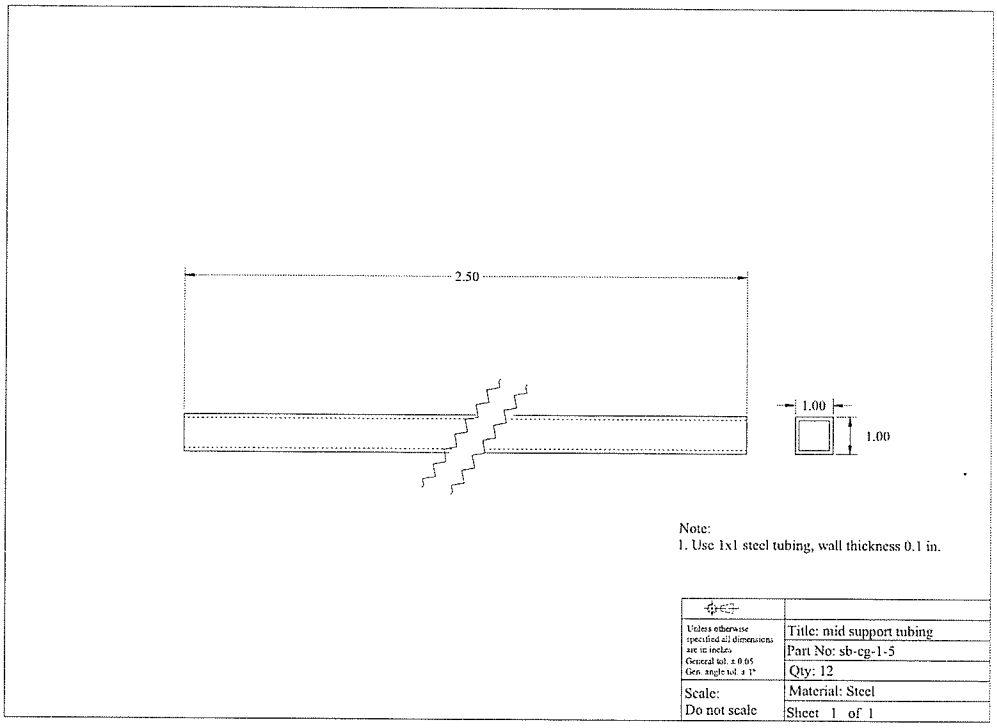

Fig. D. 56 Detail dimensions, sb-cg-1-5

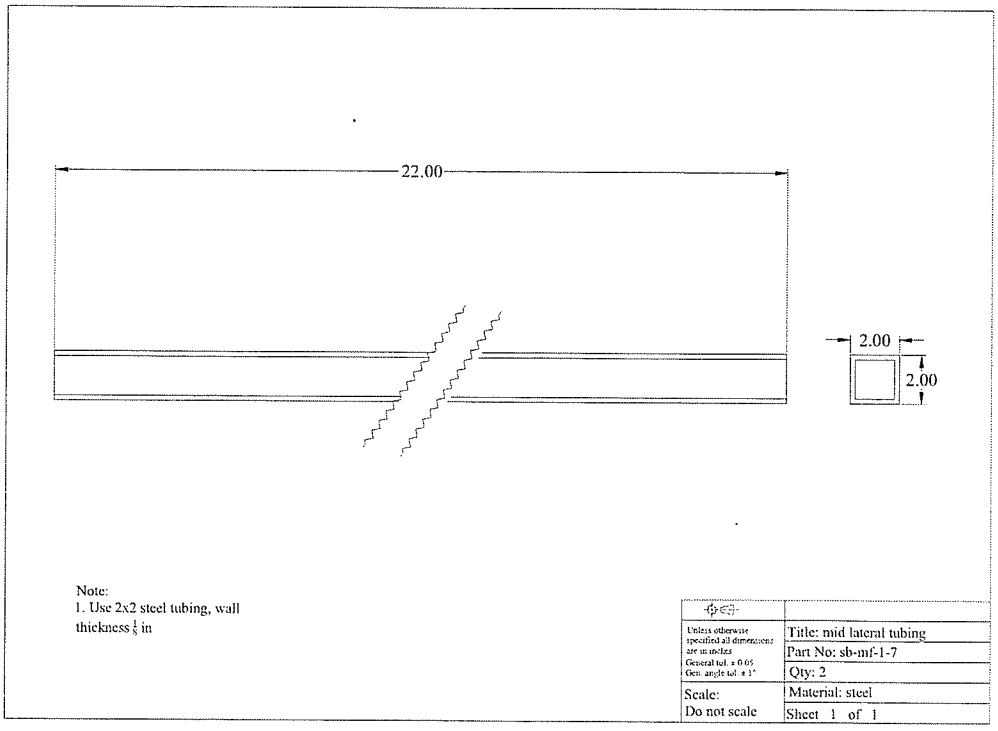

Fig. D. 57 Detail dimensions, sb-mf-1-7

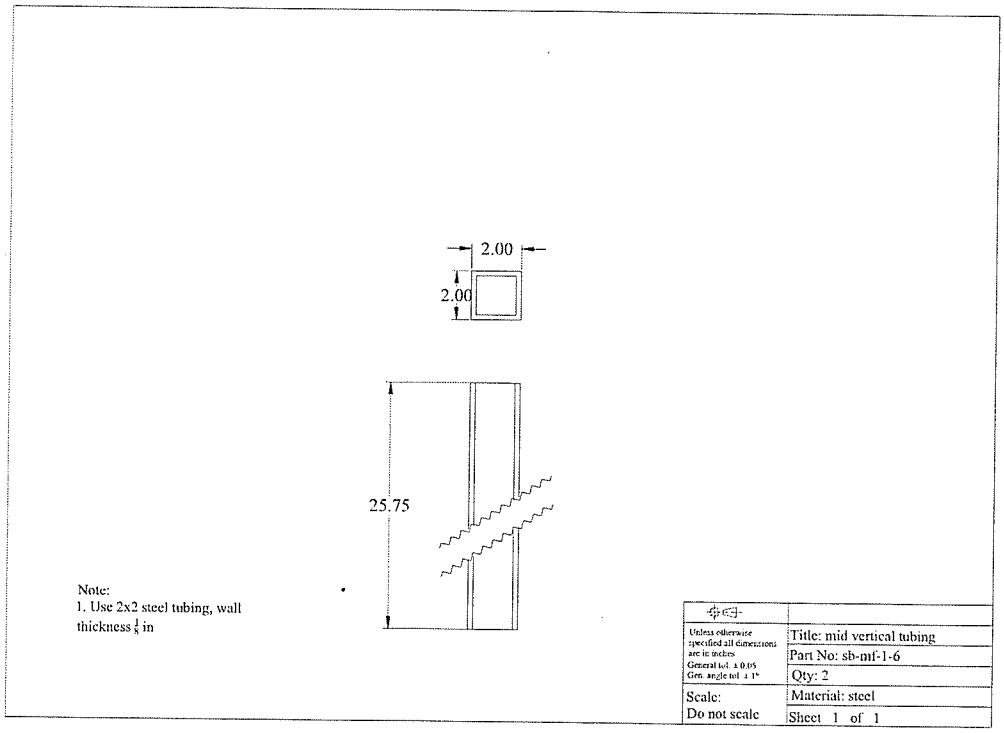

Fig. D. 58 Detail dimensions, sb-mf-1-6

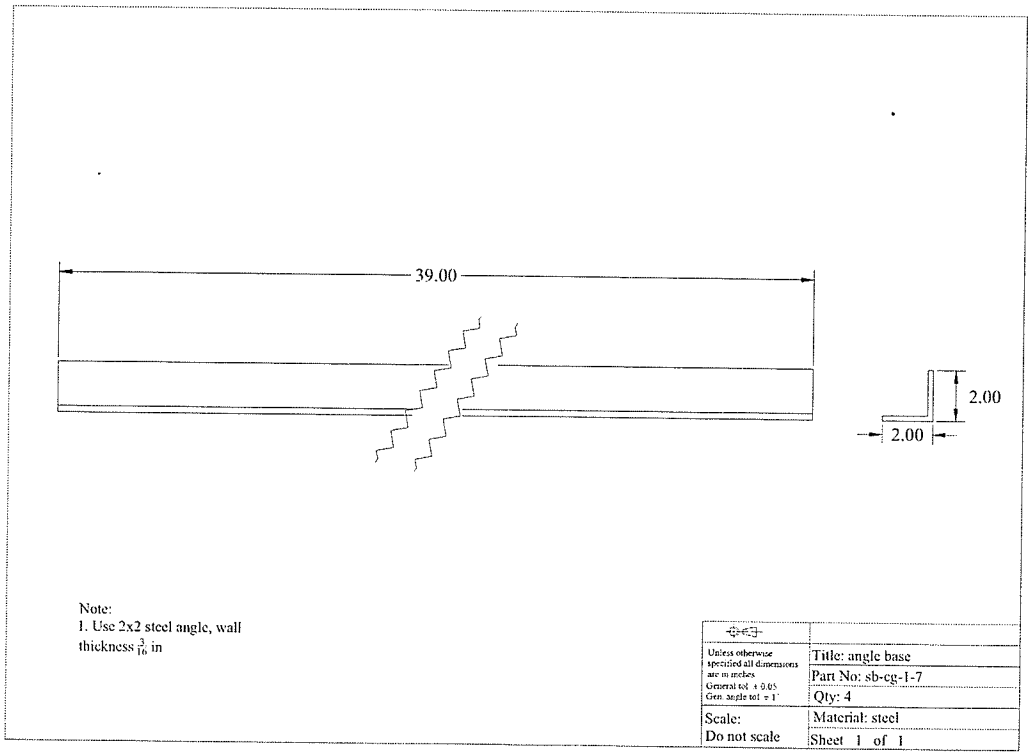

Fig. D. 59 Detail dimensions, sb-cg-1-7

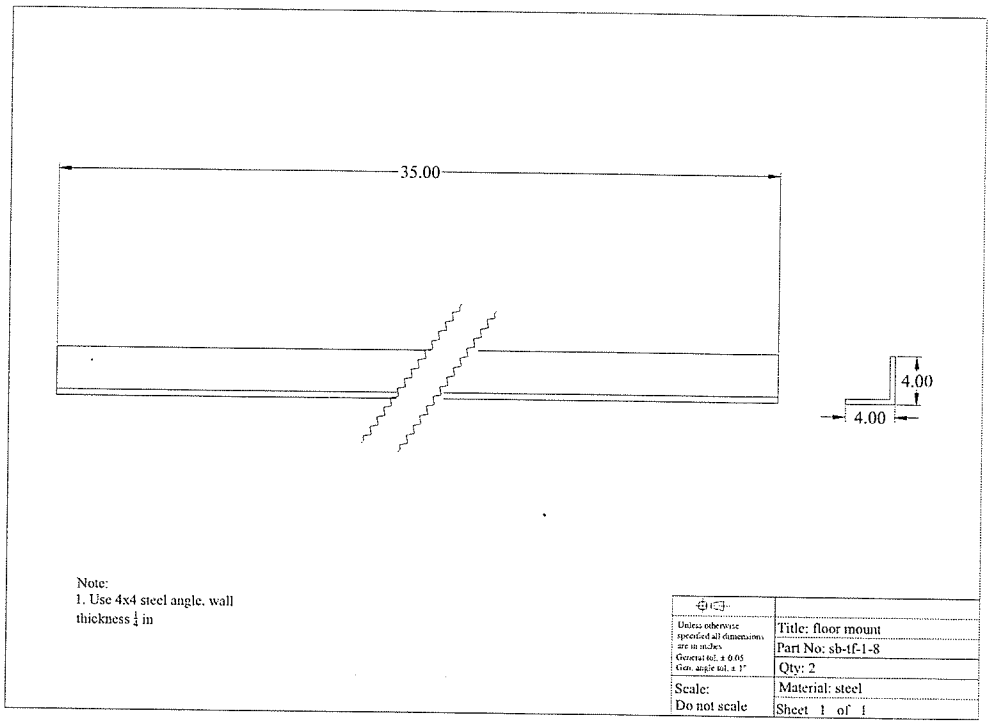

Fig. D. 60 Detail dimensions, sb-tf-1-8

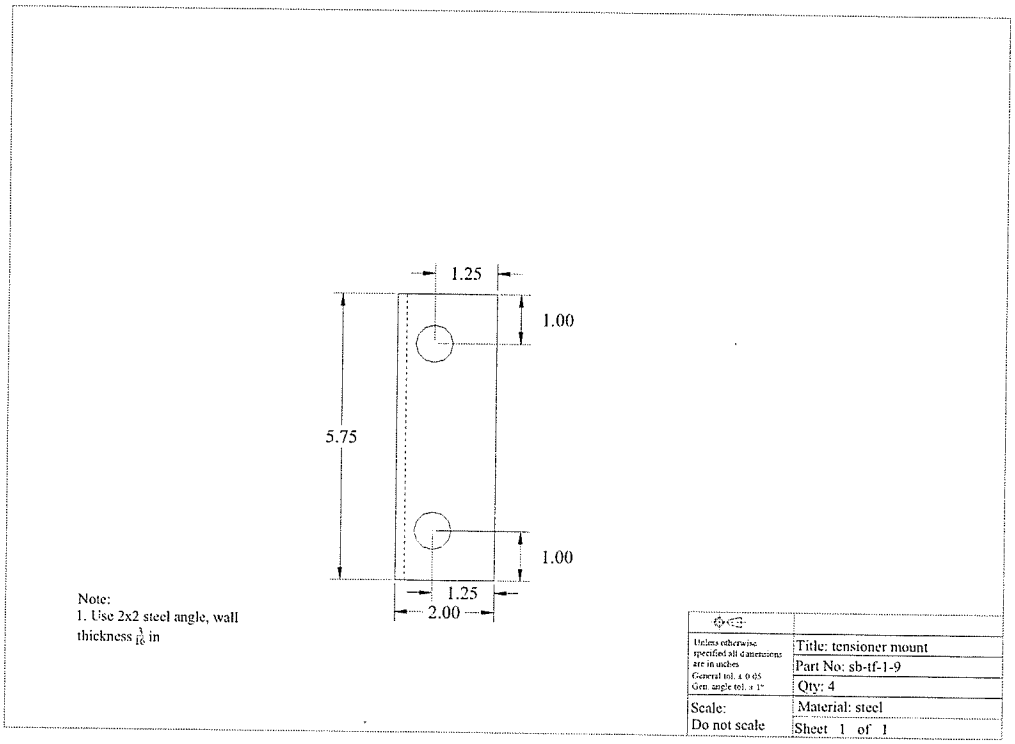

Fig. D. 61 Detail dimensions, sb-tf-1-9

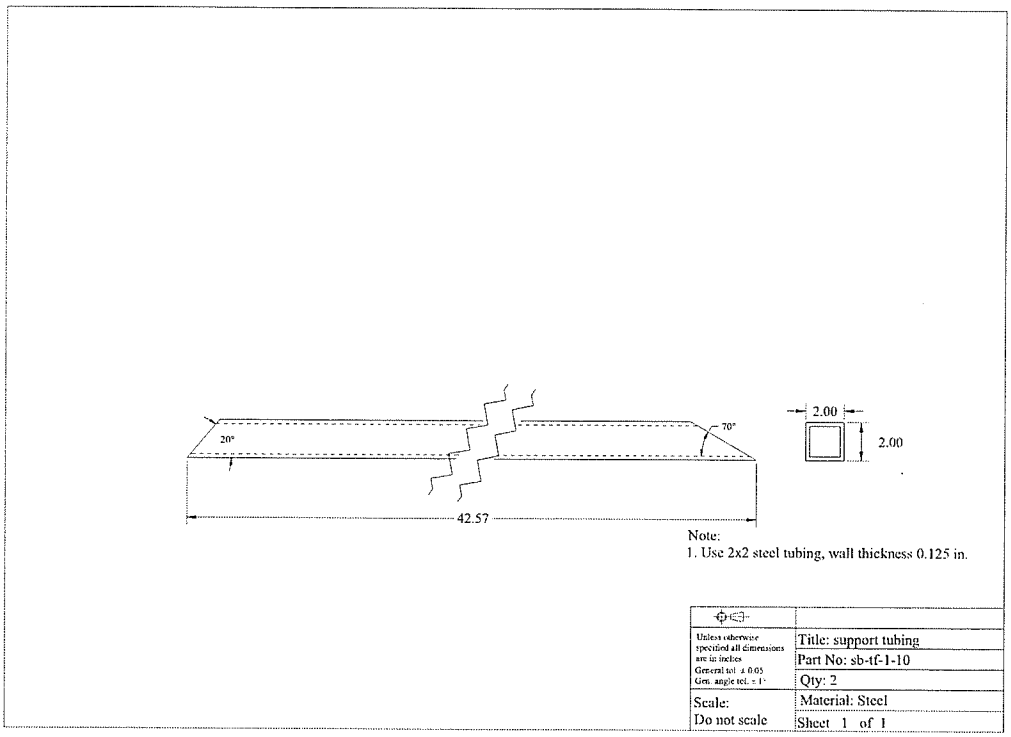

Fig. D. 62 Detail dimensions, sb-tf-1-10

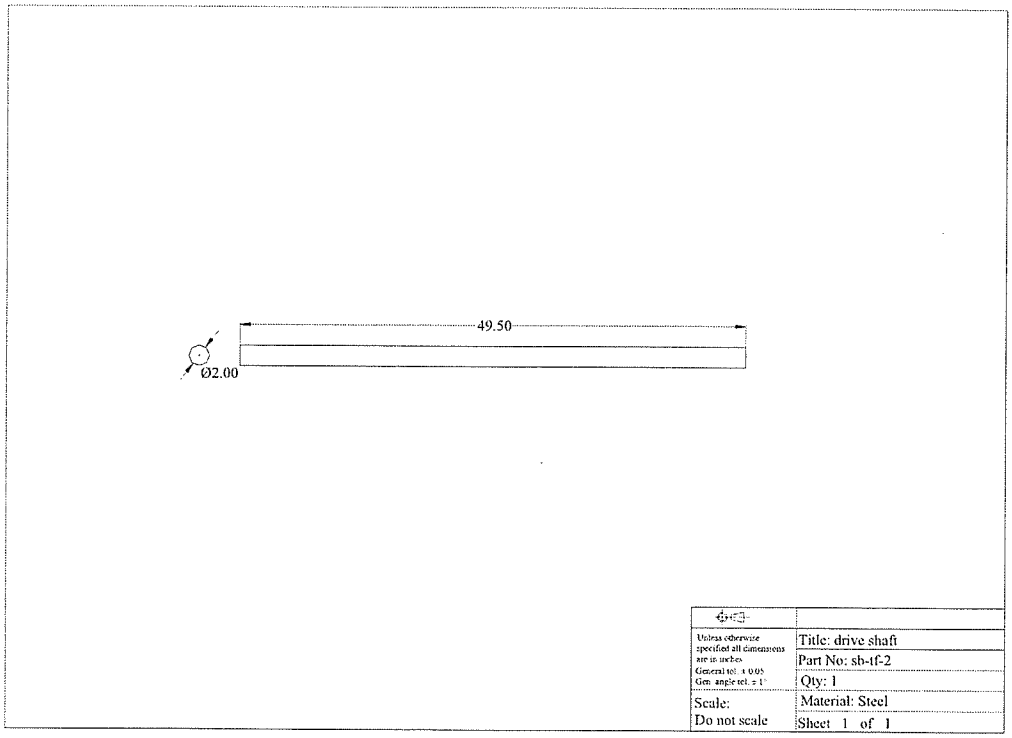

Fig. D. 63 Detail dimensions, sb-tf-2

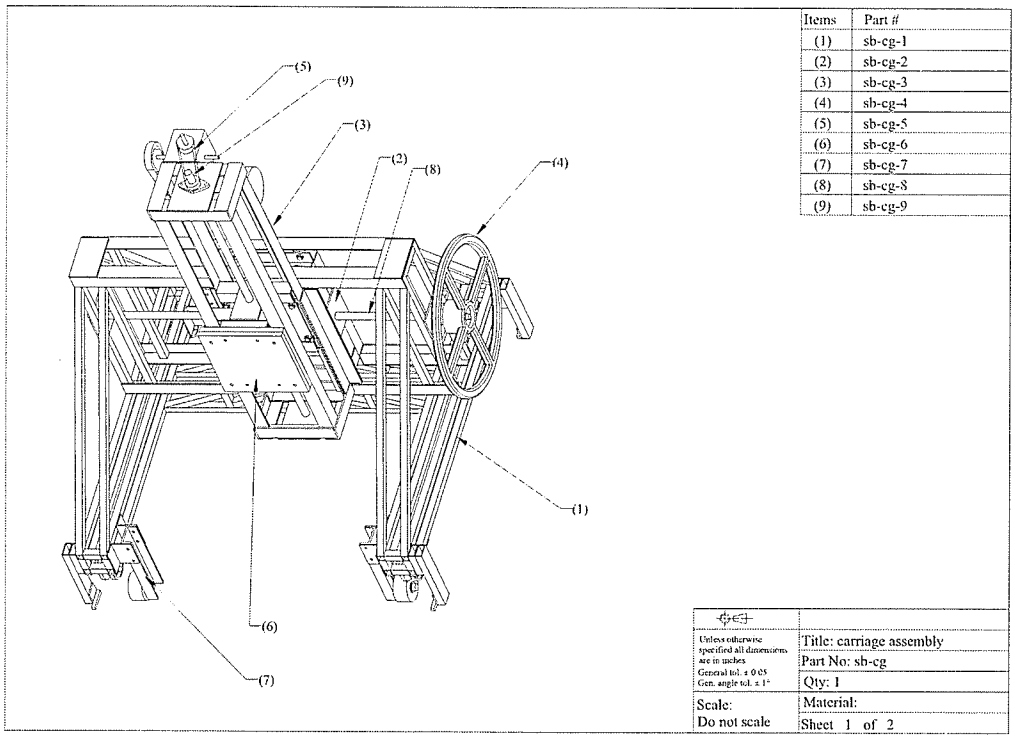

Items	Part #
(1)	sb-cg-1
(2)	sb-cg-2
(3)	sb-cg-3
(4)	sb-cg-4
(5)	sb-cg-5
(6)	sb-cg-6
(7)	sb-cg-7
(8)	sb-cg-8
(9)	sb-cg-9

Unless otherwise specified all dimensions are in inches General tol. ± 0.05 Gen. angle tol. ± 1°	Title: carriage assembly Part No: sb-cg Qty: 1
Scale: Do not scale	Material: Sheet 1 of 2

Fig. D. 64 Carriage assembly components

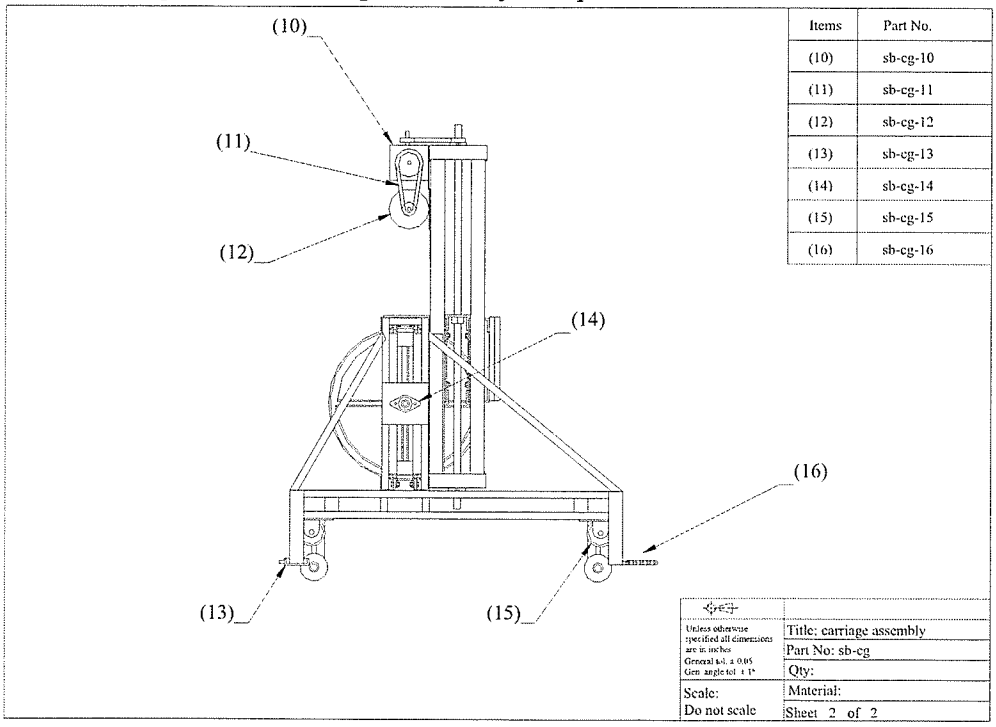

Items	Part No.
(10)	sb-cg-10
(11)	sb-cg-11
(12)	sb-cg-12
(13)	sb-cg-13
(14)	sb-cg-14
(15)	sb-cg-15
(16)	sb-cg-16

Unless otherwise specified all dimensions are in inches General tol. ± 0.05 Gen. angle tol ± 1°	Title: carriage assembly Part No: sb-cg Qty:
Scale: Do not scale	Material: Sheet 2 of 2

Fig. D. 65 Carriage assembly components (side view)

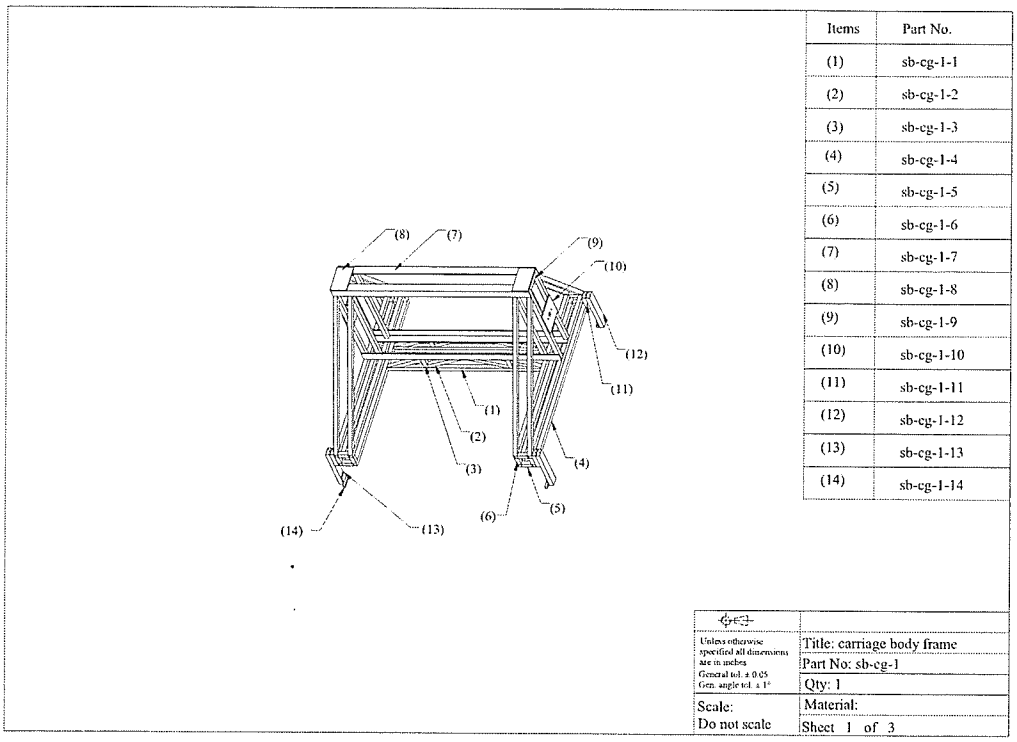

Items	Part No.
(1)	sb-cg-1-1
(2)	sb-cg-1-2
(3)	sb-cg-1-3
(4)	sb-cg-1-4
(5)	sb-cg-1-5
(6)	sb-cg-1-6
(7)	sb-cg-1-7
(8)	sb-cg-1-8
(9)	sb-cg-1-9
(10)	sb-cg-1-10
(11)	sb-cg-1-11
(12)	sb-cg-1-12
(13)	sb-cg-1-13
(14)	sb-cg-1-14

Unless otherwise specified all dimensions are in inches General tol. ± 0.05 Gen. angle tol. ± 1°	Title: carriage body frame Part No: sb-cg-1 Qty: 1
Scale: Do not scale	Material: Sheet 1 of 3

Fig. D. 66 Carriage body frame members

Items	Part No.
(15)	sb-cg-1-14
(16)	sb-cg-1-16
(17)	sb-cg-1-17
(18)	sb-cg-1-18

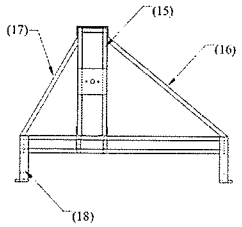

Unless otherwise specified all dimensions are in inches General tol. ± 0.05 Gen. angle tol. ± 1°	Title: carriage body frame Part No: sb-cg-1 Qty:
Scale: Do not scale	Material: Sheet 2 of 3

Fig. D. 67 Carriage body frame members

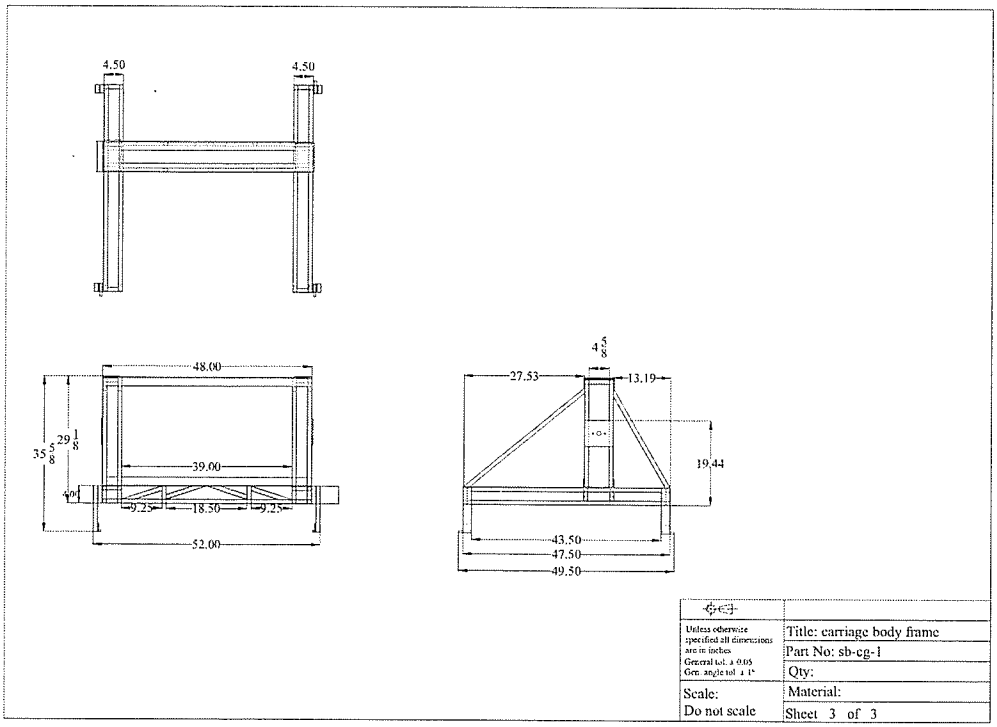

Fig. D. 68 Carriage body frame dimensions

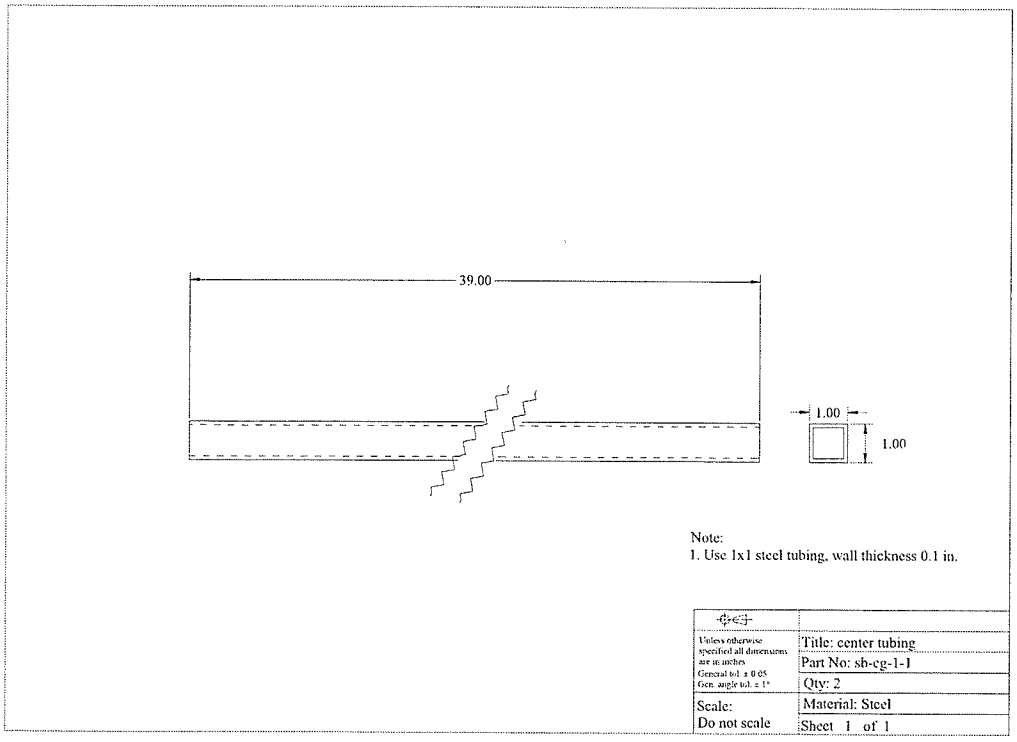

Fig. D. 69 Detail dimensions, sb-cg-1-1

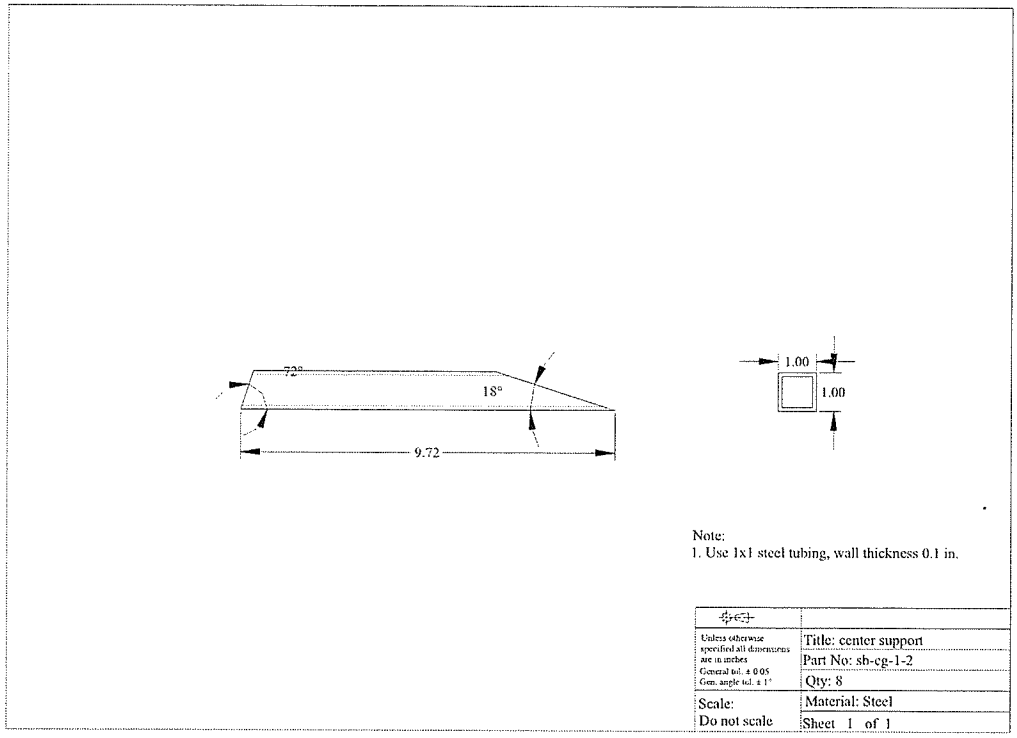

Fig. D. 70 Detail dimensions, sb-sg-1-2

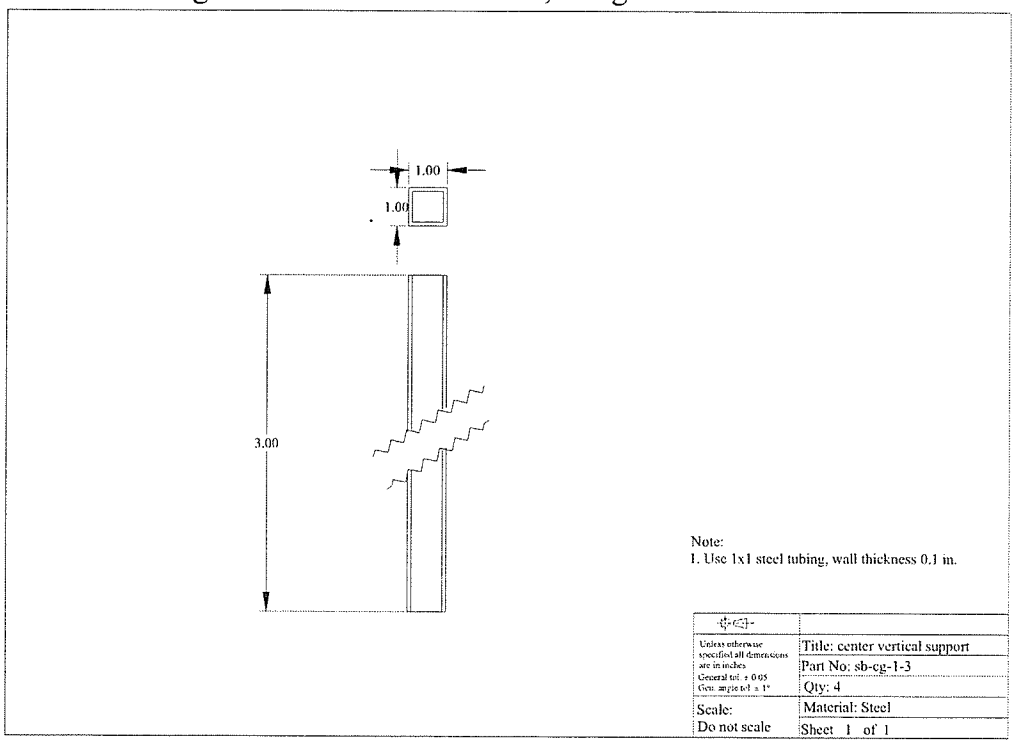

Fig. D. 71 Detail dimensions, sb-cg-1-3

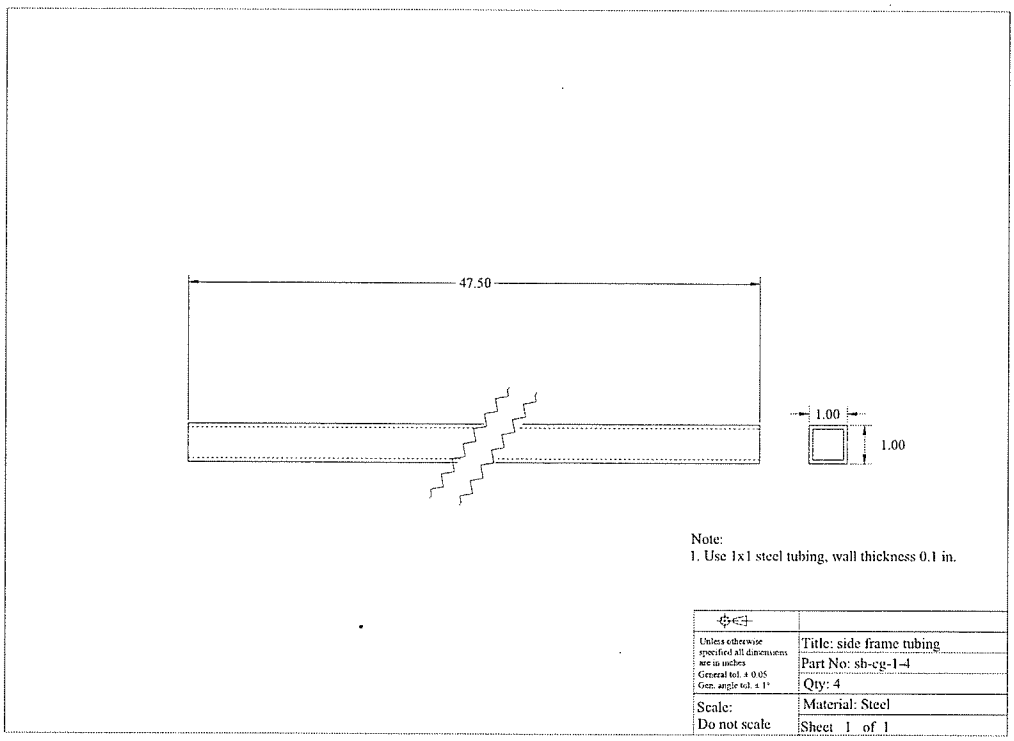

Fig. D. 72 Detail dimensions, sb-cg-1-4

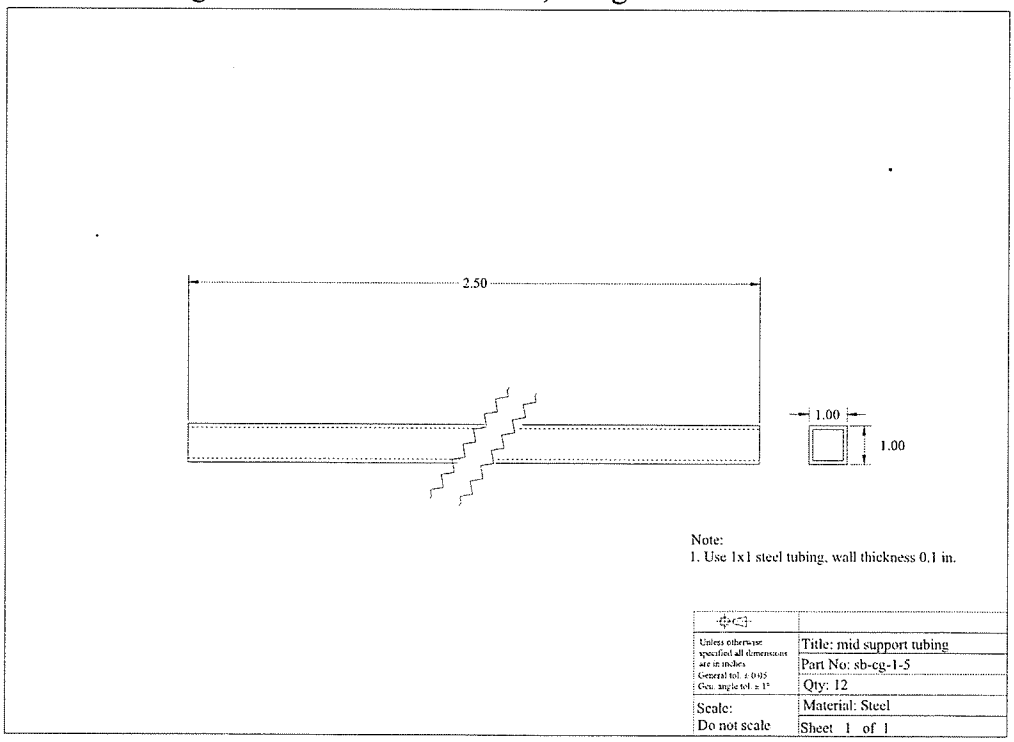

Fig. D. 73 Detail dimensions, sb-cg-1-5

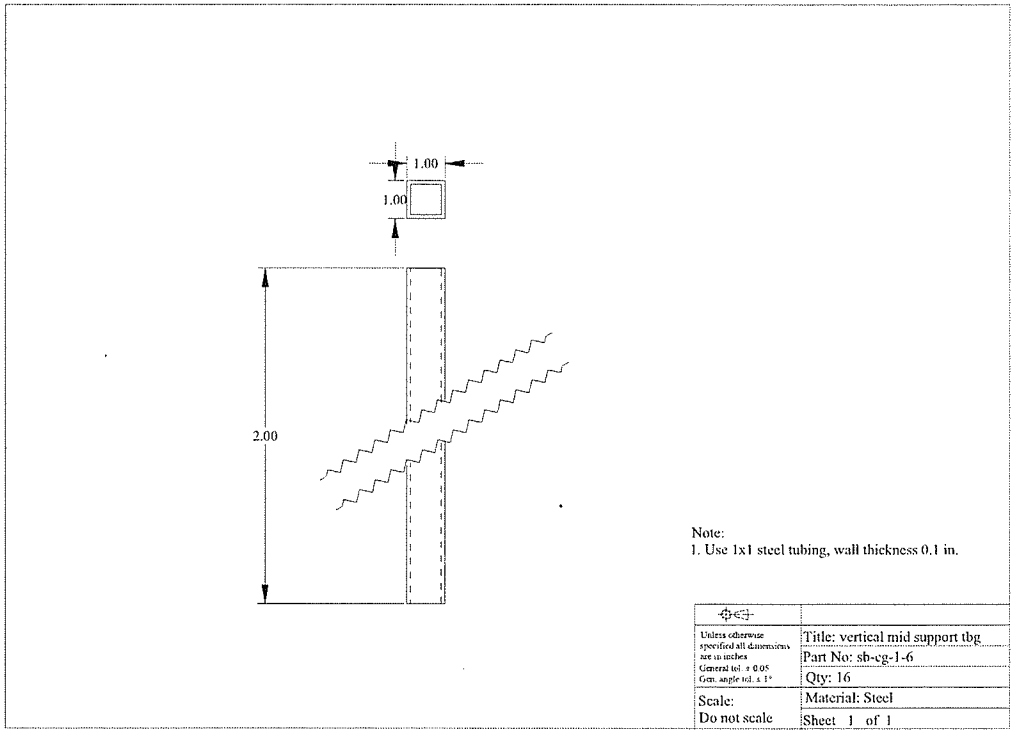

Fig. D. 74 Detail dimensions, sb-cg-1-6

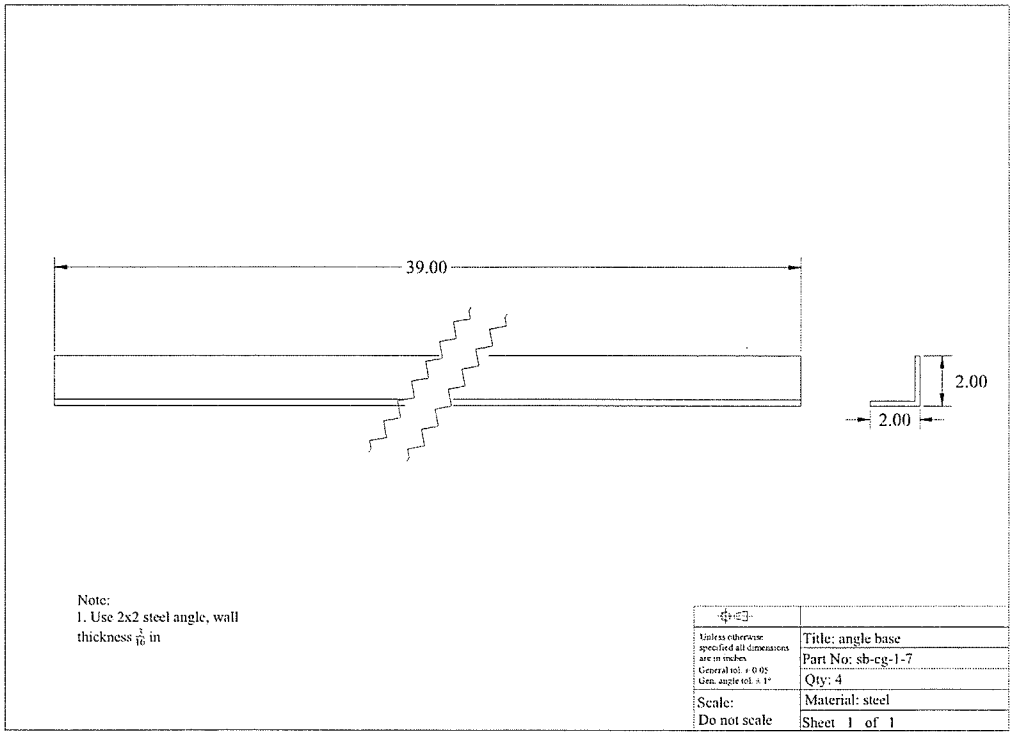

Fig. D. 75 Detail dimensions, sb-cg-1-7

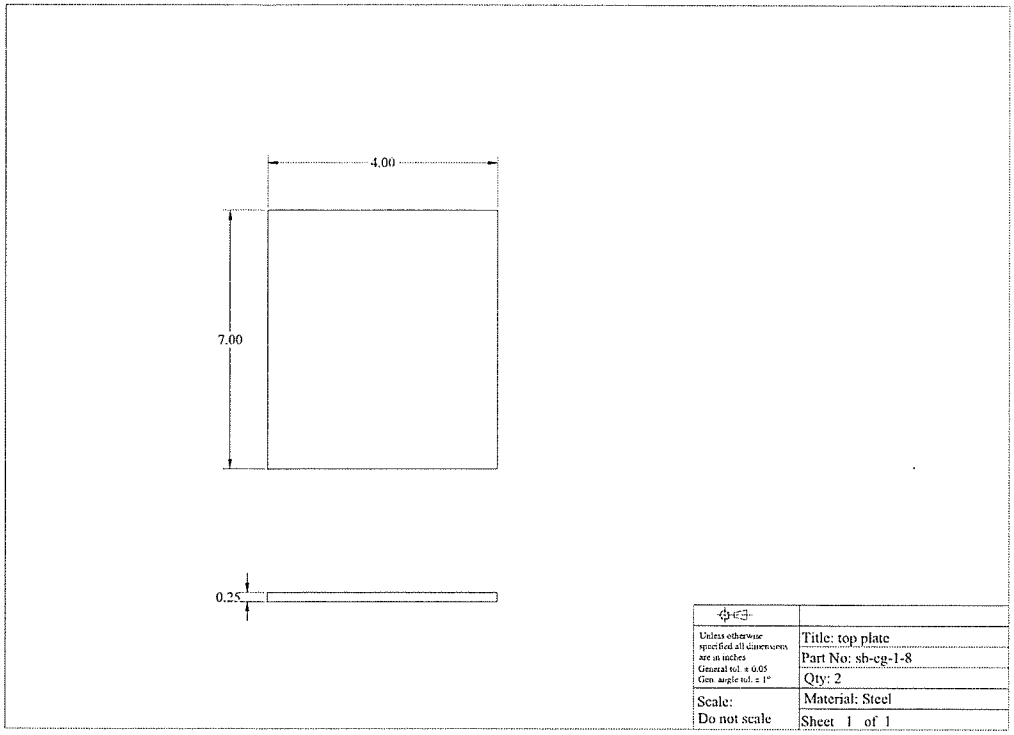

Fig. D. 76 Detail dimensions, sb-cg-1-8

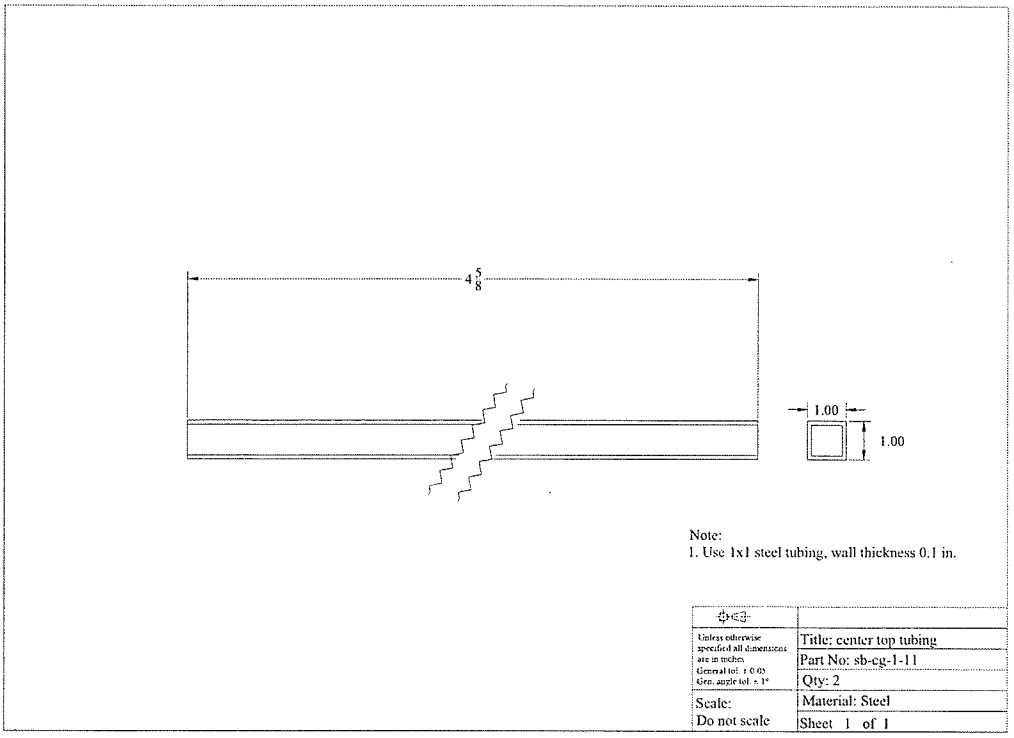

Fig. D. 77 Detail dimensions, sb-cg-1-9

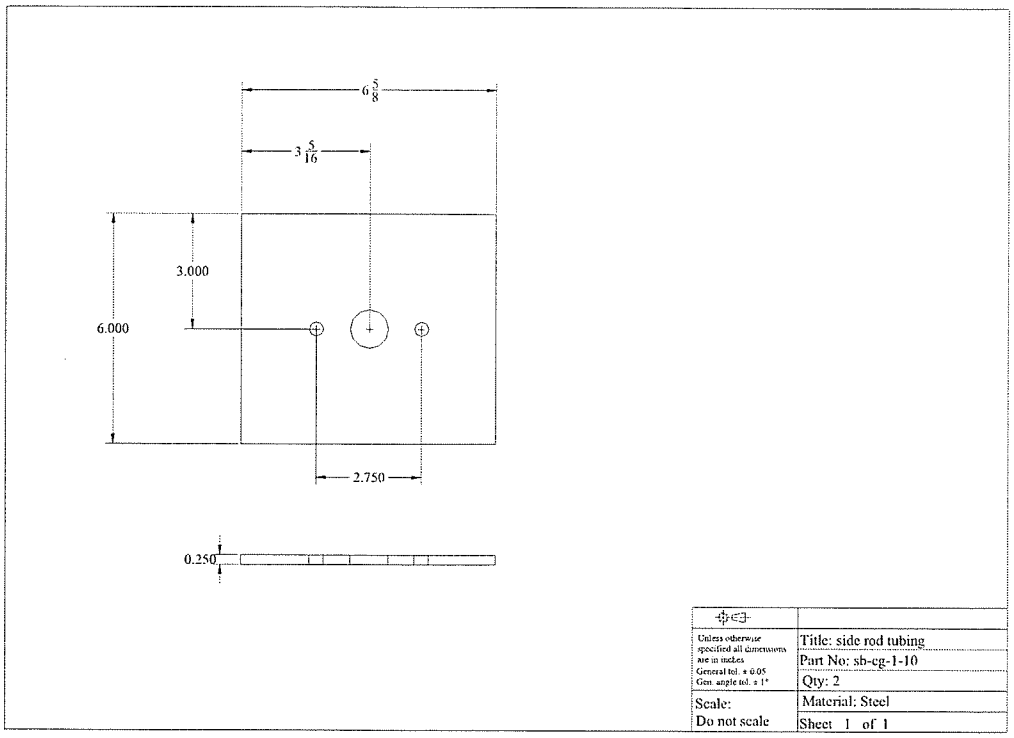

Fig. D. 78 Detail dimensions, sb-cg-1-10

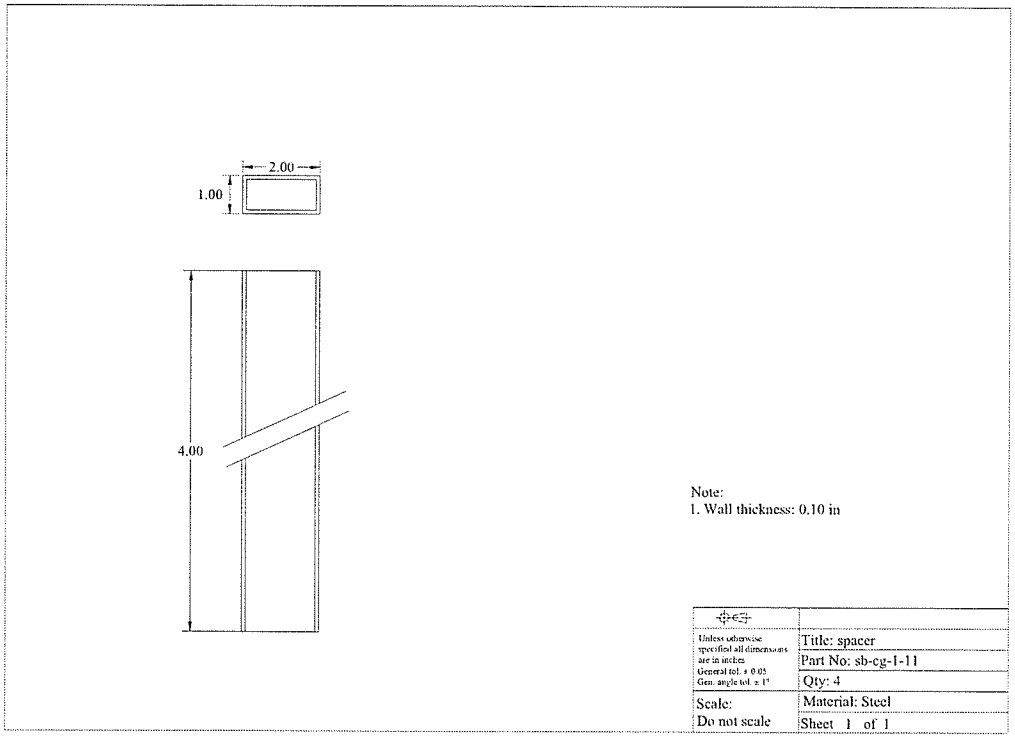

Fig. D. 79 Detail dimensions, sb-cg-1-11

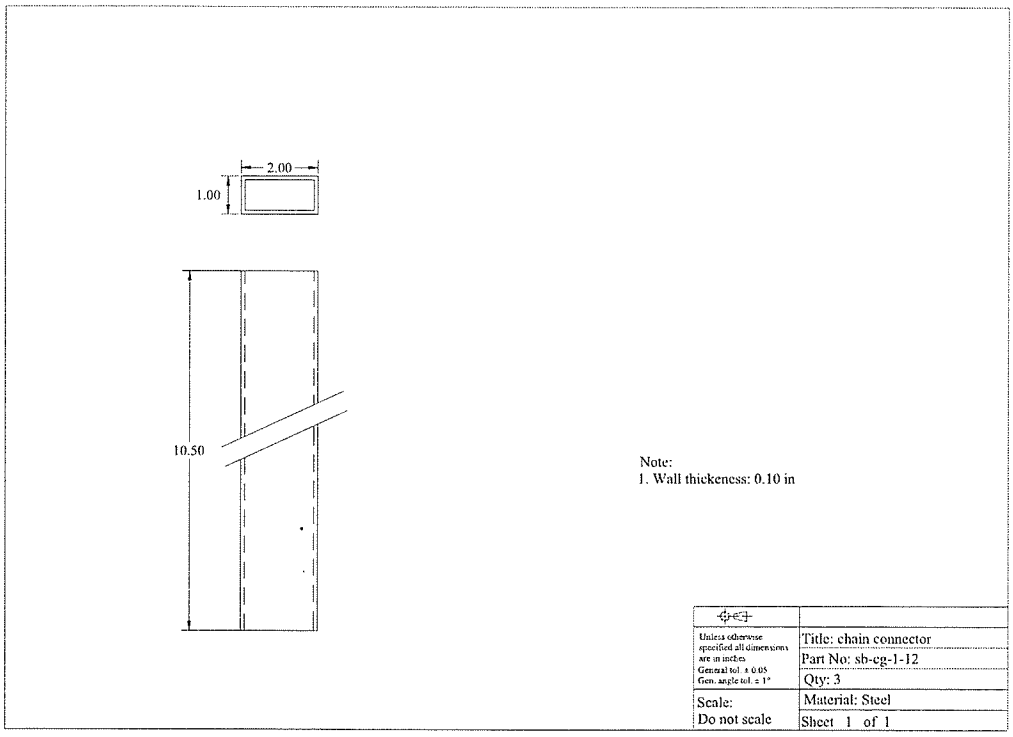

Fig. D. 80 Detail dimensions, sb-cg-1-12

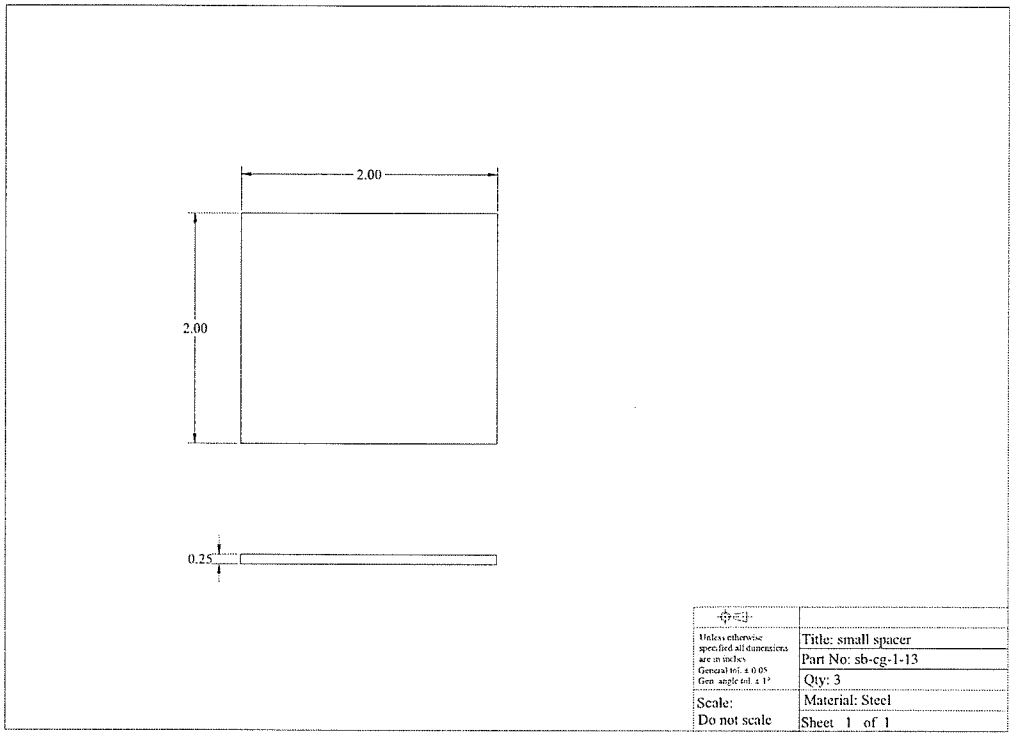

Fig. D. 81 Detail dimensions, sb-cg-1-13

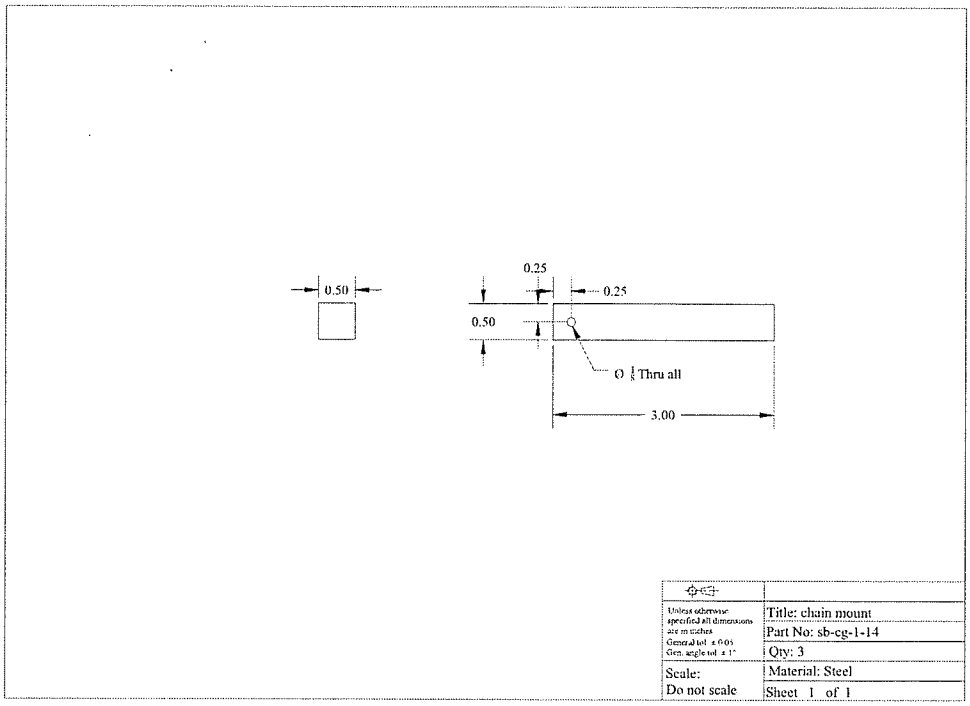

Fig. D. 82 Detail dimensions, sb-cg-1-14

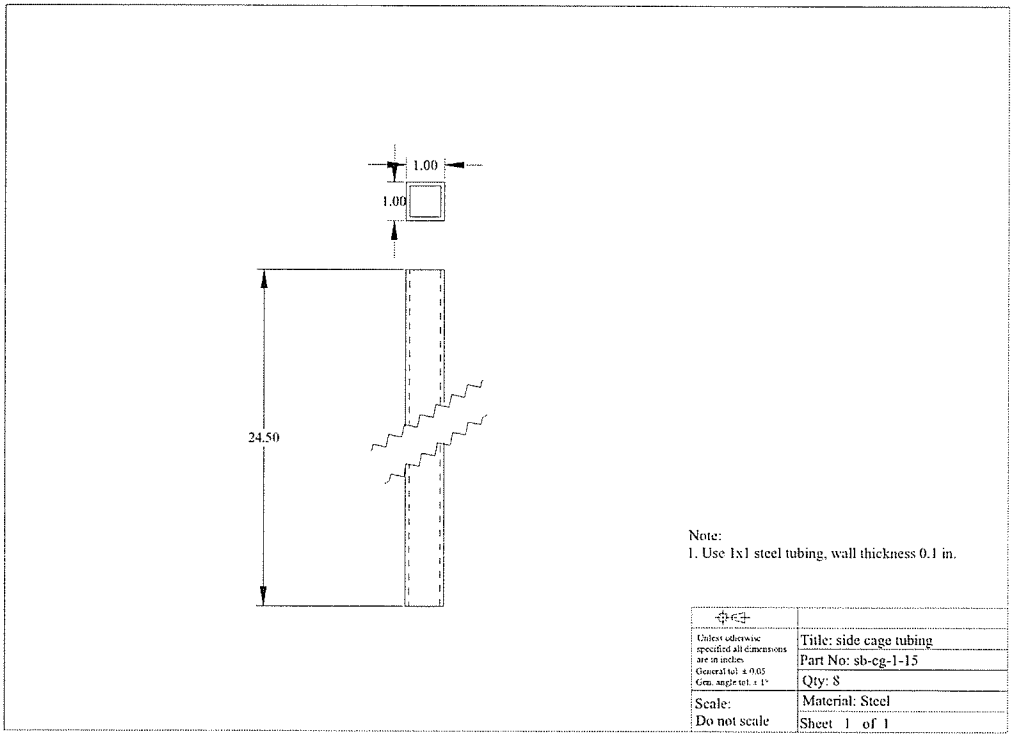

Fig. D. 83 Detail dimensions, sb-cg-1-15

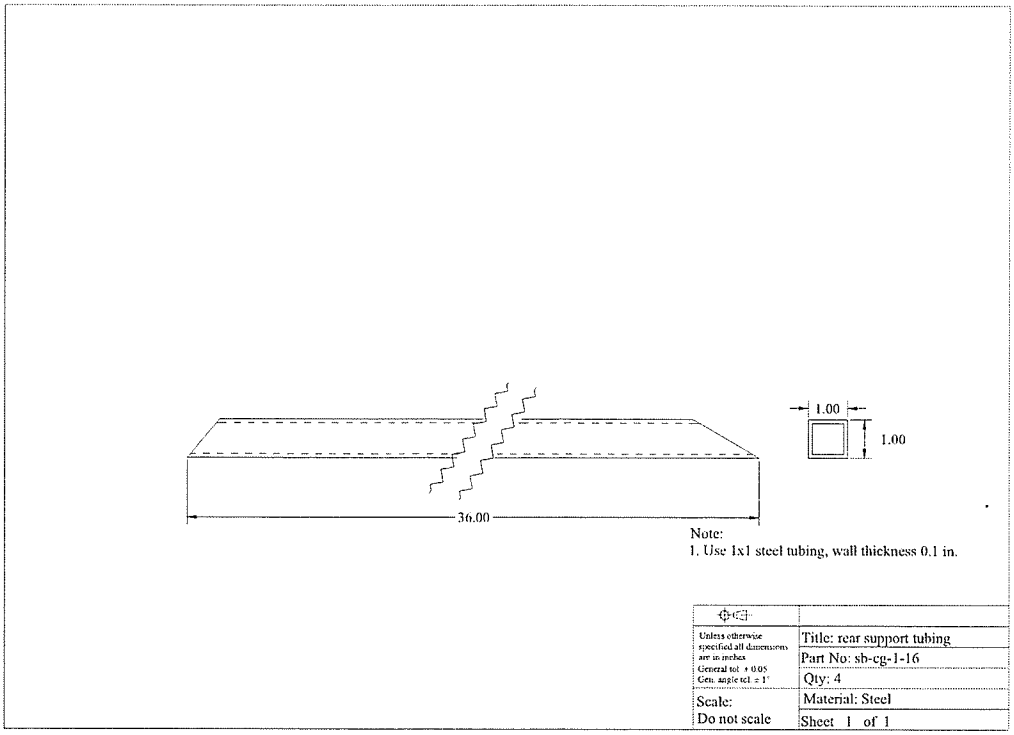

Fig. D. 84 Detail dimensions, sb-cg-1-16

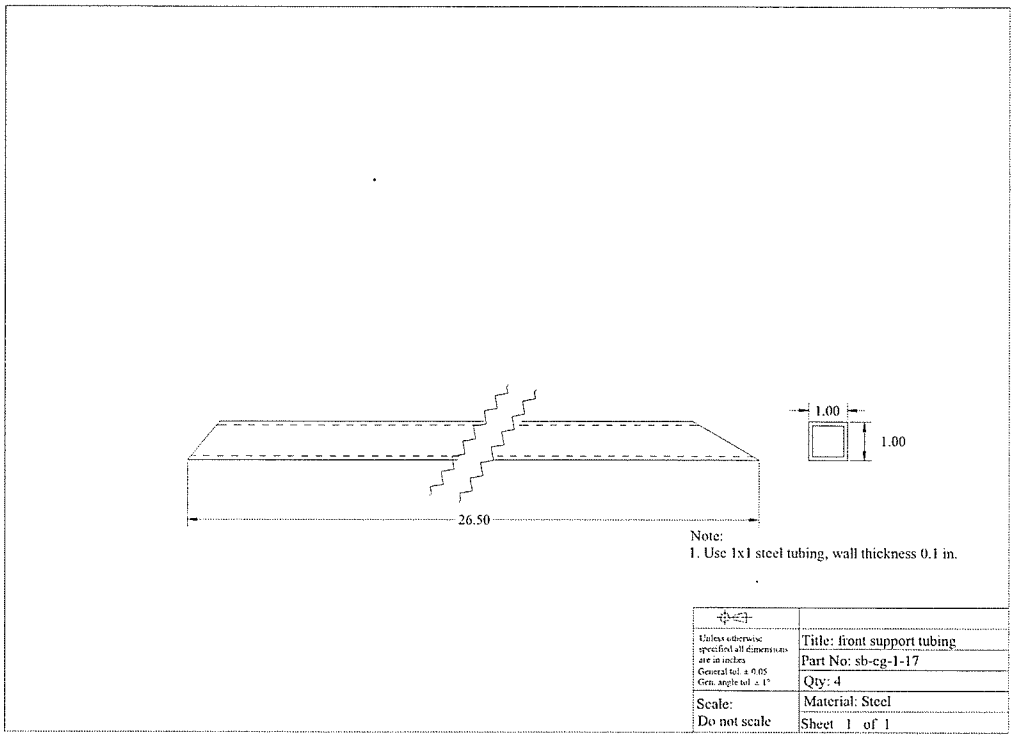

Fig. D. 85 Detail dimensions, sb-cg-1-17

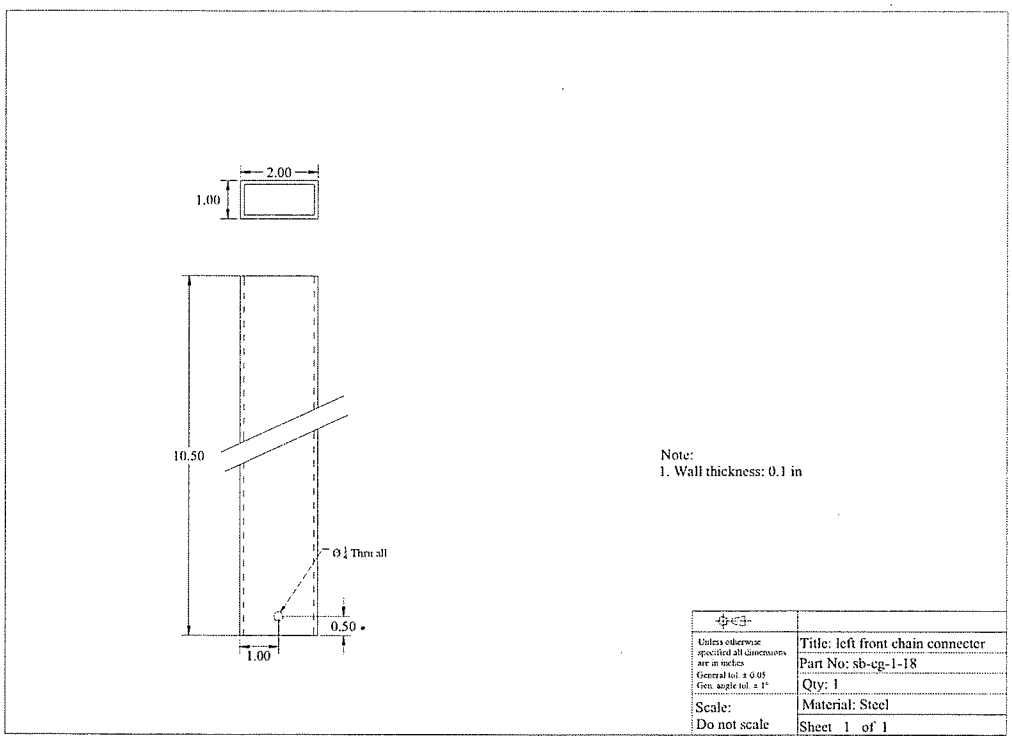

Fig. D. 86 Detail dimensions, sb-cg-1-18

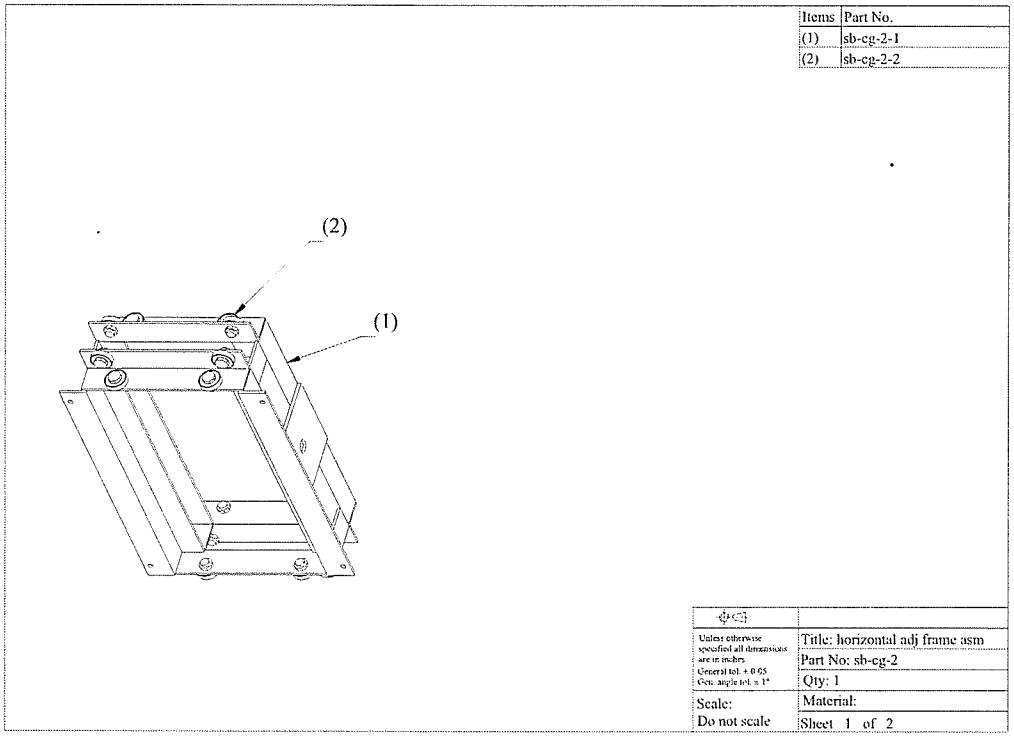

Fig. D. 87 Lateral adjustment frame assembly components

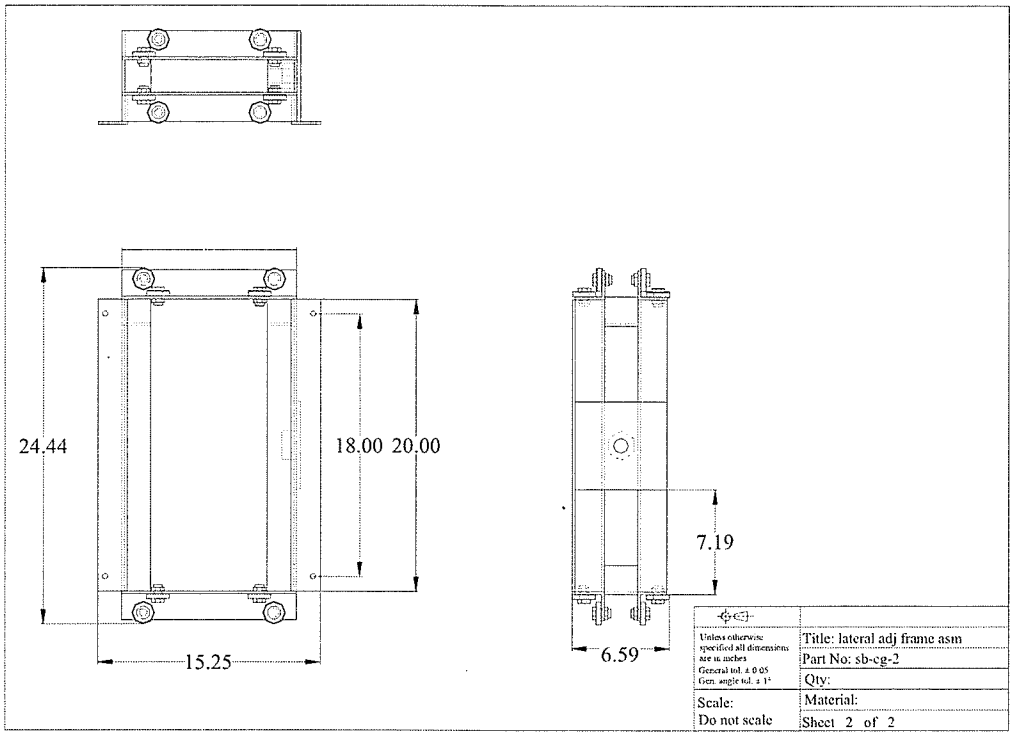

Fig. D. 88 Lateral adjustment frame dimensions

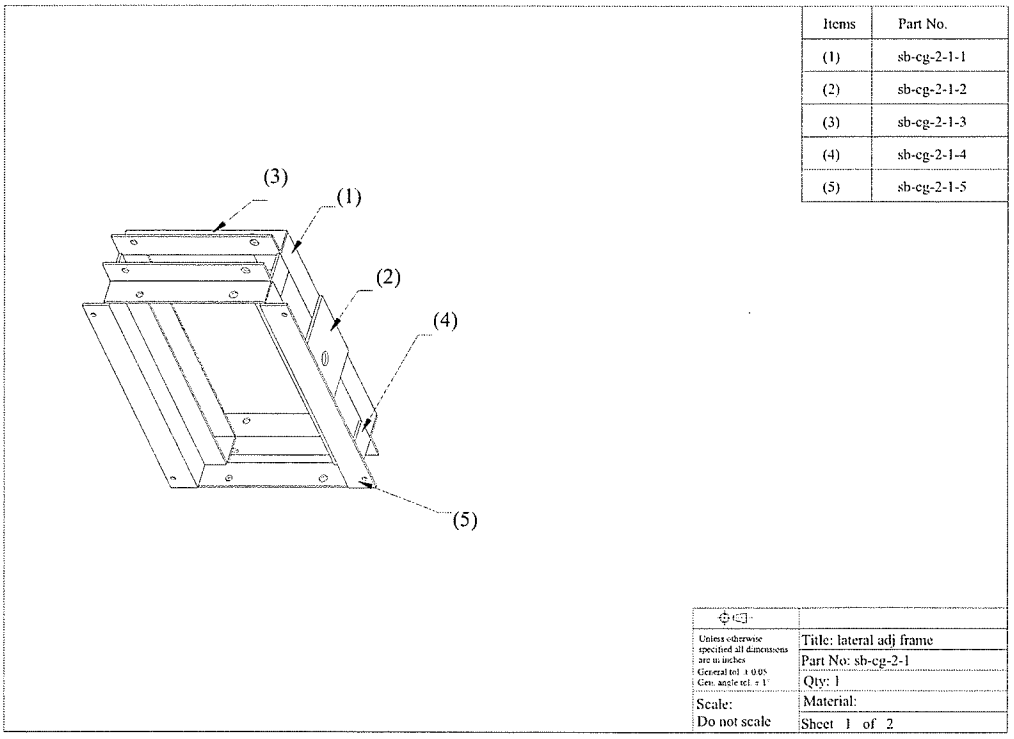

Fig. D. 89 Lateral adjustment frame members

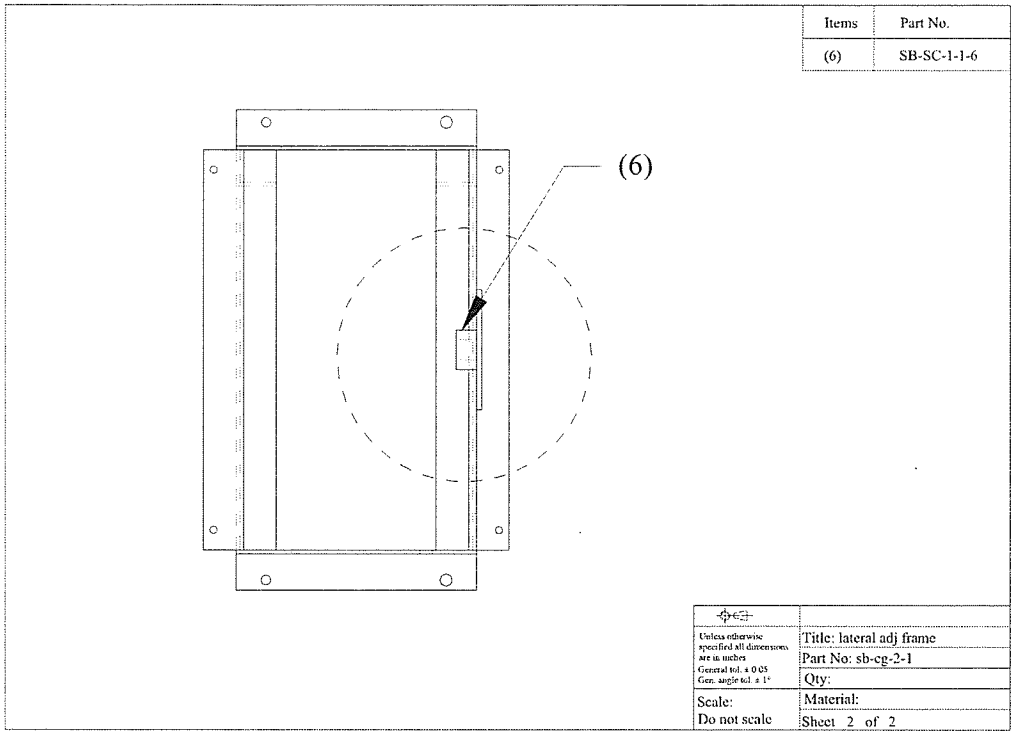

Fig. D. 90 Lateral adjustment frame members (back view)

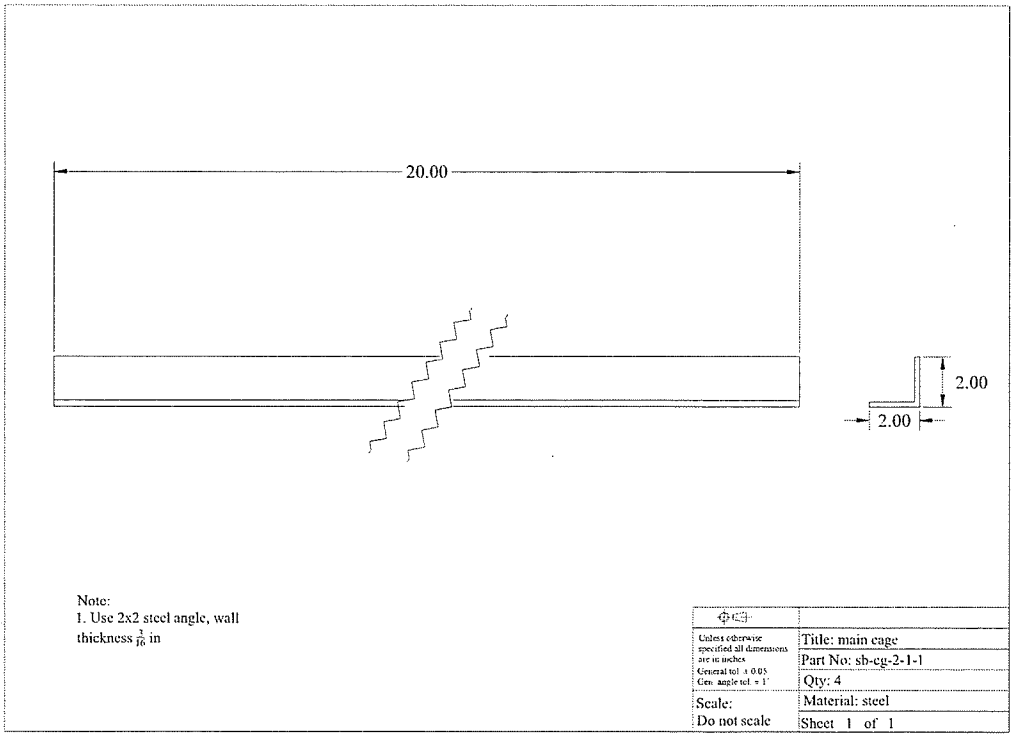

Fig. D. 91 Detail dimensions 2-1-1

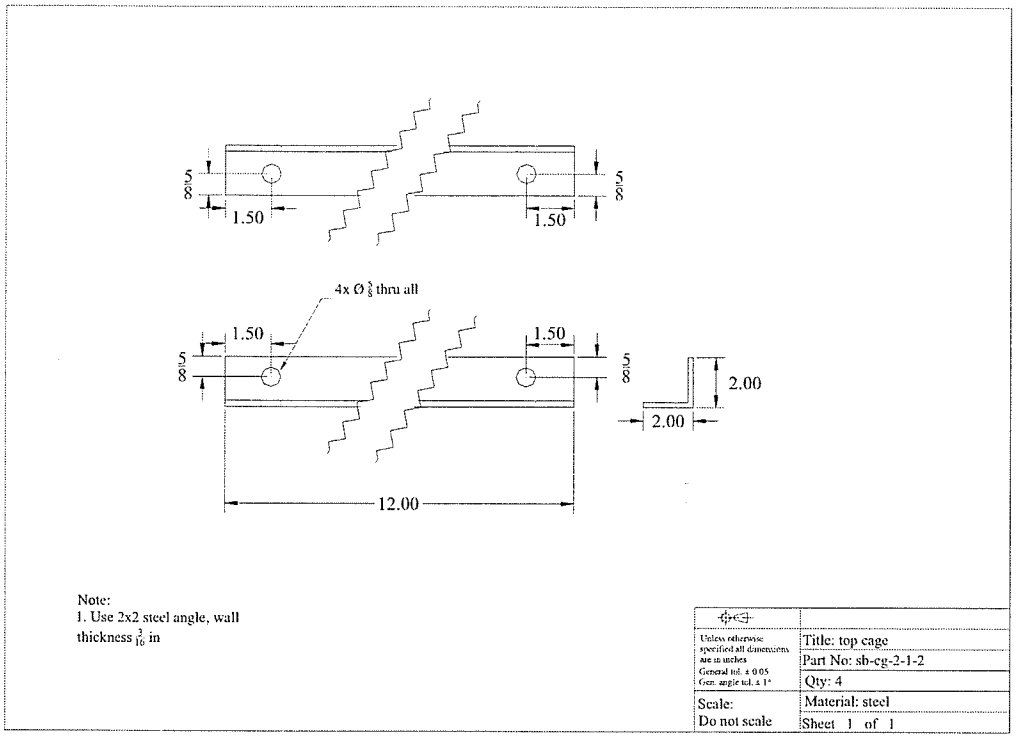

Fig. D. 92 Detail dimensions 2-1-2

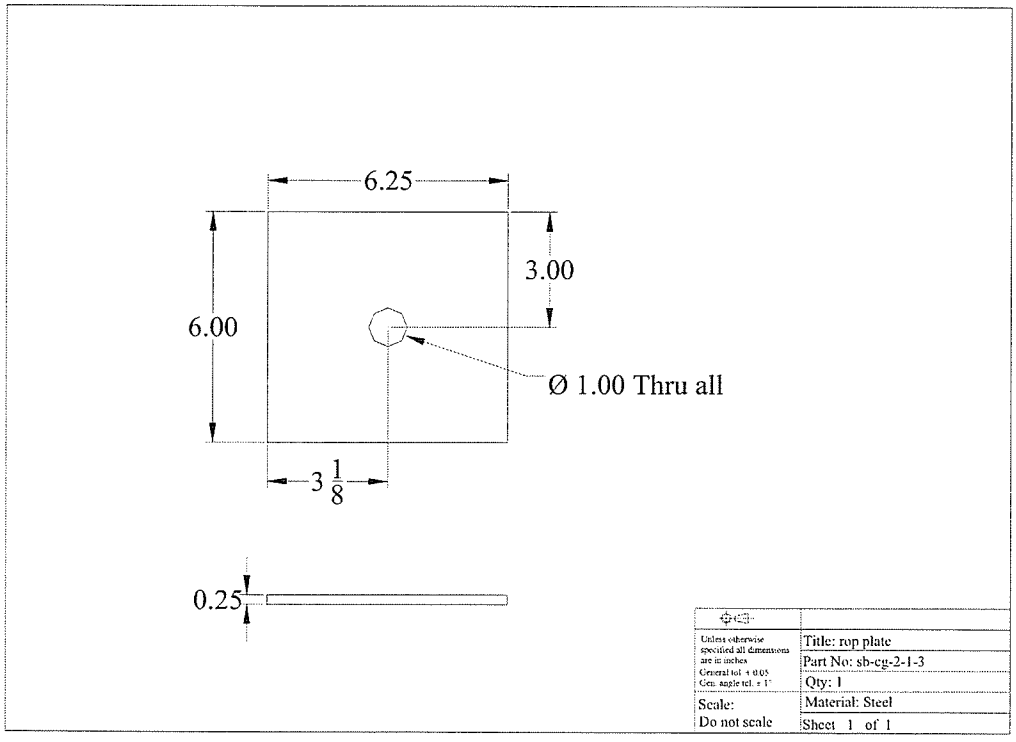

Fig. D. 93 Detail dimensions, sb-cg-2-1-3

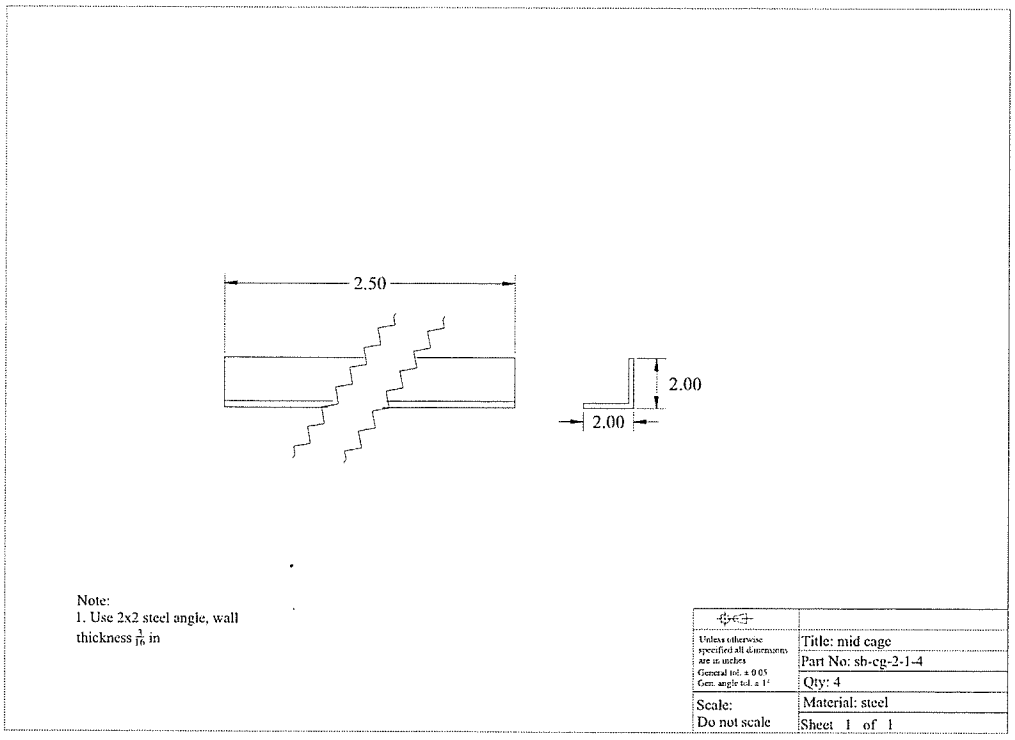

Fig. D. 94 Detail dimensions 3-1-4

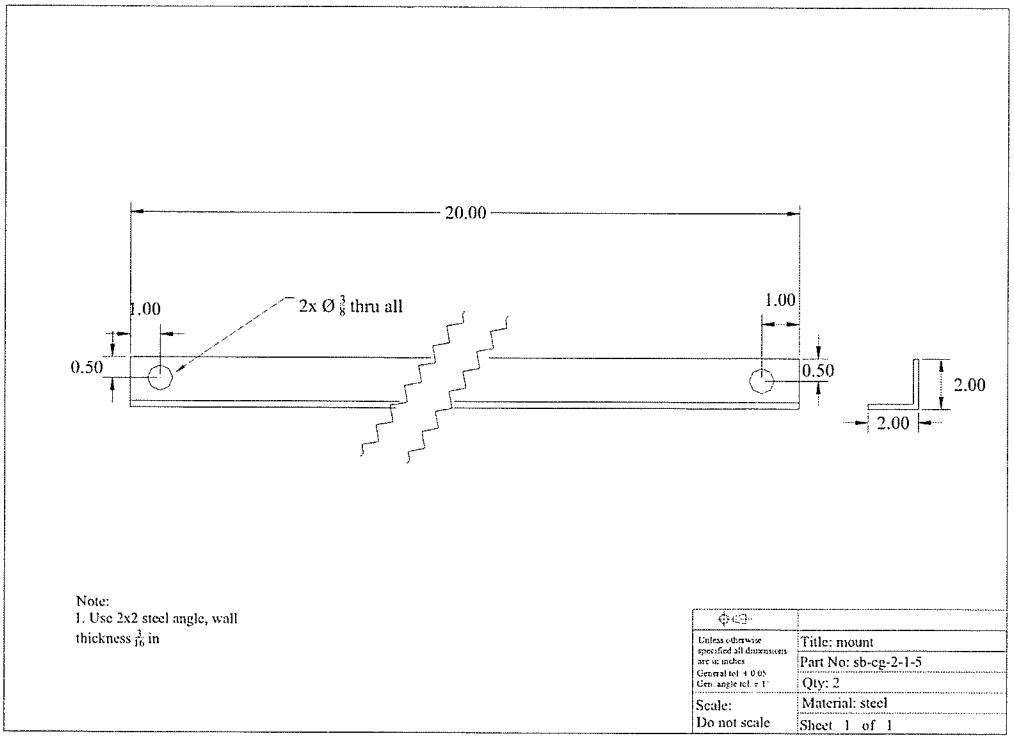

Fig. D. 95 Detail dimensions, sb-cg-3-1-5

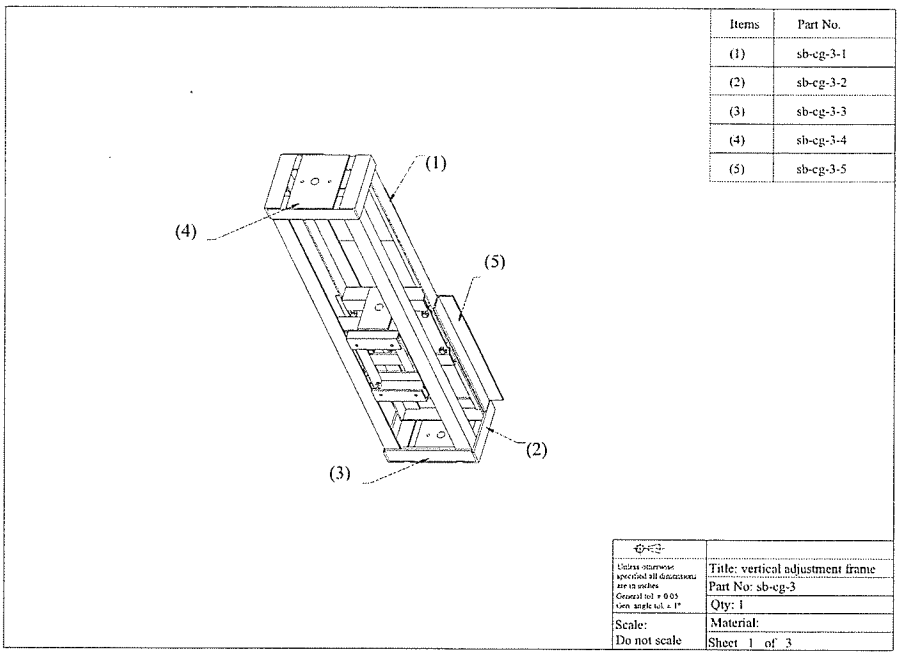

Items	Part No.
(1)	sb-cg-3-1
(2)	sb-cg-3-2
(3)	sb-cg-3-3
(4)	sb-cg-3-4
(5)	sb-cg-3-5

Unless otherwise specified all dimensions are in inches General tol. ± 0.05 Gen. angle tol. ± 1°	Title: vertical adjustment frame
	Part No: sb-cg-3
	Qty: 1
Scale: Do not scale	Material:
	Sheet 1 of 3

Fig. D. 96 Vertical frame members

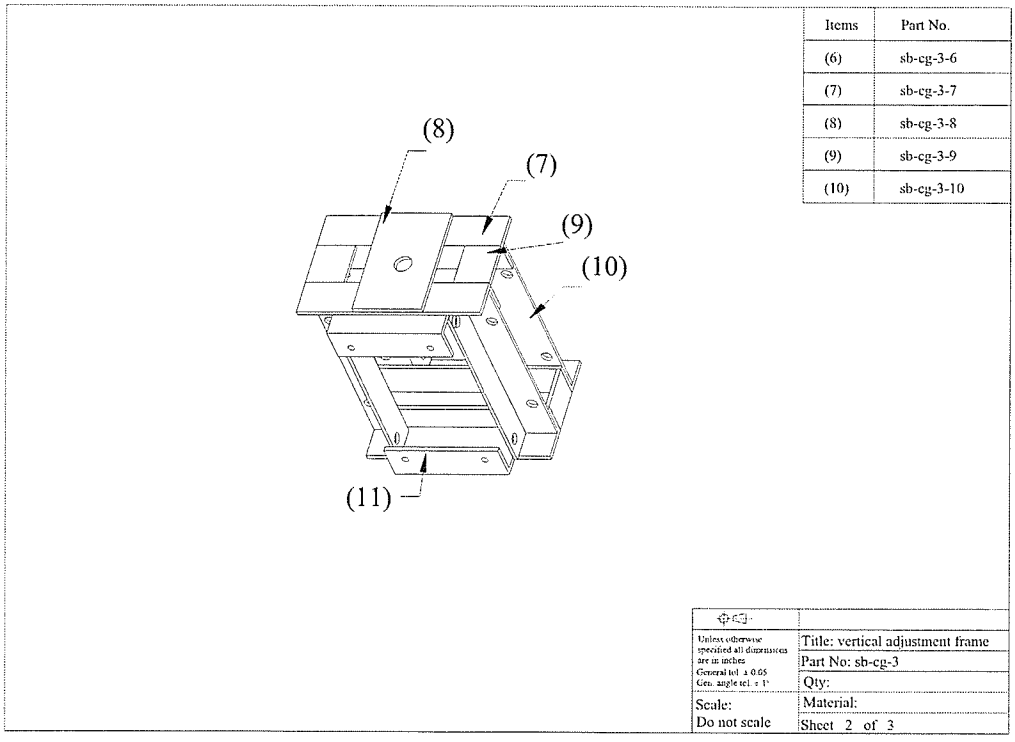

Items	Part No.
(6)	sb-cg-3-6
(7)	sb-cg-3-7
(8)	sb-cg-3-8
(9)	sb-cg-3-9
(10)	sb-cg-3-10

Unless otherwise specified all dimensions are in inches General tol. ± 0.05 Gen. angle tol. ± 1°	Title: vertical adjustment frame
	Part No: sb-cg-3
	Qty:
Scale: Do not scale	Material:
	Sheet 2 of 3

Fig. D. 97 Vertical frame members (inner frame)

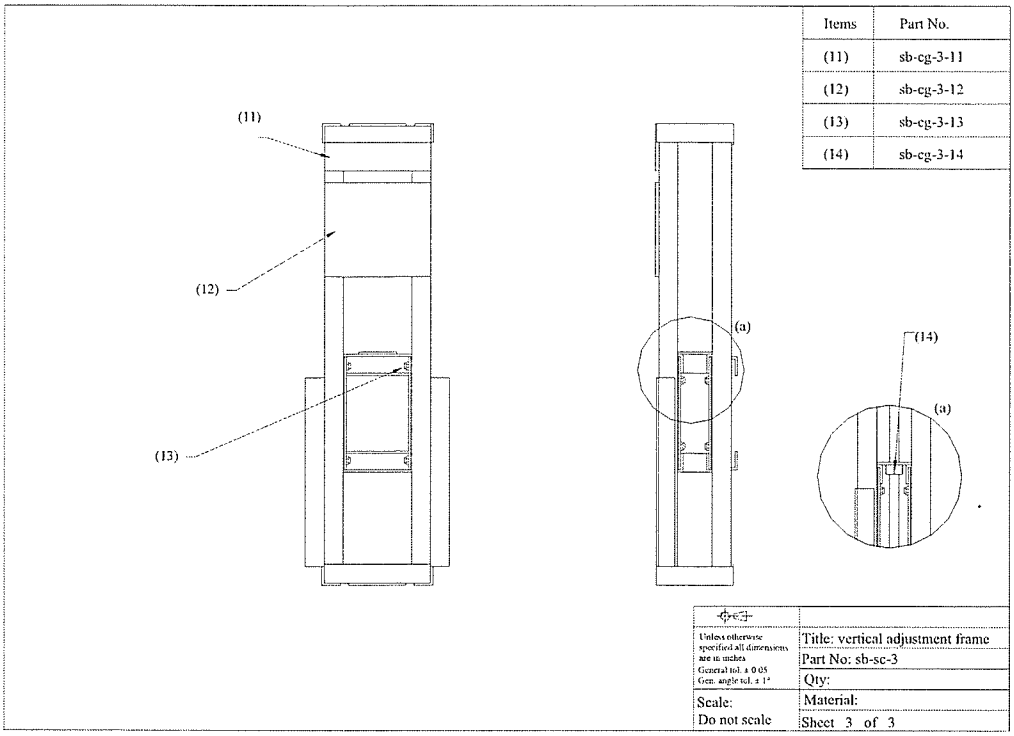

Fig. D. 98 Vertical adjustment members (alternate view)

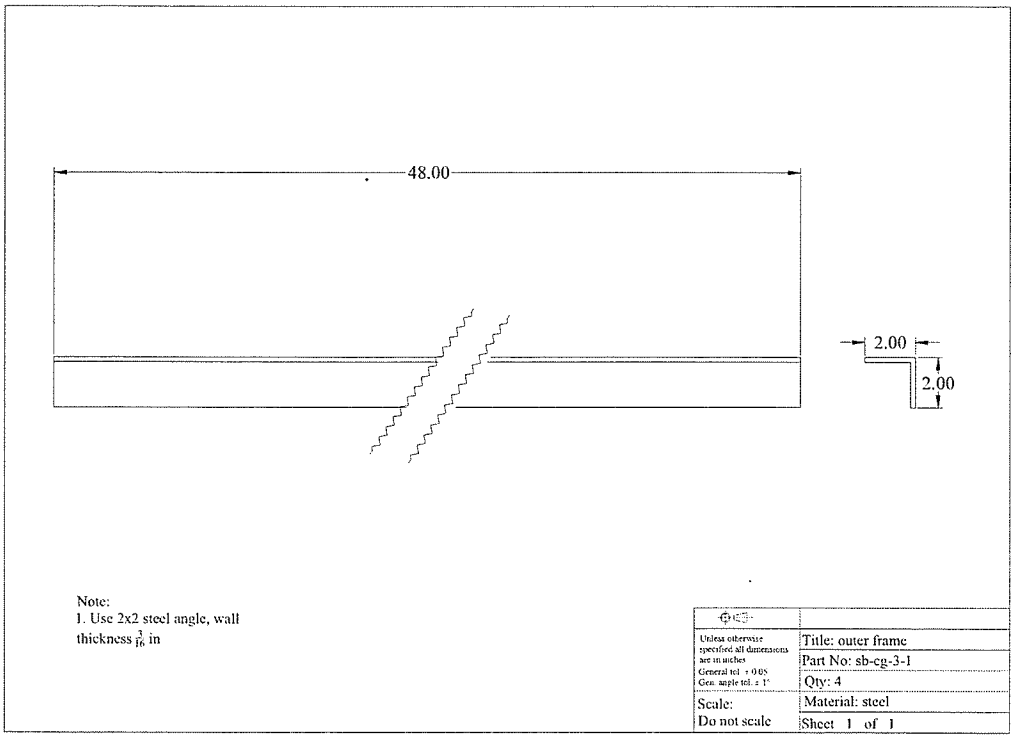

Fig. D. 99 Detail dimensions, sd-cg-3-1

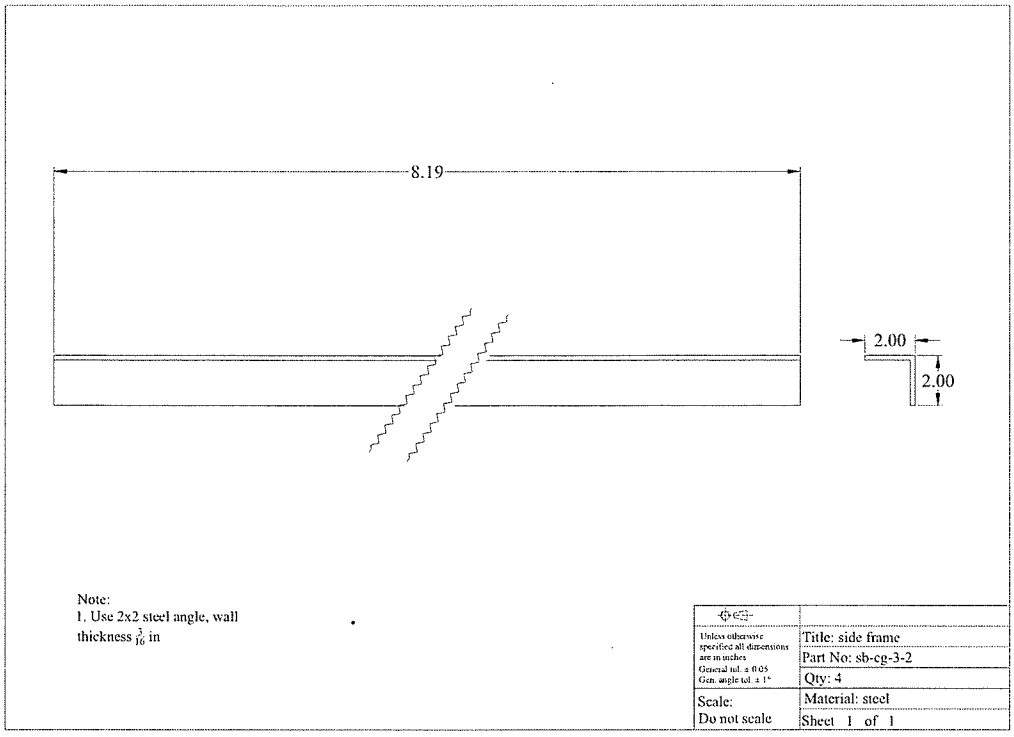

Fig. D. 100 Detail dimensions, sb-cg-3-2

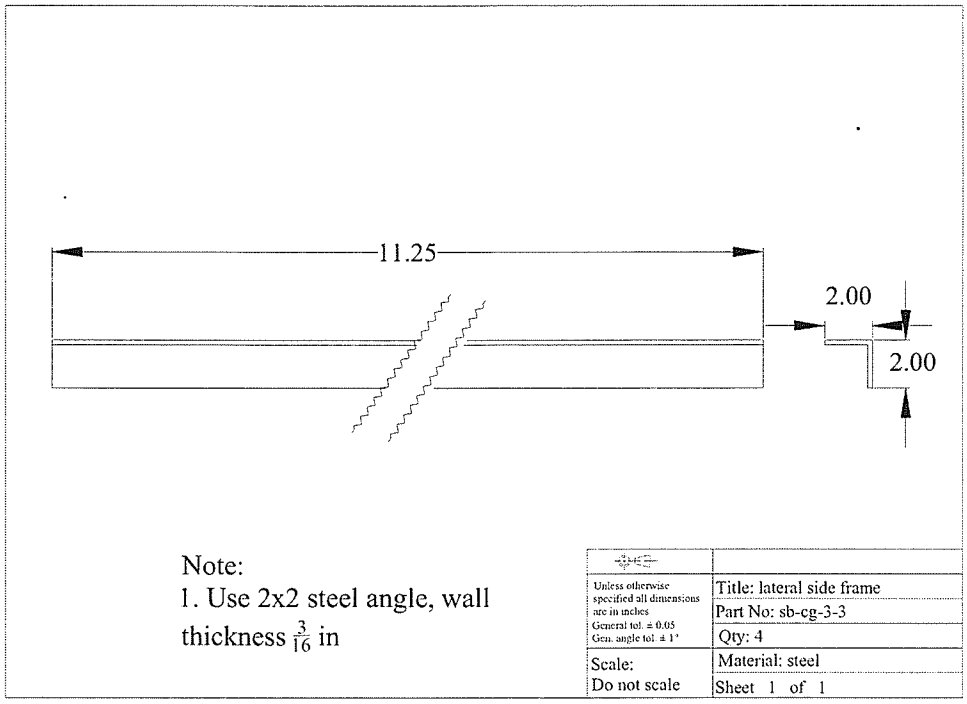

Fig. D. 101 Detail dimensions, sb-cg-3-3

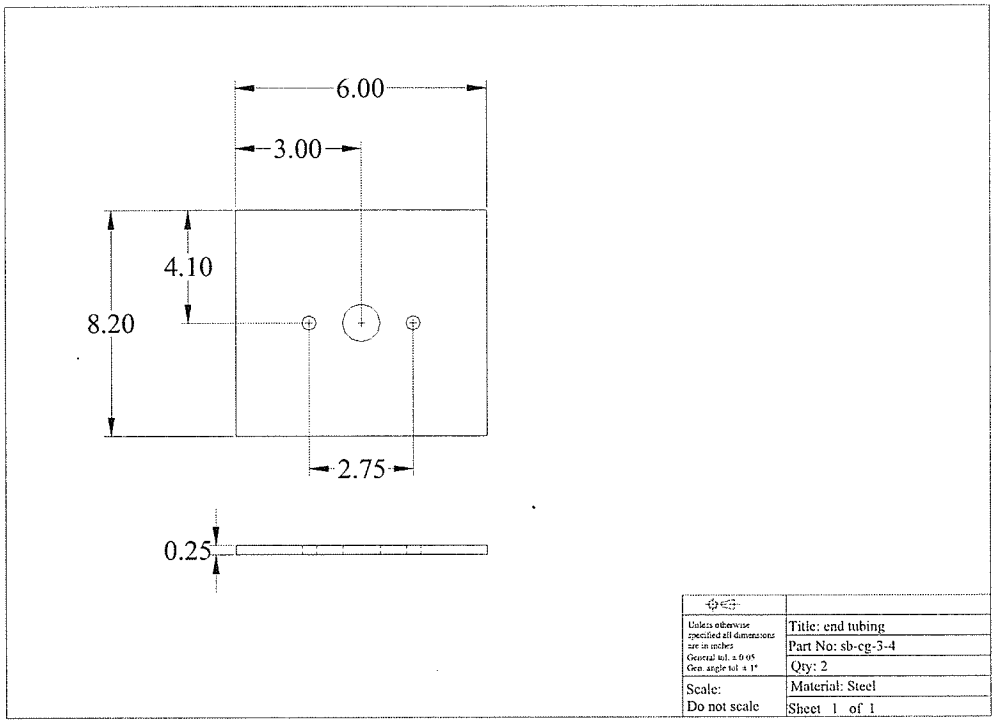

Fig. D. 102 Detail dimensions, sb-cg-3-4

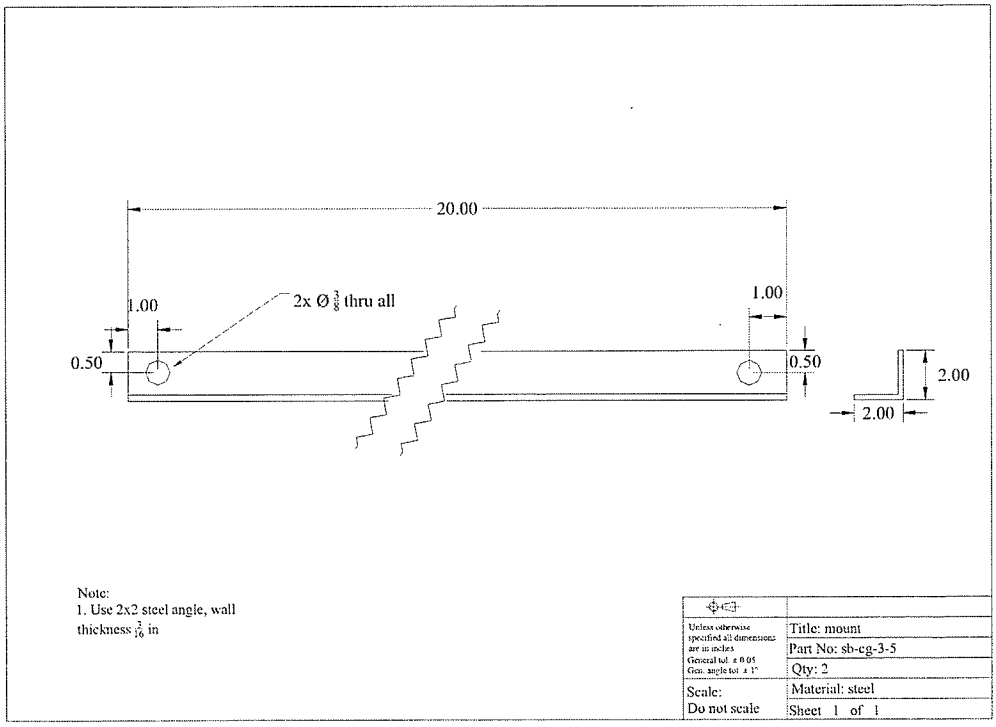

Fig. D. 103 Detail dimensions, sb-cg-3-5

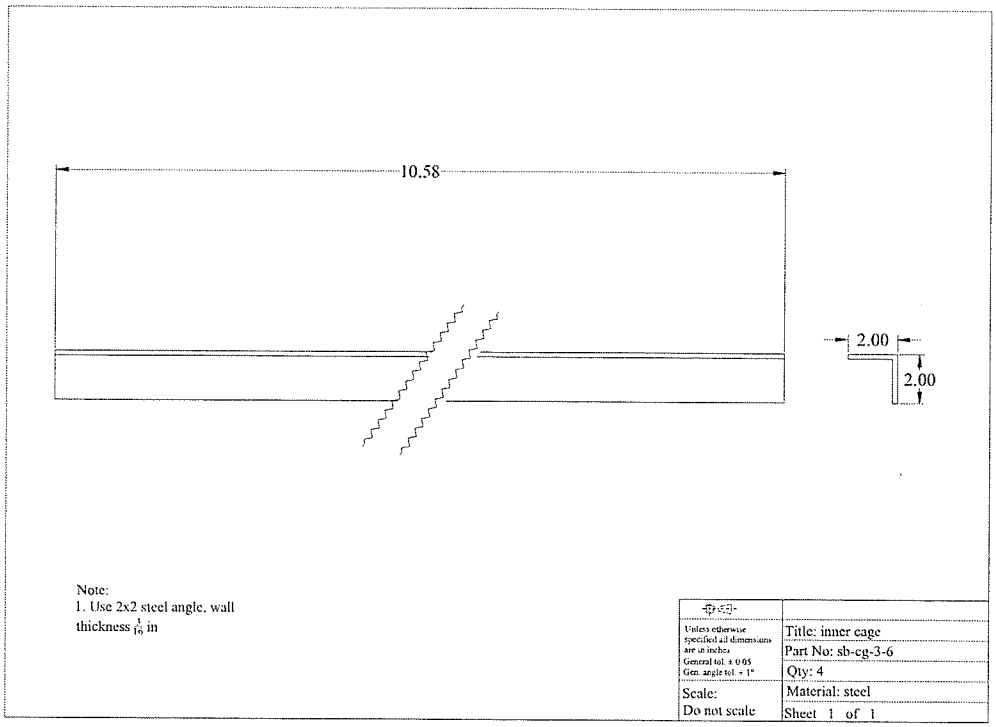

Fig. D. 104 Detail dimensions, sb-cg-3-6

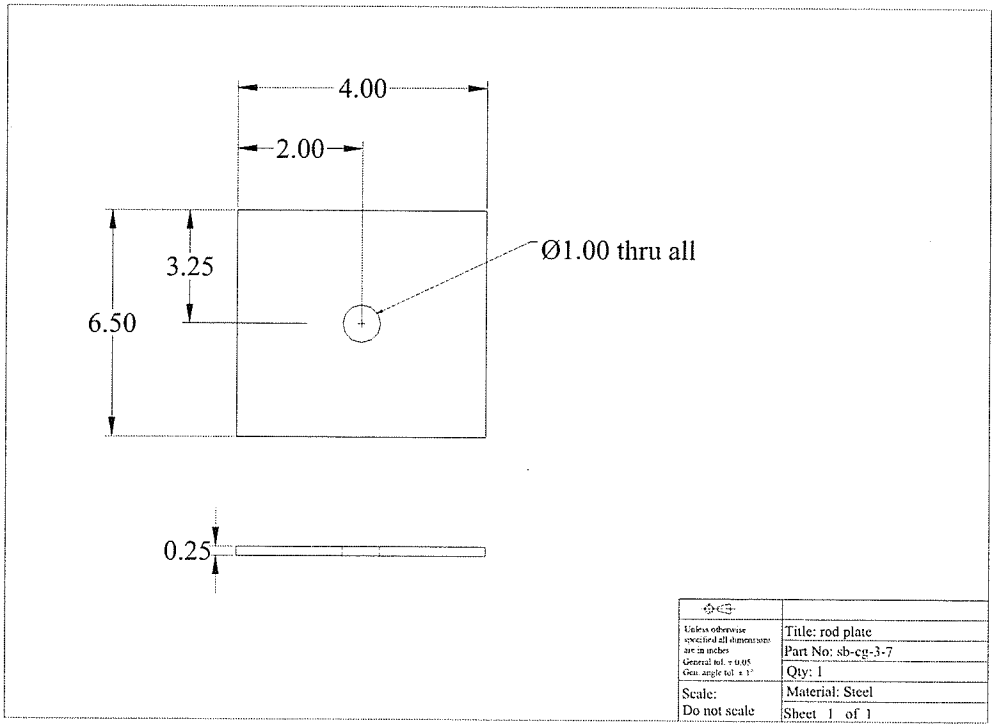

Fig. D. 105 Detail dimensions, sb-cg-3-7

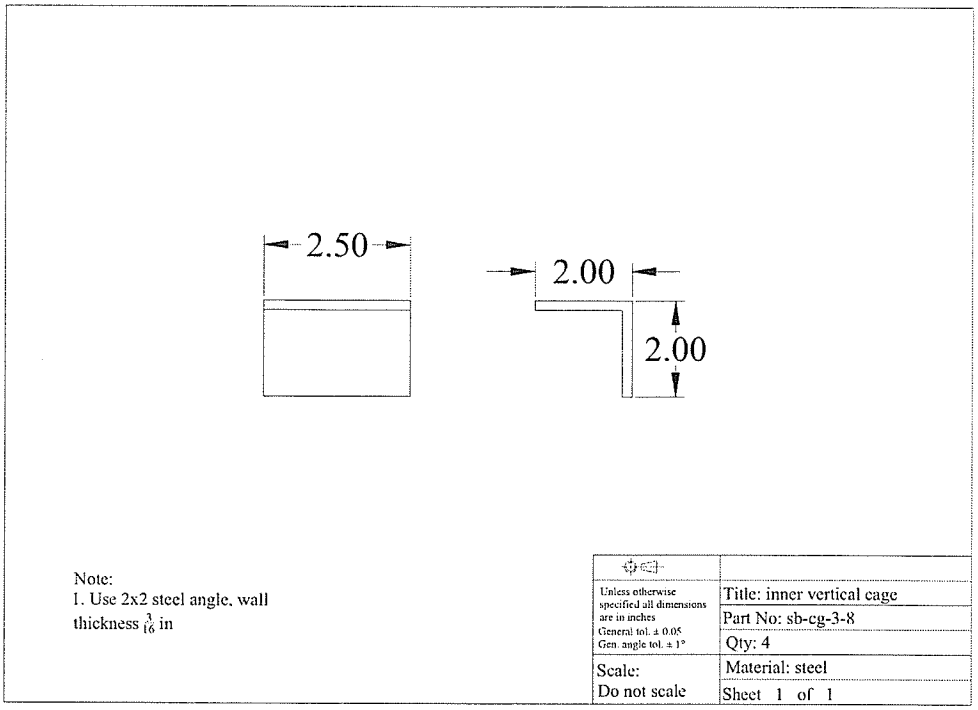

Fig. D. 106 Detail dimensions, sb-cg-3-8

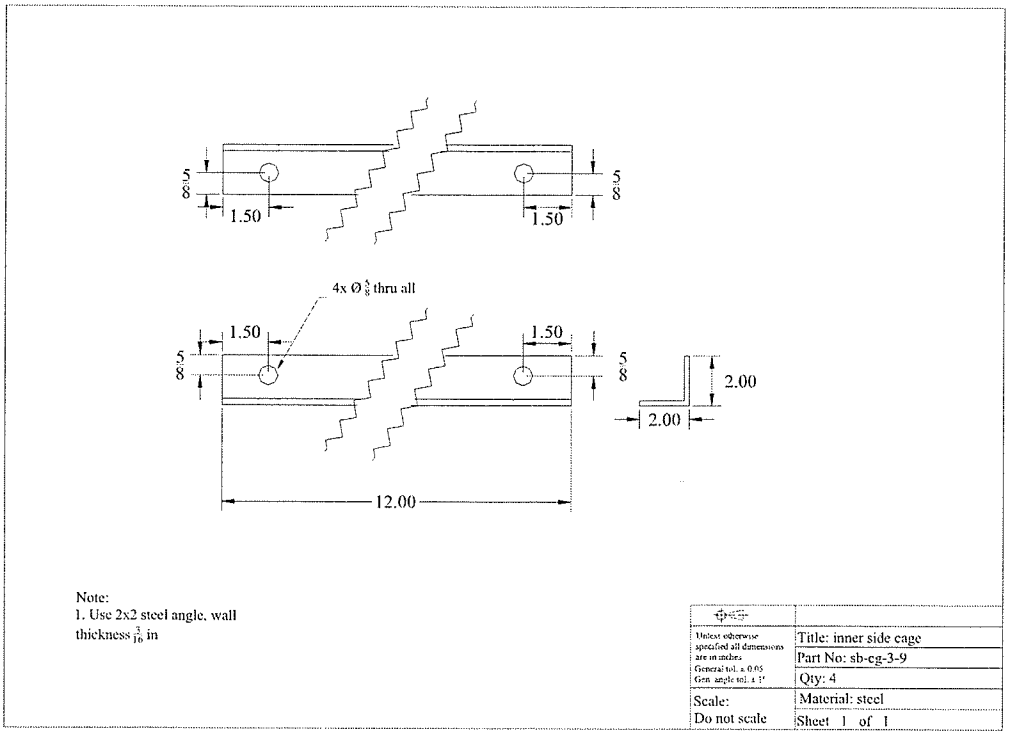

Fig. D. 107 Detail dimensions, sb-cg-3-9

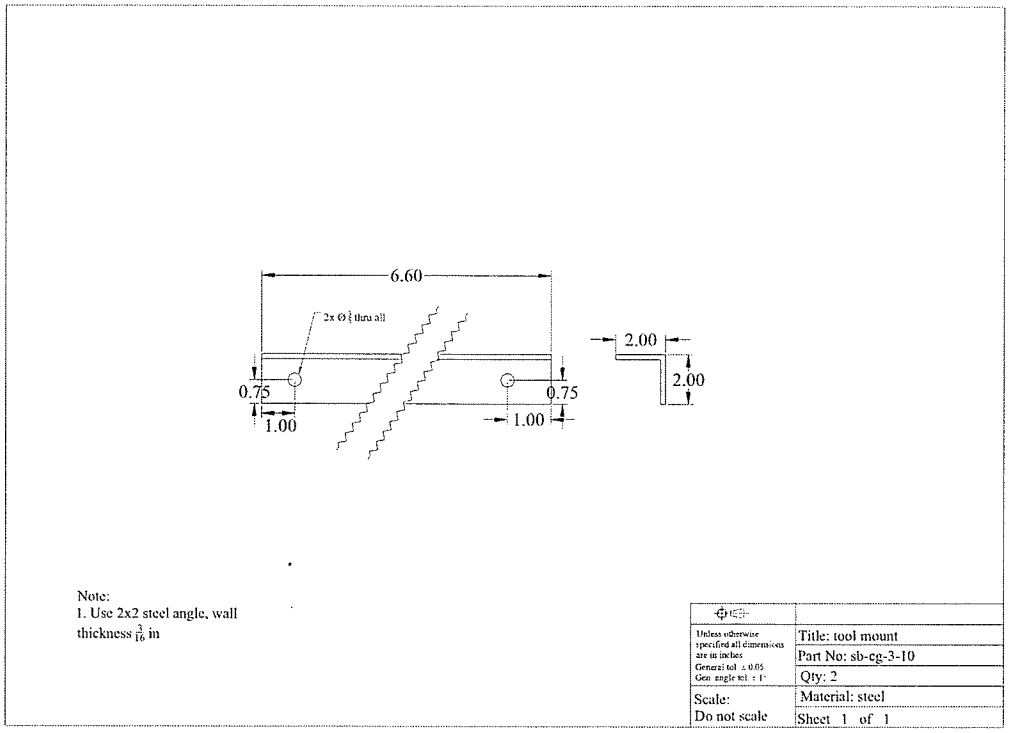

Fig. D. 108 Detail dimensions, sb-cg-3-10

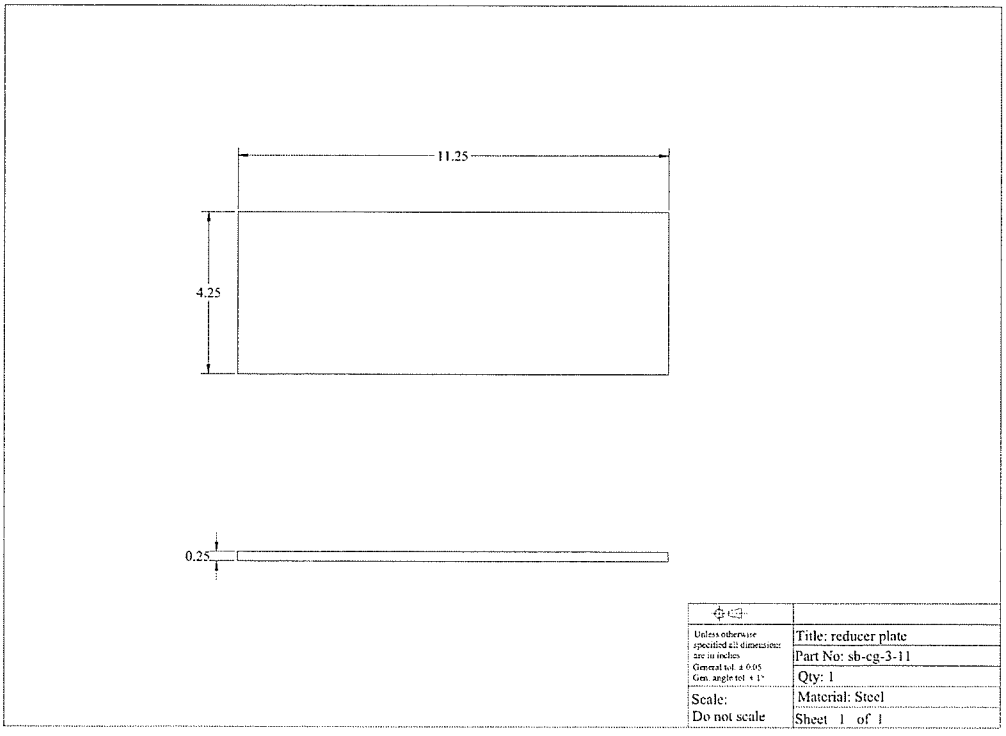

Fig. D. 109 Detail dimensions, sb-cg-3-11

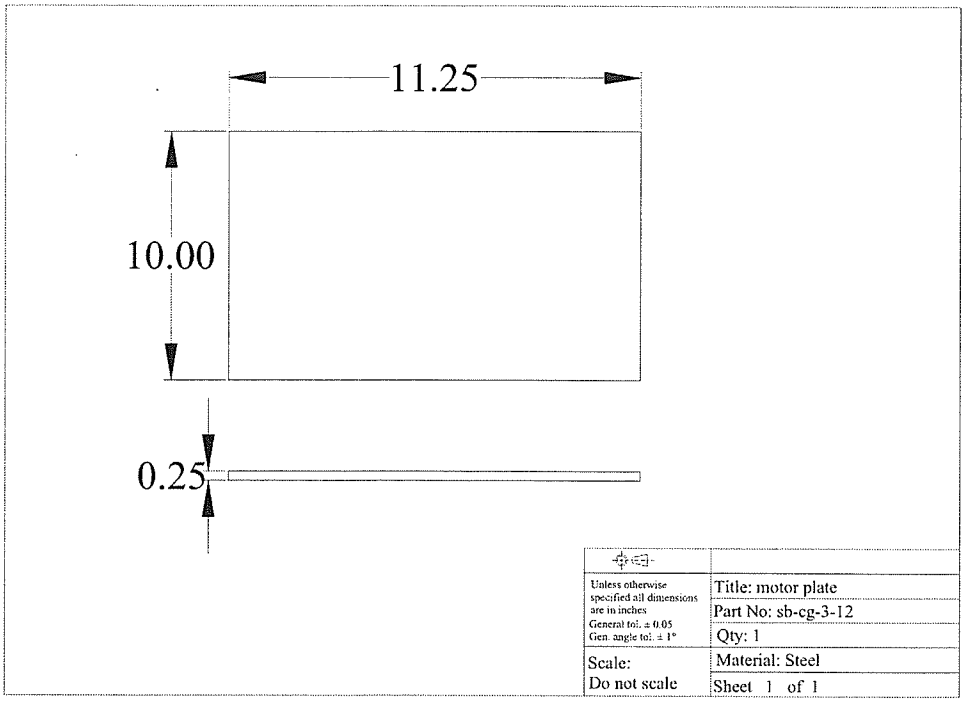

Fig. D. 110 Detail dimensions, sb-cg-3-12

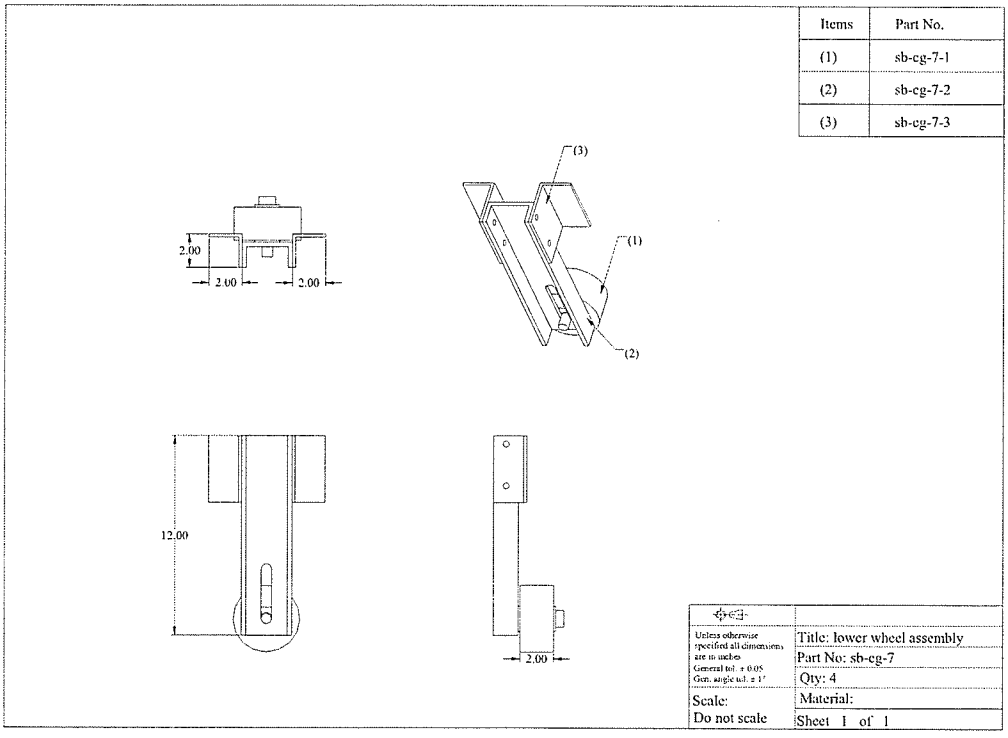

Fig. D. 111 Lower wheel assembly components and dimensions, sb-cg-7

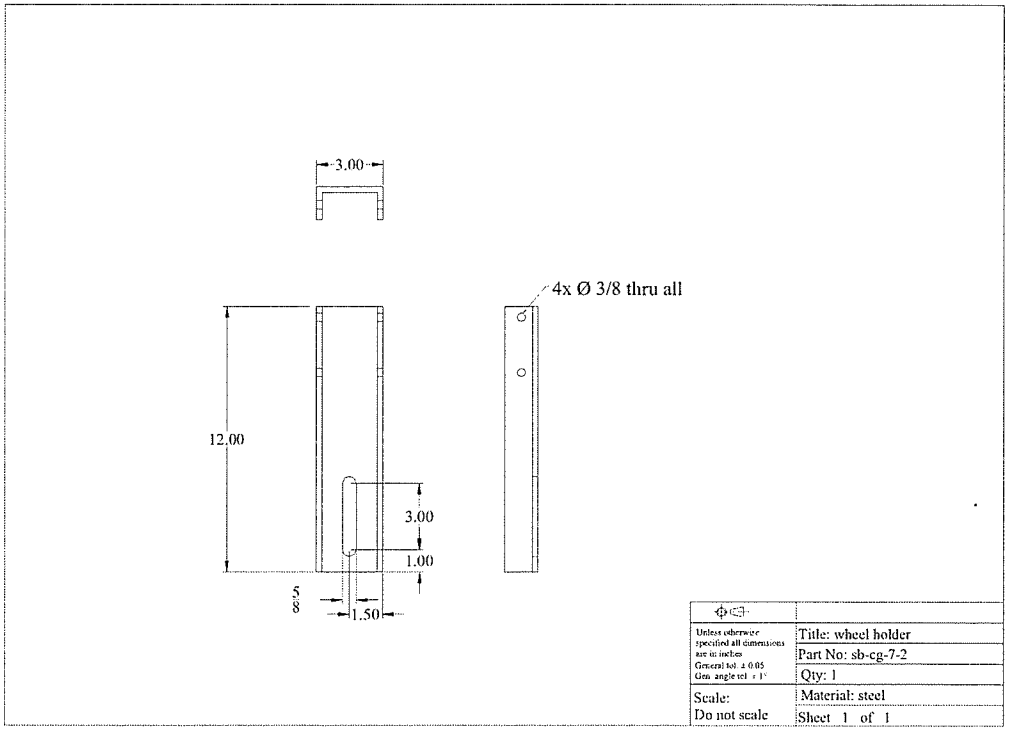

Fig. D. 112 Detail dimensions, sb-cg-7-2

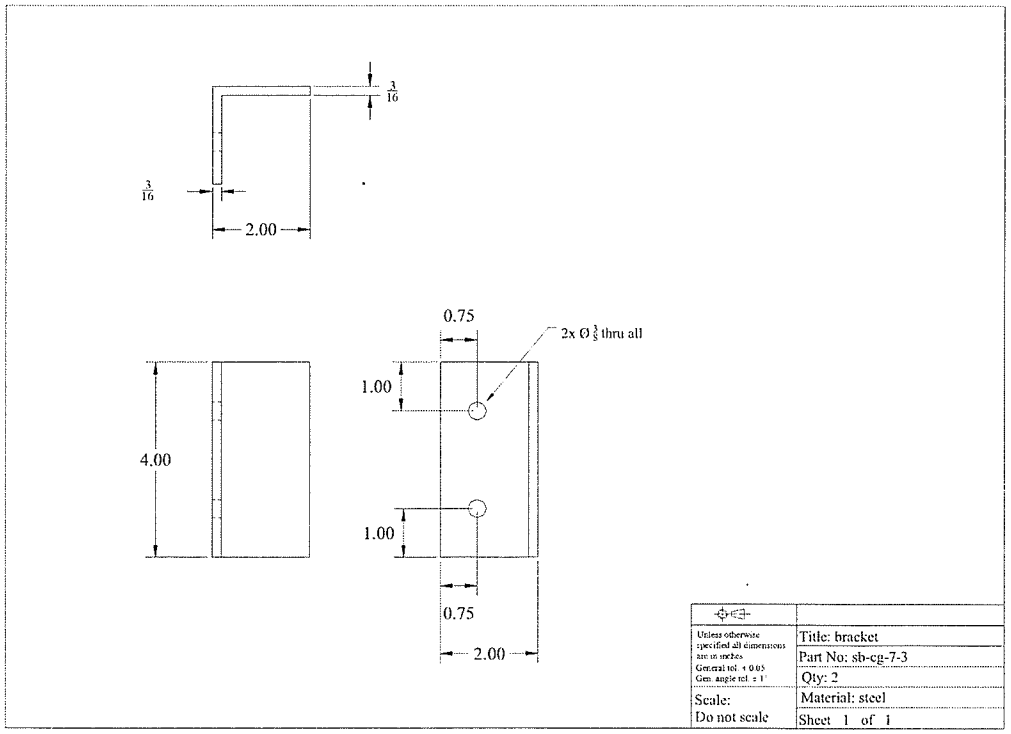

Fig. D. 113 Detail dimensions, sb-cg-7-3

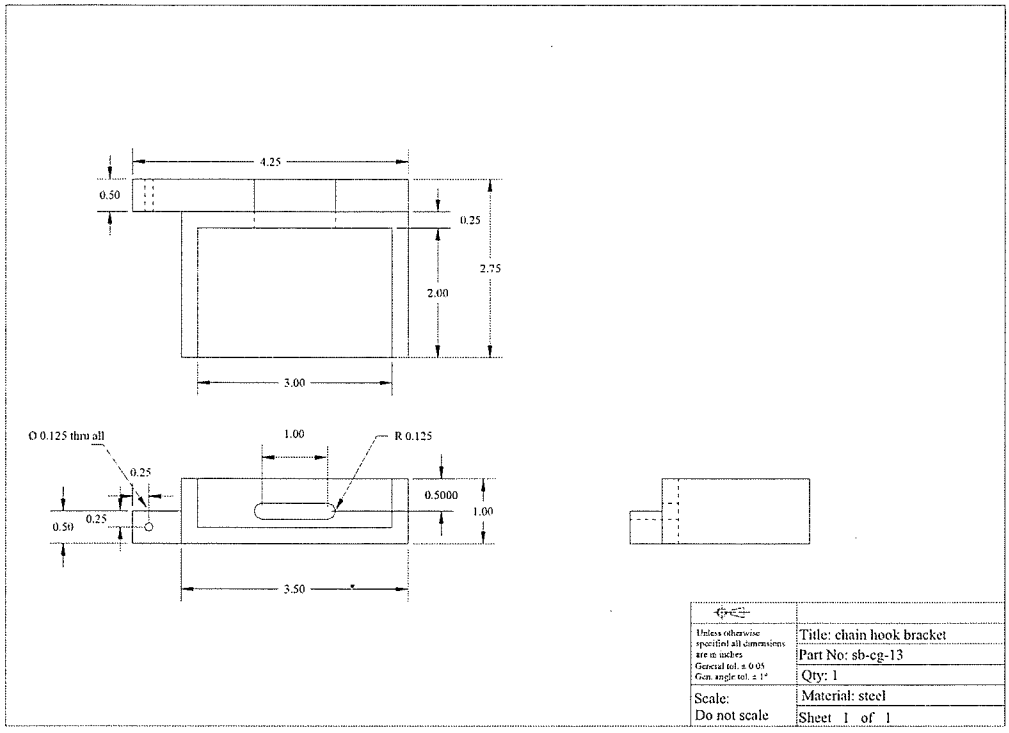

Fig. D. 114 Detail dimensions, sb-cg-13

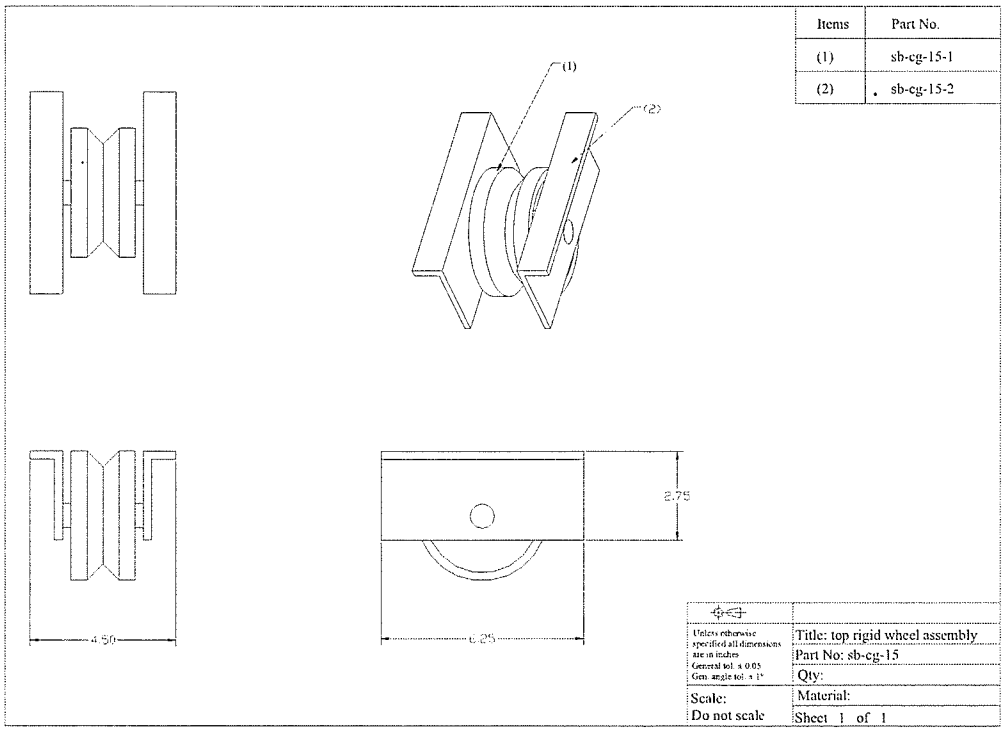

Fig. D. 115 Top rigid wheel assembly components and dimensions, sb-cg-15

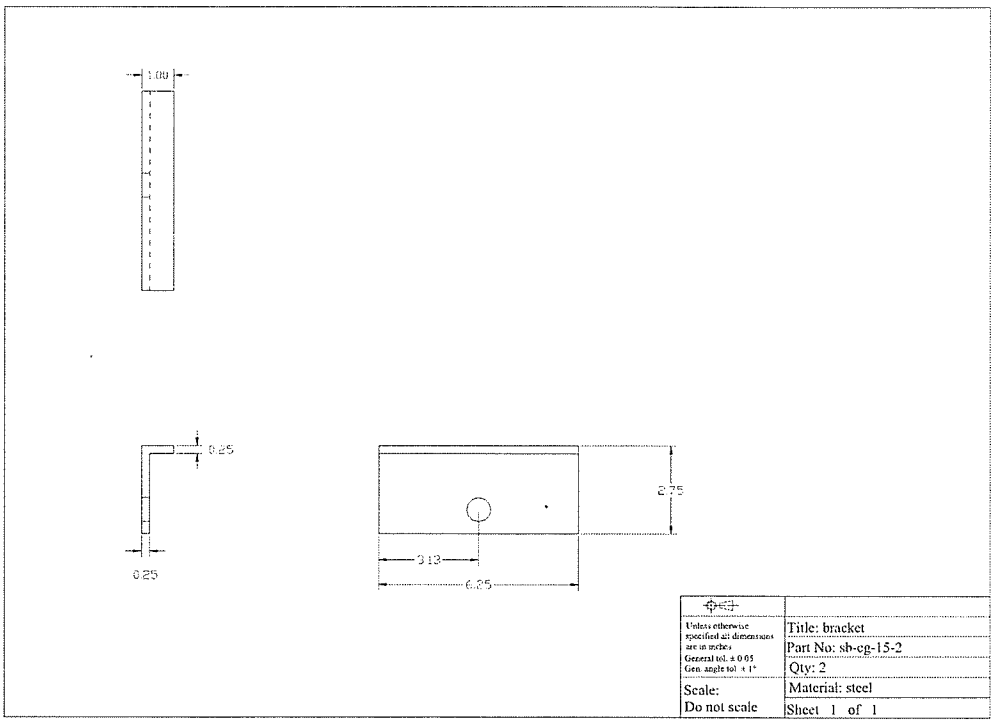

Fig. D. 116 Detail dimensions, sb-cg-15-2